
1. Introduction

1.1 Definition of Nonlinear Optics

One of the most effective techniques to overcome the spectral limitations of lasers is to exploit nonlinear optics.

Nonlinear optics is a study that deals mainly with various new optical effects and novel phenomenon arising from the interaction of intense coherent optical radiation with matter.

The potential of nonlinear optical processes is to provide a mechanism for the generation of new frequency from an already available input frequency. In other words, they provide a convenient technique for frequency conversion of light from an old to a new spectral range.

Nonlinear optical processes can take a variety of forms. The most important processes in the context of frequency conversion include second harmonic generation, sum-and difference-frequency mixing, and optical parametric oscillation. For light emission over extended spectral band, optical parametric oscillation is the key process of interest.

Optical parametric oscillators (OPOs) and optical parametric amplifiers (OPAs) constitute a class of optical frequency converting devices that have many possible applications, e.g. in range finding, molecular spectroscopy and medical applications. They can convert the frequency of the incident pump field with high efficiency, and generate two waves at new frequencies that will be continuously tunable over a wide spectral range. Virtually any wavelengths within the transparency region of the nonlinear material can be generated if the material can be phase-matched.

1.2 Optical Parametric Amplification and Oscillation

Optical parametric oscillation is a nonlinear process in which a pump beam is converted into two lower energy beams known as the signal beam (ω_s) and the idler (ω_i) beam as shown in Figure (1.2).

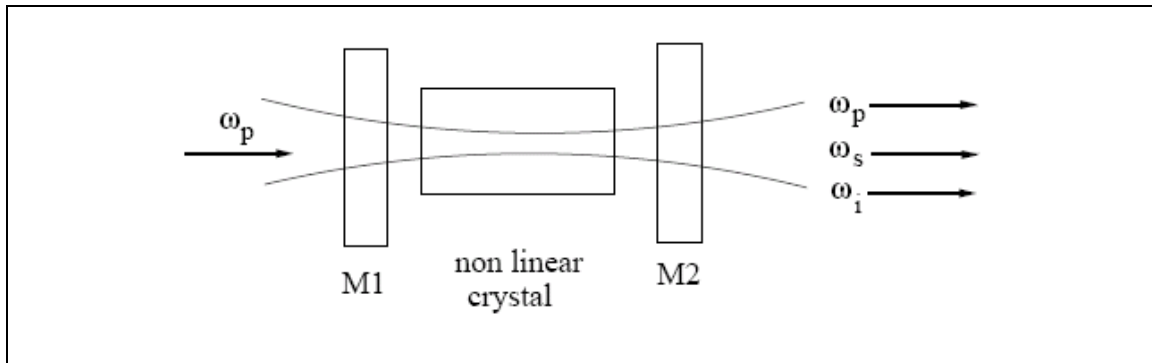


Figure (1.2): Optical parametric oscillator; the mirror M1 is highly reflective for the signal wave (ω_s) or/and idler wave (ω_i), highly transparent for the pump wavelength (ω_p). The output coupler M2 is partially reflecting (ω_s) or/and (ω_i) and highly transparent for (ω_p)[1].

As the pumped beam passes through the nonlinear medium, the spontaneous breakup of pumped photons occurs through spontaneous parametric emission. This arises from mixing of the zero point flux of the electromagnetic field at ω_s and ω_i with the incoming pump photons, through the nonlinear polarization. The field of the intense pumped beam mixes with a signal field and the idler field mixes back with the pumped beam to produce additional signal. This regenerated signal remixes with the pump to produce more idler. This process continues until power is transferred from the pump to the signal and idler field. The wavelengths of the three beams must satisfy [1]:

$1/\lambda_p = 1/\lambda_s + 1/\lambda_i$ or equivalently $\omega_p = \omega_s + \omega_i$ illustrating conservation of energy. Where (λ_p) is the pump wavelength and (λ_s) , (λ_i) are the signal and idler wavelengths respectively.

OPOs may be operated continuously, with Q-switched pulses, or with mode-locked lasers. In the latter case, synchronous pumping is required where the length of the OPO cavity is adjusted so that the cavity round-trip frequency matches the repetition rate of the pump, or is an integer fraction of that. Since two down converted waves (the signal and the idler) are generated within an OPO, there is the choice of resonating one of these two waves (singly resonant oscillator (SRO)), or to resonate both simultaneously (doubly resonant oscillator (DRO)). The DRO results in two intense fields within the nonlinear crystal at the same time, thus reducing the threshold as compared to the SRO. However, stability and smooth tuning are compromised in a DRO. An intra-cavity OPO may be employed to alleviate the reduced threshold in the SRO where the nonlinear crystal is situated inside the cavity of the pumped laser, allowing the large circulating laser field to be accessed and hence reducing the external pump threshold.

A parametric oscillator is similar to a laser, but based on optical gain from parametric amplification rather than on stimulated emission. Although OPOs are in many respects similar to lasers, there are also several of important differences. For instance, the parametric amplification process requires phase matching to be efficient. Also, no heat is deposited in the nonlinear crystal, assuming that there is no parasitic absorption. Energy is not stored in the nonlinear crystal for an OPO as in a laser, thus, gain is present only as long as the pump wave is there, and pump fluctuations directly affect the signal power.

In current OPO devices, the generated wavelengths are limited by the availability of nonlinear materials that can simultaneously satisfy the phase-matching, energy conservation and optical transmission conditions. Given a material that meets these criteria, a periodic reversal of the sign of the nonlinear susceptibility can be introduced every coherence length (typically achieved by electric field poling), and the generated fields do not cancel.

This quasi-phase matching (QPM) principle allows a cumulative growth of the generated field. For a given crystal temperature and propagation direction, phase matching may be satisfied only for one combination of frequencies. By changing the temperature, and thus the refractive index of the crystal, the frequency of the output from the crystal may be tuned.

Angular tuning results in restricted angular acceptance and walk-off, which restricts the interaction length. In the case of QPM, additional tuning flexibility is also possible using several uniform gratings on a single crystal, thus, it is possible to achieve frequency tuning through simple mechanical translation of the crystal [1].

1.3 OPO Technique: Past and Present

The first nonlinear optics experiment was conducted by Franken *et al.* with the demonstration of second harmonic generation in crystal quartz in 1961 [2], using a normal – mode ruby laser. The conversion efficiency was less than one part per billion because of the lack of phase matching.

The idea of parametric amplification and generation of tunable light was proposed and analyzed by Armstrong *et al.* [3], Kingston [4], and by Kroll [5] in 1962.

Three years later in 1965, the first experimental demonstration parametric gain by three – wave mixing was achieved by Wang and Rachetti [6]. In the same year, parametric oscillation was achieved by Giordmaine and Miller [7]. They used a *Q*-switched Nd:CaWO₄ laser, frequency – doubled to the green in LiNbO₃, to pump a monolithic LiNbO₃ tunable parametric oscillator. Shortly thereafter, the parametric oscillator was demonstrated in Russia at Moscow State University by Akhmanov *et al.* [8]. The Russian parametric oscillator, based on the nonlinear crystal KDP, had a tuning range that extended from 957.5 to 1177.5 nm. It was pumped by *Q*-switched frequency – doubled Nd:Glass laser.

In 1966, Boyd and Askin [9] suggested that CW parametric oscillation might be possible in the crystal LiNbO₃ with a threshold as low as 10mW. Two years later in 1968, Smith *et al.* achieved CW oscillation in the near infrared in Ba₂NaNb₅O₁₅ [10]. Almost simultaneously, the first CW visible parametric oscillator was demonstrated by Byer *et al.* [11]. The CW LiNbO₃ optical parametric oscillator (OPO) was pumped by the 514nm output from an argon ion laser. The OPO threshold at greater than 400mW was just below the maximum power generated by the experimental argon ion laser source.

The progress in nonlinear optical devices was reviewed by Harris [12] in 1969 as the decade drew to a close. Harris also reviewed the status of

nonlinear materials. Only four nonlinear crystals had been used successfully to achieve parametric oscillation by 1969.

The availability of the tunable optical parametric oscillator with a tuning range that extended into the near infrared molecular fingerprint region of the spectrum opened the possibility for lasers to become the critical tool for remote sensing applications.

In the 1970's the requirements for wavelength tuning with linewidth control, especially in the near infrared molecular fingerprint region, led to develop an infrared (IR) tunable parametric oscillator. The first tunable IR – OPO was based in CdSe and pumped by Nd:YAG operating at an unusual 1.83 μm wavelength [13]. The second tunable IR – OPO was an angle phase-matched LiNbO₃ OPO pumped by a *Q*-switched Nd:YAG laser [14], [15]. The *Q*-switched Nd:YAG pumped tunable 1.4 to 4.4 μm LiNbO₃ OPO was reported in 1975 [16]. The LiNbO₃ OPO had an extended 1.4 to 4.4 μm tuning range required for remote sensing, but was well short of the required energy.

In the 1980's, Chen introduced the new nonlinear crystal beta barium borate (BBO). In 1986, Chen visited Stanford, where the crystals were evaluated by second – harmonic generation [17], [18]. The visible BBO – OPO was demonstrated at Stanford and elsewhere in 1988 [19], [20].

Tang *et.al.* reviewed progress in parametric oscillators in 1992 [21]. Improvement in the growth and the optical quality of BBO led to the reorientation of a commercial tunable parametric oscillator product by spectra physics in 1993. Continued progress in the frequency control of the BBO-OPO by injection seeding [22], [23] led to the application of these all

solid-state tunable sources to spectroscopy. Today, BBO parametric oscillators, with their broad 0.41 – 2.5 μm tuning range, have replaced high-peak power dye lasers as the preferred tunable coherent source. The characterization of type I ($e + o + o$) phase matching in beta-barium borate (BBO) optical parametric oscillators pumped by the third harmonic of a Q-switched Nd:YAG laser in a collinear phase-matched geometry and three separate non-collinear configurations was presented by Lawrence Gloster *et.al.* [24]. They showed that the optical conversion efficiency increases from 10.7% in the collinear case to 40% with a non-collinearity of 90.8mrad, and a corresponding fall in the operational threshold from 274 to 188 mJ.cm^{-2} .

Ultrafast parametric processes investigated so far have mostly sought to increase the efficiency of the collinear OPG and OPA by means of suppressing the accompanying non-collinear process. Several approaches such as seeding with white-light continuum pulses and multiple-pass amplification in two or more crystals have been used. Broadband non-collinear generation was recently used to produce, after compression, sub-20-fs pulses [25], sub-8-fs and sub-10-fs pulses [26], [27]. Less attention has been devoted, however, to more systematic study of the relation between the collinear and non-collinear effects in BBO as well as in other nonlinear crystals.

In the year 2000 Krylov *et.al.* [28], presented a comprehensive theoretical and experimental analysis of femtosecond parametric generation and amplification in type-I phase-matched BBO crystal, pumped with 390 nm wavelength, both in non-collinear and collinear geometry. For excitation they used 150-fs-duration pulses from frequency-doubled regenerative-

amplified Ti:sapphire laser. They analyzed theoretically the conditions for group-velocity matched generation and amplification, seeded with white light continuum pulses by considering mean propagation velocity of pump and parametric pulses.

In the near- and mid-infrared spectral region up to 4- μm KTP is well suited for frequency conversion due to its wide transparency range, comparatively large nonlinearity and high damage threshold. In 2002 Finsterbusch *et.al.* [29], report on OPO seeded, high-repetition-rate parametric amplification in KTP. Pumped at 1053 nm this device shows quantum efficiency as high as 37%. Moreover, pumping at 1053 nm avoids problems induced by two-photon absorption and gray-tracking, which are observed at shorter pumping wavelengths [30]-[32] and which substantially decrease the conversion efficiency and reliability. Using difference frequency mixing, this high-power OPA is an optimal source for the generation of narrow linewidth mid-infrared radiation tunable between 5 and 20 μm for signal and idler wave tuning ranges near 2 μm .

A compact eye-safe optical parametric oscillator (OPO) using a noncritically phase-matched KTP crystal intracavity pumped by a passively Q-switched Nd :YVO₄ laser was experimentally demonstrated in 2003 [33]. To enhance the performance of passive Q-switching, a Cr⁴⁺ :YAG saturable absorber crystal is coated as an OPO output coupler in a nearly hemispherical cavity. With an incident pump power of 2.5W, the compact intracavity OPO cavity, operating at 62.5 kHz, produces average powers at 1573 nm up to 255 mW and peak powers higher than 1 kW.

The development of compact high efficiency optical parametric oscillators (OPO) which generate widely tunable coherent radiation with small divergence and high angular pointing stability is currently a topical problem. In the past, many efforts had been made to reduce the spectral bandwidth and the divergence of the OPO output beam. The spatial and spectral properties of a 355nm pumped pulsed nanosecond (ns) BBO OPO were improved by using type II phase matching and pump beam back reflection [34]. In this way the OPO bandwidth was reduced by more than a factor of 20 to less than 0.1nm, and the divergence of the OPO beam was reduced in the phase matching plane by a factor of 5 to 1mrad. Kondr, *et.al.* [35] investigated the spectral properties of the type II BBO OPO and KTP OPO pumped at 532nm and pump beam reflected. It was found, that the OPO bandwidth was reduced by more than a factor of 5 to less than 0.3nm at 680nm and 0.7nm at 1064nm. They determined that in collinear OPO with inclined nonlinear crystal in the forward direction the output signal beam deviates from the pump beam. After reflection at the OPO out coupling mirror the signal and pump beams inside crystal are non-collinear. After passing through the crystal in backward direction and reflection at the OPO rear mirror the signal and pump beams inside crystal are again collinear.

In 2004 an efficient diode-pumped passively Q-switched Nd:GdVO₄/Cr⁴⁺:YAG laser was employed to generate a high repetition rate, high-peak-power eye-safe laser beam with an intracavity optical parametric oscillator (OPO) based on a KTP crystal [36]. The conversion efficiency for the average power is 8.3% from pump diode input to OPO signal output and the slope efficiency is up to 10%. At an incident pump power of 14.5W, the

compact intracavity OPO cavity, operating at 46 kHz, produces average powers at 1571 nm up to 1.2W with a pulse width as short as 700 ps.

In 2005 a new method for characterization of periodically poled crystals is developed based on spontaneous parametric down-conversion. The method is demonstrated on crystals of Y:LiNbO₃, Mg:Y:LiNbO₃ with non-uniform periodically poled structures, obtained directly under the Czochralski growth procedure and designed for application of 1.064 μm pumped OPO in the mid- infrared range. Infrared dispersion of refractive index, effective working periods and wavelengths of OPO were determined by special treatment of frequency angular spectra of spontaneous parametric down-conversion in the visible range. Two-dimensional mapping via spontaneous parametric down-conversion is proposed for characterizing spatial distribution of bulk quasi-phase matching efficiency across the input window of a periodically poled sample [37].

In 2006 Vodchits and his team studied an optical parametric oscillator (OPO) with an unstable telescopic cavity, placed inside the cavity of an actively Q-switched multimode Nd³⁺:KGW pump laser [38]. They used a KTP crystal as the nonlinear medium for the OPO. They have compared the emission characteristics of OPOs with unstable telescopic and planar cavities. They have established that compared with the planar cavity, the unstable cavity reduces the OPO beam divergence and improves the spatial distribution of the radiation energy in the far wave zone.

Based on their investigations, they have designed a compact eye-safe ($\lambda = 1.578 \mu\text{m}$) laser source with natural cooling, emitting (for electrical pumping energy 7.3 J) pulses with pulse energy 22 mJ and pulse duration

6 nsec. The FWHM beam divergence for the source is no greater than 3.5 mrad.

A non-collinear, 1064 nm pumped, 10 kHz repetition rate ns-OPO which consists of a 13mm long periodically poled lithium niobate (PPLN) crystal in a hemispherical optical cavity was demonstrated in 2007 [39]. The non-collinear phase-matching is achieved by tilting the domains by 60° with respect to the pump beam. This phase-matching avoids back conversion of signal and idler radiation into pump radiation and thus improves the spatial quality of the generated OPO radiation considerably. At a pump power of 5.5W the OPO provided a conversion efficiency of up to 34%. The generated OPO pulses with a total power of up to 1.85W were emitted in an almost diffraction limited beam with a M^2 -value of 1.1. The beam quality did not change when the pump power was varied in the range of 2–5W.

1.4 Aim of the Project

The aim of this work is to investigate a method of calculating the characteristics of non-collinear phase matching in both uniaxial and biaxial crystals. The method in the present study allows a far larger set of nonlinear crystals and configurations to be studied as follows:

- a. Determine the optimum design parameters for the nonlinear crystals (both uniaxial and biaxial) parametric oscillators.
- b. Design a nanosecond AgGaS_2 type-I singly resonant (DSR) optical parametric oscillator to achieve continuously tunable radiation in the range of atmospheric transparency (3-5 μm).

- c. Design a confocal positive – branch unstable KTP OPO for the generation of eye-safe wavelength radiation.

2. Second Order Nonlinear Optical Conversions

2.1 Basic Principles of Second Order Nonlinear Optical Conversions

Optical phenomena that are observed in our every day life, e.g. refraction in a glass prism or the colors from the interference pattern of an oil film on water can to a very high degree of accuracy be described by linear equations. Dielectric media like glass or water may be thought of as an assembly of positive ion cores, where each core is surrounded by a negatively charged electron cloud. In linear optics, the electromagnetic wave induces a polarization in the dielectric material, i.e. a separation of charges, which is directly proportional to the electric field and hence oscillates with the same frequency as the applied field. The linearity also implies that the electromagnetic waves passing through the material do not interact with each other or themselves to create waves at new frequencies and that the observed phenomena is not dependant of the light intensity.

However, if the electric fields become sufficiently strong it will disturb the electron cloud to the degree when the restoring forces between the heavy ion cores and electrons are not linear to the electric field anymore as shown in figure 2.1.

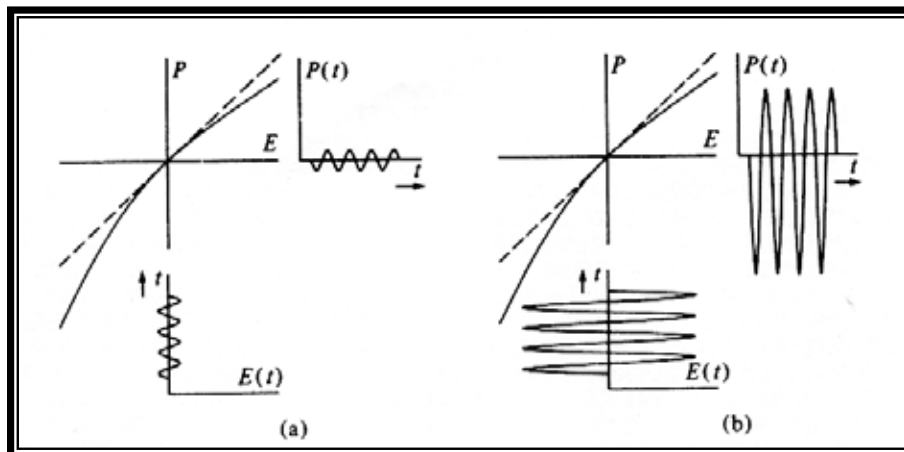


Figure 2.1 The nonlinear dependence of the polarisation versus the applied electric field. (a) small input fields result in a linear response. (b) strong input fields causes a distorted waveform of the polarisation, which contains harmonic frequencies[40].

It is then not enough to describe the induced polarization with a linear term; instead a full series expansion of the polarization in terms of successively higher orders of the electric field is needed [40].

$$P = \varepsilon_0 \chi^{(1)} E + \varepsilon_0 (\chi^{(2)} E^2 + \chi^{(3)} E^3 + \dots) = P^L + P^{NL} \quad (2.1)$$

where P^L denotes the linear part of the polarization, P^{NL} the nonlinear part, ε_0 is the permittivity of vacuum, E is the electric field component of the electromagnetic wave and $\chi^{(m)}$ represents the susceptibility tensor of m th order with the rank $(m+1)$. To observe consecutively higher orders of nonlinear phenomenon the electric field must become stronger and stronger, since the magnitude of the susceptibility tensor elements falls off rapidly with increasing order.

The quadratic polarization $P^{(2)} = \varepsilon_0 \chi^{(2)} E_1 E_2$ is responsible for many interesting effects. In the case when both electric fields oscillate with optical frequencies, different types of frequency conversion processes occur, figure 2.2, while if one field is static the refractive index of the media is affected through the linear electro-optic effect, (the Pockel's effect). For all frequency conversion processes the energy of the photons that take part in the mixing has to be conserved. The frequency conversion processes may be divided into two groups.

In the first, two electromagnetic waves with different frequencies are impinging on the media. Sum-frequency generation (SFG) take place when the photon energies from the different fields are added and a photon with higher energy is created. Difference-frequency generation (DFG) occurs when the photons with lower energy are subtracted from the photons with

higher energy. At the same time the light waves can also interact with themselves and create a polarization, which contains both a static component (dc-rectification) and one at the double original frequency, second harmonic generation (SHG).

In the second group there is only one field, the pump field, incident to the material. A pump photon is split up into two photons with lower energy, this is called optical parametric generation (OPG). The generated photons are denoted signal and idler photons, where the former has higher frequency than the latter. If a cavity is used to enhance the efficiency by resonating one or both of the generated fields, the device is named an optical parametric oscillator (OPO). Finally, optical parametric amplification (OPA) is essentially an OPG process where either the signal or the idler fields are seeded on the incoming side. OPA may also be considered to be a sort of difference frequency process, but in the case of OPA the amplification of the seed field is studied, while on the other hand for DFG the idler field gets most attention.

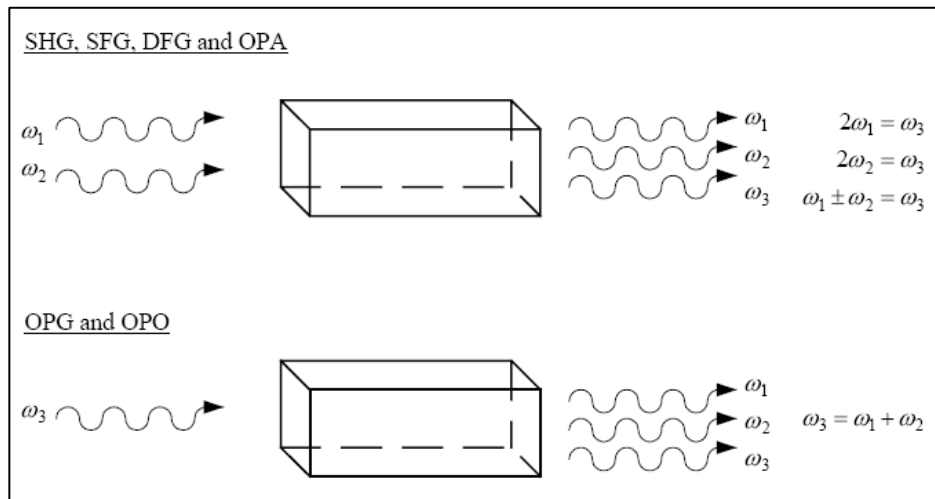


Figure 2.1 frequency conversion processes arising from $\chi^{(2)}$ [40].

The cubic polarization $\mathbf{P}^{(3)} = \epsilon_0 \chi^{(2)} \mathbf{E}_1 \mathbf{E}_2 \mathbf{E}_3$ causes the quadratic electro-optic effect (the Kerr effect), dc induced SHG, four wave mixing processes, the optical Kerr effect, two photon absorption, Raman and Brillouin scattering.

This study focuses on parametric down conversion in particular OPOs and OPAs.

2.1.1 Three Wave Interactions in 2nd Order NLO Process

For the $\chi^{(2)}$ mixing the three waves couple to each other through three polarizations, which give the following set of equations [41]:

$$\frac{d}{dr} E_i(w_1, r) = i \left(\frac{K_1}{2k_1} \right) 2 \chi_2^{ijk}(-w_1, w_2, w_3) E_j(w_2, r) E_k(w_3, r) \exp(-i\Delta K r) \quad (2.2)$$

$$\frac{d}{dr} E_j(w_2, r) = i \left(\frac{K_2}{2k_2} \right) 2 \chi_2^{jik}(-w_2, w_1, -w_3) E_i(w_2, r) E_k^*(w_3, r) \exp(i\Delta K r) \quad (2.3)$$

$$\frac{d}{dr} E_i(w_3, r) = i \left(\frac{K_3}{2k_3} \right) 2 \chi_2^{ikj}(-w_3, w_1, -w_2) E_i(w_1, r) E_j^*(w_2, r) \exp(i\Delta K r) \quad (2.4)$$

Where $\Delta K = K_1 - (K_2 + K_3)$, $w_1 = w_2 + w_3$ and $\chi_2^{ijk}(-w_1, w_2, w_3) = \chi_2^{*ijk}(-w_2, w_1, -w_3) = \chi_2^{*ijk}(-w_3, w_1, -w_2)$. Exact solutions of the above equations have been obtained with various amounts of radiation present initially at the three different frequencies [3].

The sum and difference frequency generation will be considered. Here two frequency components are initially present with comparable intensity, and a wave at the third frequency is created through the nonlinear interaction. Thus, if the waves at w_2 and w_3 are initially present, the initial growth of a wave at the sum frequency w_1 will be given from (2.2) by [41]:

$$E_i(w_1, r) = E_i(w_1, 0) + i \left(\frac{K_1}{2k_1} \right) 2\chi_2^{ijk}(-w_1, w_2, w_3) E_j(w_2, 0) E_k(w_2, 0) \left[\frac{1 - \exp(-i\Delta Kr)}{i\Delta K} \right] \quad (2.5)$$

The three-wave interactions through $\chi^{(2)}$ can also lead to parametric amplification and parametric oscillation. In this case, parametric amplification refers to the coupled growth of two frequency components in the presence of a strong frequency component, which will be referred to as the pump [42]. To describe these possibilities, it is convenient to write w_p , w_s , and w_i as the pump, signal, and idler frequencies. The corresponding wave number vectors are written k_p , k_s , and k_i . Here $w_p = w_s + w_i$ and $\Delta K = K_p - (K_s + K_i)$. It is assumed that the percentage energy conversion is small so that the amplitude and phase of the pump radiation remain approximately constant. Under index matched conditions, solutions of (2.3) and (2.4) give [41]:

$$E_j(w_s, r) = E_j(w_s, 0) \cosh(gr) \quad (2.6)$$

$$E_k(w_i, r) = i \left(\frac{w_i}{w_s} \right)^{\frac{1}{2}} E_j(w_s, 0) \sinh(gr) \quad (2.7)$$

$$g = \left[\frac{K_i K_s}{k_i k_s} \right]^{\frac{1}{2}} \chi_2^{ijk}(-w_i, w_p, w_s) E_s(w_p, 0) \quad (2.8)$$

Where the initial amplitude $E_k(w_i, 0)$, at the idler frequency has been neglected. From an exact solution of (2.2-2.3), it can be shown that energy and momentum are conserved.

The nonlinear optical interactions involve optical waves whose frequencies w_i are much smaller than the lowest resonance frequency of the

material system. Under these conditions, the nonlinear susceptibility is essentially independent of frequency and the nonlinear polarization can be described in the time domain by the relation

$$\bar{P}(t) = \chi^{(2)} \bar{E}(t)^2 \quad (2.9)$$

Where $\chi^{(2)}$ can be taken to be a constant.

Since the medium is necessarily lossless whenever the applied field frequencies w_i are very much smaller than the resonance frequency w_0 , the condition of full permutation symmetry must be valid under these circumstances. This condition states that the indices can be permuted as long as the frequencies are permuted simultaneously, and it leads to the conclusion that

$$\begin{aligned} \chi_{ijk}^{(2)}(w_3 = w_1 + w_2) &= \chi_{jki}^{(2)}(w_1 = -w_2 + w_3) = \chi_{kij}^{(2)}(w_2 = w_3 - w_1) \\ &= \chi_{ikj}^{(2)}(w_3 = w_2 + w_1) = \chi_{jik}^{(2)}(w_1 = w_3 - w_2) \\ &= \chi_{kji}^{(2)}(w_2 = -w_1 + w_3) \end{aligned} \quad (2.10)$$

However, under the present conditions $\chi^{(2)}$ does not actually depend on the frequencies, therefore the indices can be presented without permuting the frequencies, leading to the result

$$\begin{aligned} \chi_{ijk}^{(2)}(w_3 = w_1 + w_2) &= \chi_{jki}^{(2)}(w_3 = w_1 + w_2) = \chi_{kij}^{(2)}(w_3 = w_1 + w_2) \\ &= \chi_{ikj}^{(2)}(w_3 = w_1 + w_2) = \chi_{jik}^{(2)}(w_3 = w_1 + w_2) \\ &= \chi_{kji}^{(2)}(w_3 = w_1 + w_2) \end{aligned} \quad (2.11)$$

This result is known as the Kleinman symmetry condition. It is valid whenever dispersion of the susceptibility can be neglected [43].

2.1.2 Effective second-order nonlinear coefficient

Even orders of the polarization can only exist in material that lacks a centre of inversion. Among the 32 different crystal classes in nature 21 are acentric [40]. The second order susceptibility is in the literature most often replaced by the second order nonlinear tensor, the d-tensor [40]. The relation between the tensors is:

$$\chi_{ijk}^{(2)}(-\omega_3; \omega_1, \omega_2) = 2d_{ijk}(-\omega_3; \omega_1, \omega_2) \quad (2.12)$$

The d-tensor consists of 27 elements, but in the case of frequency doubling the intrinsic permutation symmetry of the tensor allows it to be contracted to a matrix of 3 by 6 independent elements. This contraction of the original tensor can be done for any second-order mixing process, if Kleinmann symmetry holds [43], i.e. all interacting frequencies are far from resonance. Furthermore, if the symmetry of the specific crystal class is taken into account the number of independent elements can be reduced further.

The connection between the polarization and the electric fields via the contracted tensor is written in matrix form as follows:

$$\begin{bmatrix} \left(P_{\omega_3}^{(2)} \right)_x \\ \left(P_{\omega_3}^{(2)} \right)_y \\ \left(P_{\omega_3}^{(2)} \right)_z \end{bmatrix} = 2\varepsilon_0 K \begin{bmatrix} d_{11} & d_{12} & d_{13} & d_{14} & d_{15} & d_{16} \\ d_{21} & d_{22} & d_{23} & d_{24} & d_{25} & d_{26} \\ d_{31} & d_{32} & d_{33} & d_{34} & d_{35} & d_{36} \end{bmatrix} \begin{bmatrix} \left(E_{\omega_1} \right)_x \left(E_{\omega_2} \right)_x \\ \left(E_{\omega_1} \right)_y \left(E_{\omega_2} \right)_y \\ \left(E_{\omega_1} \right)_z \left(E_{\omega_2} \right)_z \\ \left(E_{\omega_1} \right)_y \left(E_{\omega_2} \right)_z + \left(E_{\omega_2} \right)_y \left(E_{\omega_1} \right)_z \\ \left(E_{\omega_1} \right)_x \left(E_{\omega_2} \right)_z + \left(E_{\omega_2} \right)_x \left(E_{\omega_1} \right)_z \\ \left(E_{\omega_1} \right)_x \left(E_{\omega_2} \right)_y + \left(E_{\omega_2} \right)_x \left(E_{\omega_1} \right)_y \end{bmatrix} \quad (2.13)$$

$K(-\omega_3; \omega_1, \omega_2)$ is the degeneracy factor, which takes the value $\frac{1}{2}$ for SHG and optical rectification and 1 for the other conversion processes. ω is the carrier frequency of the electromagnetic wave.

2.2 Nonlinear Optical Materials

2.2.1 Basic Properties

Nonlinear materials useful for optical parametric oscillator applications in general have the same properties and requirements as those materials useful for optical second-harmonic generation [44]. Among the requirements and desirable properties are those materials:

- Lack a center of symmetry.
- Posses a large value of $(\chi^{(2)})^2/n^3$.
- Phase-matchable.
- Transparent for all wavelengths of interest.
- Homogeneous and of good optical quality.
- Resistant to optical damage.

2.2.2 Optical Properties of Materials

If the lengths of all the axes of the optical indicatrix are equal the crystal has only one refractive index and is referred to as isotropic. If any axes of the optical indicatrix are not equal the crystal is termed anisotropic.

There are two types of anisotropic crystals encountered in nature. If two axes of the optical indicatrix are equal, the crystal is termed uniaxial. The term uniaxial is used because in this case the crystal has one optic axis that is perpendicular to the plane formed by the two equal axes of the indicatrix. (An optic axis is defined as the wave vector direction that has a refractive index value that is independent of the direction of polarization, or in other

words, it is the wave vector direction perpendicular to a circular cross-section of the optical indicatrix). A uniaxial crystal is called positively birefringent when $n_e > n_o$ and negatively birefringent for $n_e < n_o$, as shown in figure 2.3.

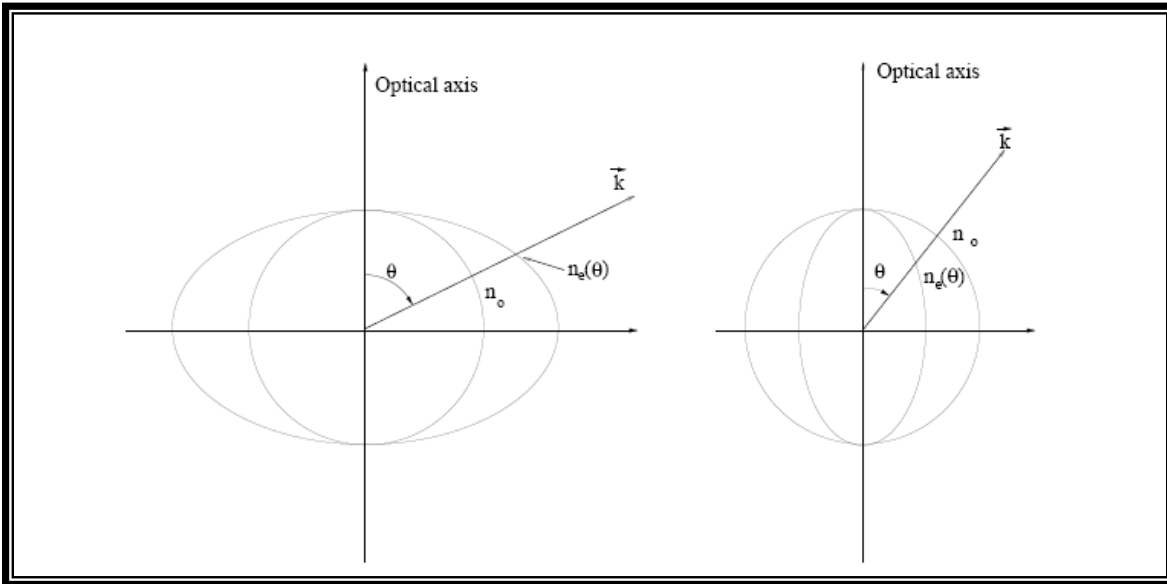


Figure 2.3 Dependence of the angle θ between the wave vector K and the optical axis of a positive (right) and negative (left) birefringent crystal [45].

If all three axes of the indicatrix are unequal (three different values for the principal refractive indices), the crystal is called biaxial. The term biaxial is used because in this case the crystal has two primary optic axes [46]. For a biaxial crystal with $n_x < n_y < n_z$, the two optic axes lie in the xz principal plane [47]. If n_y is closer in value to n_x the crystal is called positive biaxial and if n_y is closer to n_z the crystal is called negative biaxial [47]. For a positive biaxial crystal, the z -axis is the acute bisector of the angle between the two optic axes. For a negative biaxial crystal, the x -axis is the

acute bisector of the angle between the two optic axes. Figure 2.4 shows the optical indicatrix for a negative biaxial crystal.

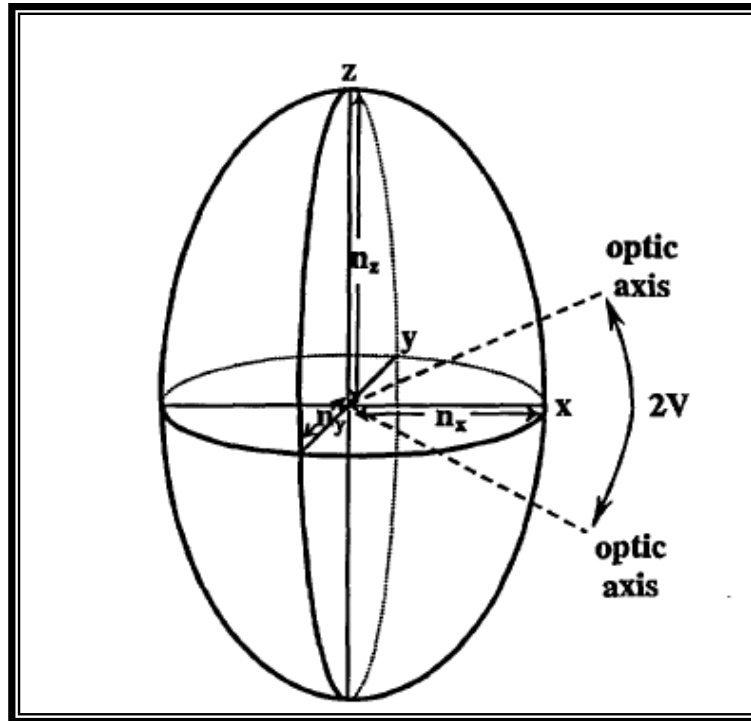


Figure 2.4. Optical indicatrix for a negative biaxial crystal where $n_x < n_y < n_z$. The x , y , and z -axes are the crystal's dielectric axes and n_x , n_y and n_z are the principal refractive indices. Note that the optic axes lie in the xz plane where the x dielectric axis is the acute bisectrix and V is the optic angle [47].

Whether a crystal is isotropic or anisotropic, and in the anisotropic case, whether it is uniaxial or biaxial, is determined by the crystal's point group symmetry. Crystals with cubic symmetry are isotropic. Crystals with trigonal, tetragonal, or hexagonal symmetry are uniaxial. Crystals with orthorhombic, monoclinic, or triclinic symmetry are biaxial.

2.3 Phase Matching and Conversion Efficiency

The phase matching ($\Delta k = k_p - k_s - k_i = 0$) of the three waves is the key requirement for second-order nonlinear processes to occur [48]. From a quantum mechanical point of view, this condition can also be viewed as the condition for conservation of momentum of photons in the process. In materials with normal dispersion the refractive index of the medium increases with increasing frequency.

To simultaneously satisfy the conservation of energy ($w_p = w_s + w_i$) and phase matching conditions, the interacting fields must be subject to different refractive indices.

The effect of imperfect phase-matching on the efficiency of the nonlinear process is given by [49]:

$$efficiency = l_c^2 \left(\frac{\sin^2 \left(\frac{\Delta K l_c}{2} \right)}{\left(\frac{\Delta K l_c}{2} \right)^2} \right) \quad (2.14)$$

For high overall efficiency we need a large (l_c) and a small $\Delta K l_c$, i.e. $\Delta K=0$. The momentum of a photon is ($\hbar K$). Therefore the $\Delta K=0$ condition for a down-conversion process implies that the momentum of the incident photon is equal the sum of the momentum of the generated photons. Hence the phase-matching condition is equivalent to the conservation of momentum.

2.3.1 Methods for phase-matching

For very short lengths of non linear material phase-matching is not important since the product $\Delta k l_c$ is still small. However, for most nonlinear systems this length of material is insufficient to observe efficient non linear interactions. Phase-matching is important because

- Increases efficiency of nonlinear process.
- Acts to select the nonlinear process of interest.

In all nonlinear materials, dispersion in the phase velocity (a refractive index which depends on wavelength) ensures that the requirements for energy conservation

$$\omega_3 = \omega_1 + \omega_2 \quad (2.15)$$

and momentum conservation

$$\Delta k = k_3 - k_2 - k_1 = 1/c (n_3\omega_3 - n_2\omega_2 - n_1\omega_1) = 0 \quad (2.16)$$

cannot be satisfied simultaneously.

A number of methods for phase-matching can be employed [49].

- Dielectric waveguide phase-matching.
- Birefringent phase-matching.
- Quasi phase-matching.
- Non-collinear phase-matching.

One of the surprising points to arise from the tensor nature of the nonlinear coefficient is the fact that the generated light need not have the same polarization state as the incident light.

Phase-matching types are characterised in term of the relative polarization states of the three fields as shown in Figs.2.5-2.7. This is particularly significant with respect to birefringent phase-matching.

Type-I phase-matching ($\omega_3 = \omega_1 + \omega_2$)

- $E(\omega_1)$ and $E(\omega_2)$ have parallel polarizations.
- $E(\omega_3)$ is orthogonally polarized with respect to $E(\omega_1)$ and $E(\omega_2)$.

Type-II phase-matching ($\omega_3 = \omega_1 + \omega_2$)

- $E(\omega_1)$ and $E(\omega_2)$ have orthogonal polarizations.
- $E(\omega_3)$ has parallel polarization with respect to $E(\omega_1)$ or $E(\omega_2)$.

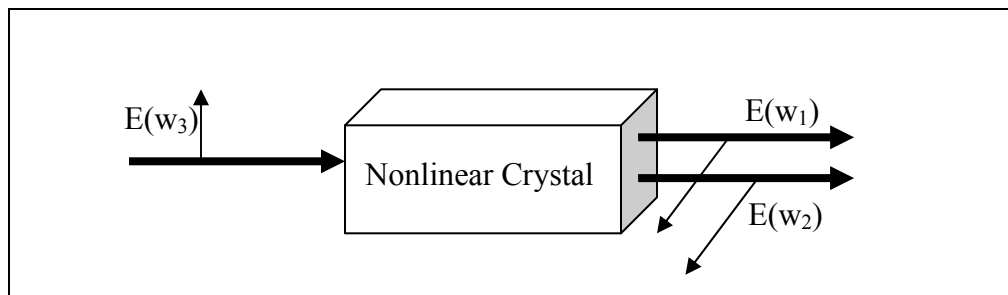


Figure 2.5 Type I phase matching

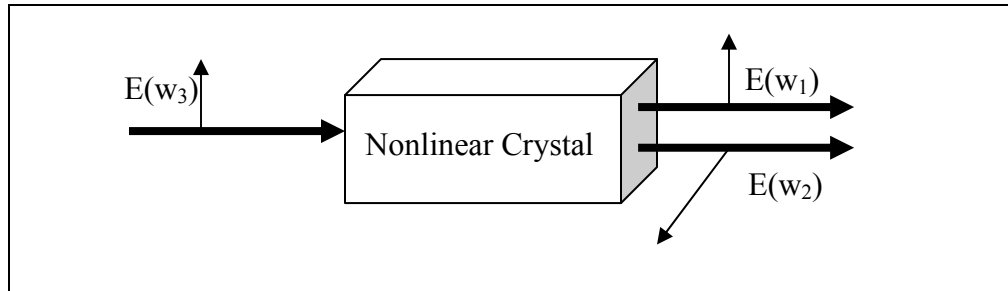


Figure 2.6 Type II phase matching

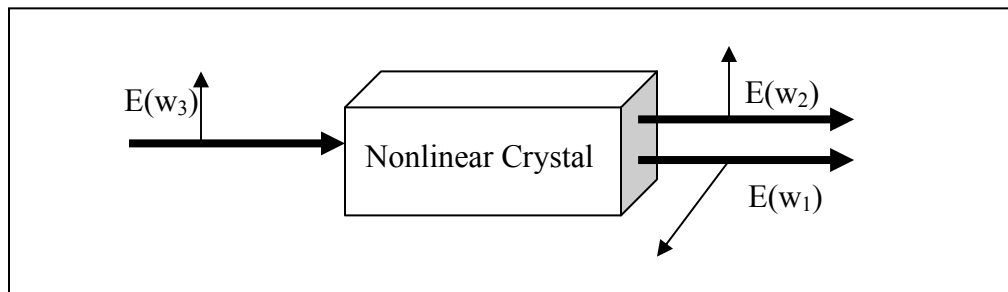


Figure 2.7 Type II phase matching

2.3.1.1 Dielectric waveguide phase-matching

The propagation of light within a dielectric waveguide is more complicated than that through bulk material. The transverse boundary conditions within the solution of Maxwell's equations lead to allowed transverse modes of propagation. These modes have characteristic intensity profiles (which decay to zero outside the guiding layer) and travel with a phase velocity which differs from that of the bulk material. Assuming that the refractive indices of the guiding and cladding layers are n_g and n_c respectively then the effective mode index, N , of the transverse mode can take on a range of values

$$n_c < N < n_g \quad (2.17)$$

Different modes within the guide have different values of N . By appropriate design of the waveguide geometry, the mode index of two or more different modes with different frequencies can be made such that [49]:

$$N_{\text{mode A}}(w_3) - N_{\text{mode B}}(w_2) - N_{\text{mode C}}(w_1) = 0 \quad (2.18)$$

i.e. phase-matching.

2.3.1.2 Birefringent Phase matching

In a uniaxial crystal a special direction exists called the optic axis (typically labeled the Z -axis). The plane containing the Z -axis and the wave vector K of the light wave is termed the principle plane. A light beam whose polarization is normal to the principle plane is called an ordinary ray, or o-ray, while a beam polarized parallel to the principle plane is known as an extraordinary ray, or e-ray. The refractive index of an o-ray does not depend on the propagation direction, while that for the e-ray does. Thus, the refractive index in a nonlinear optical crystal generally depends both on the light polarization and propagation direction. The difference between the refractive indices of the o-ray and the e-ray is known as birefringence, Δn . The Δn is equal to zero along the optic axis Z , and reaches a maximum in the direction normal to this axis. In the plane normal to the Z -axis, the refractive indices of the o-ray and the e-ray are termed the principle values of the refractive index, and are labeled by n_o and n_e , respectively.

The refractive index of the e-ray depends on the polar angle θ between the Z-axis and the vector K. It is determined by the equation [50]

$$\frac{1}{n_e^2(\theta)} = \frac{\cos^2(\theta)}{n_o^2} + \frac{\sin^2(\theta)}{n_e^2} \quad (2.19)$$

Where, the subscript “e” in “ $n_e(\theta)$ ” denotes the change of refractive index for the e-ray and the index $n_e(\theta)$ is thus bounded by n_o and n_e . If the signal and idler are ordinary rays with indices of refraction n_s and n_i respectively then the index of refraction for the pump wave necessary to achieve collinear phase matching is given by [44]:

$$n_3' = \left(\frac{w_s}{w_p} \right) n_s + \left(\frac{w_i}{w_p} \right) n_i \quad (2.20)$$

If the pump is an extraordinary wave then phase matching can be achieved for some angle θ_p if n_3' lies between $n_o(w_p)$ and $n_e(w_p)$. Where the angle θ_{PM} refers to phase matching angle and is given by [44]:

$$\theta_p = \sin^{-1} \left[\left[\frac{n_{op}^2 \cdot n_{ep}^2}{n_{op}^2 - n_{ep}^2} \right] \cdot \left[\frac{1}{\left[n_{es} + \frac{w_i}{w_p} (n_{ei} - n_{es}) \right]^2} - \frac{1}{n_{op}^2} \right] \right]^{\frac{1}{2}} \quad (2.21)$$

It should be noted that phase matching can in practice be achieved only in a limited number of crystals.

In negative uniaxial crystals ($n_e < n_o$), phase matching can in principle be achieved for an extraordinary pump with either one or both of the signal and idler being ordinary rays. The case when the signal and idler are both

ordinary rays is referred to as type I or parallel phase matching; when either is an extraordinary ray it is referred to as type II or orthogonal phase matching. In positive uniaxial crystals the pump beam must be an ordinary ray and either or both of the signal and idler rays giving rise to type II or type I phase matching respectively. It should be noted that type II phase matching requires more birefringence to compensate for dispersion than does type I phase matching.

In biaxial crystals, the refractive index sphere will be a 3-dimensional structure which not only involves the change of θ , but also the angle ϕ . Thus, phase matching in biaxial crystals is much more complicated than that in uniaxial crystals. The principle, however, remains the same only with different polarizations can the three light wave phase matching be obtained in birefringent crystal [51].

The index surface in a biaxial crystal is determined analytically by the two real solutions of the Fresnel's equation to obtain n_{fast} and n_{slow} [50].

$$\frac{S_x^2}{\frac{1}{n^2(\hat{S})} - \frac{1}{n_x^2}} + \frac{S_y^2}{\frac{1}{n^2(\hat{S})} - \frac{1}{n_y^2}} + \frac{S_z^2}{\frac{1}{n^2(\hat{S})} - \frac{1}{n_z^2}} = 0 \quad (2.22)$$

S being the propagation direction of the cosine vector, i.e.

$$\vec{S}_x = \sin \theta \cos \phi, \quad \vec{S}_y = \sin \theta \sin \phi \quad \text{and} \quad \vec{S}_z = \cos \theta \quad (2.23)$$

Equation (2.22) can be written in the following form

$$\begin{aligned}
& x^2 - \left[S_x^2 \left(\frac{1}{n_y^2} + \frac{1}{n_z^2} \right) + S_y^2 \left(\frac{1}{n_x^2} + \frac{1}{n_z^2} \right) + S_z^2 \left(\frac{1}{n_x^2} + \frac{1}{n_y^2} \right) \right] x \\
& + \left[\frac{S_x^2}{n_y^2 n_z^2} + \frac{S_y^2}{n_y^2 n_z^2} + \frac{S_z^2}{n_x^2 n_y^2} \right] = 0
\end{aligned} \tag{2.24}$$

where $x = \frac{1}{n(\hat{S})}$. Solving for x , we obtain one solution for each possible

polarization (fast or slow):

$$n_{fast} = \sqrt{\frac{2}{B + \sqrt{B^2 - 4C}}} \tag{2.25}$$

$$n_{slow} = \sqrt{\frac{2}{B - \sqrt{B^2 - 4C}}}$$

where

$$\begin{aligned}
B &= \left[S_x^2 \left(\frac{1}{n_y^2} + \frac{1}{n_z^2} \right) + S_y^2 \left(\frac{1}{n_x^2} + \frac{1}{n_z^2} \right) + S_z^2 \left(\frac{1}{n_x^2} + \frac{1}{n_y^2} \right) \right] \\
C &= \left[\frac{S_x^2}{n_y^2 n_z^2} + \frac{S_y^2}{n_y^2 n_z^2} + \frac{S_z^2}{n_x^2 n_y^2} \right]
\end{aligned}$$

Refractive index measurements give values as functions of wavelength. Frequently, it is desirable to have a functional form for the dispersion of the refractive index (i.e., for calculations and value interpolation). There are many formulas used for representing the refractive index. One of the most widely used is the Sellmeier (or Drude or Maxwell-Helmholtz-Drude) [52] dispersion model, which arises from treating the absorption like simple

mechanical or electrical resonances. The usual form of this equation for optical applications gives refractive index as a function of wavelength rather than wave number, frequency, or energy. In this form, the Sellmeier's equation is:

$$n^2(\lambda) - 1 = \sum_{i=1} \frac{A_i \cdot \lambda^2}{\lambda^2 - \lambda_i^2} \quad (2.26)$$

Another common formula for the index of refraction is the Herzberger equation, first developed for glasses [53] and later applied to infrared crystalline materials [54].

$$n = A + \frac{B}{(\lambda^2 - 0.028)} + \frac{C}{(\lambda^2 - 0.028)^2} + D\lambda^2 + E\lambda^4 \quad (2.27)$$

Where the choice of the constant (0.028) is arbitrary in that it is applied to all materials.

To get an idea of the wide variety of Sellmeier equations, some Sellmeier equations are given in the Appendix B.

2.3.1.2.1 Walk off

For any phase matching other than in the crystal's x,y plane, the interacting waves will physically separate from each other, since they have orthogonal polarizations. This separation is called "walk-off". The propagation direction of the energy of a wave in a crystal is given by the Poynting vector (\vec{S}). The direction of the Poynting vector is the normal to the tangent of the wave vector (\vec{k}) and the curve of the refractive index (see figure 2.8).

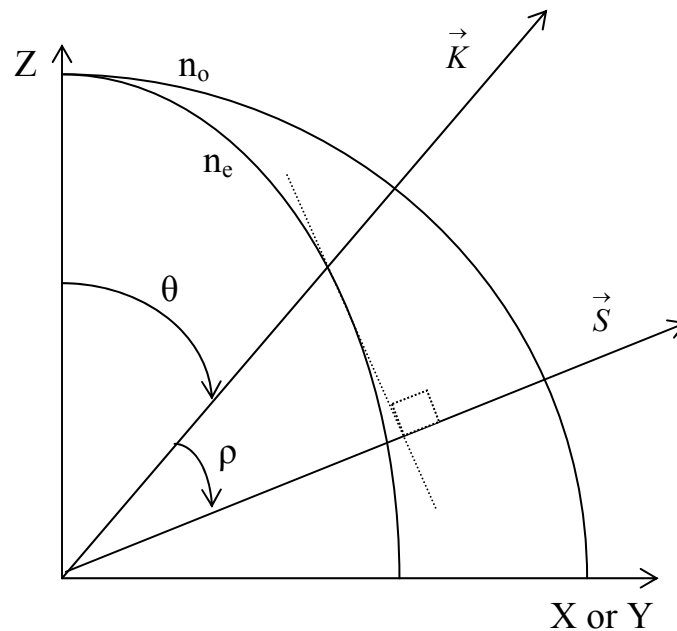


Figure 2.7 The walk-off angle ρ between the wave vector \vec{k} and the Poynting vector \vec{S} in a negative uniaxial crystal [45].

For the ordinary wave the curve of the index of refraction $n_o(\theta)$ is a circle, and the direction of the Poynting vector (\vec{S}) is equal to the direction of the wave vector (\vec{K}) . For the extraordinary wave, on the other hand, the curve of the index of refraction $n_e(\theta)$ is an ellipsoide. Here the wave vector and the Poynting vector do not overlap. The walk-off angle (ρ) is defined as the angle between the wave vector of the generated wave(s) and the Poynting vector (\vec{S}) (the direction of the energy propagation).

From figure 2.8 it is seen that when $\theta = 0^\circ$ or $\theta = 90^\circ$, the walk-off angle (ρ) is zero. However, phase matching cannot take place along the optical axis of the crystal ($\theta = 0^\circ$), since then $n_o = n_e$. It is possible to phase match at $\theta = 90^\circ$, this is known as noncritical phase matching. Obviously, in this case the angle cannot be tuned, so phase matching is achieved by changing the temperature of the crystal, which changes the refractive index n_e .

When the walk-off is too large, the interacting waves will not overlap spatially in the entire crystal, and the conversion process will be terminated. When walk-off is present, but a longer nonlinear interaction length is desired, two separate crystals can be used instead of one longer crystal. The second crystal has to be oriented such that the optical axis is at an angle of 180° with respect to the optical axis of the first crystal. Hence, the walk-off in the first crystal is compensated in the second crystal.

2.3.1.3 Quasi Phase-Matching

Until recent years birefringent phase matching has been by far the most common form of phase matching in both commercial and laboratory laser systems. However, birefringent phase matching imposes a number of limitations

- Only works for birefringent materials.
- Only works for certain geometries.
- May require angle tuning to a critical phase-matching condition and associated walk off.

Another technique has been developed, quasi phase matching. In quasi phase matching the crystal is effectively divided into sections L_c long as illustrated in figure 2.9. By turning each successive section upside down the phase relation between the pump and the generated light can be maintained [3].

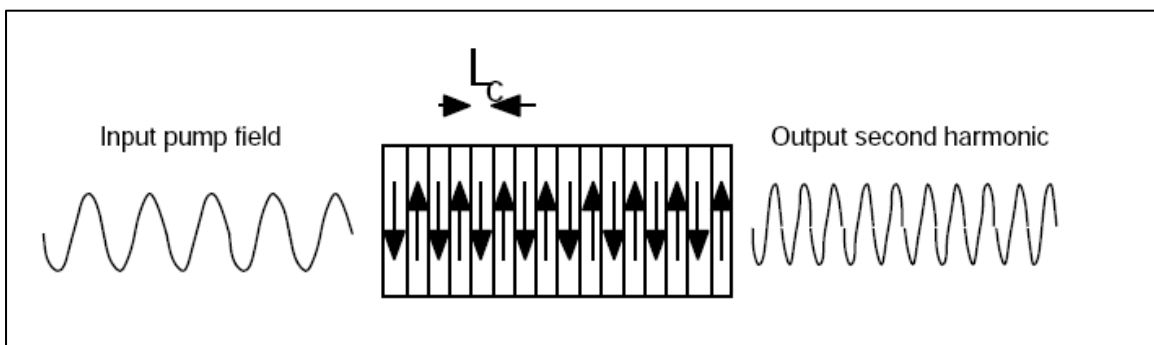


Figure 2.9 Quasi phase-Matching Technique [49].

Quasi phase matching can give high efficiency over a long length of crystal

Quasi phase matching (QPM) can also be applied to OPO's and other nonlinear interactions.

Rather than physically cut the crystal into short sections it is usual to process bulk crystals to orient the crystal structure. This orientation is frequently performed using an electrode pattern on the crystal and applying an electric field at elevated temperatures. After cooling the crystal is "poled" and no further fields are required.

Such crystals are said to be "periodically poled". Amongst others Lithium niobate and KTP have both been widely used (PPLN, PPKTP).

2.3.1.4 Non-collinear Phase-Matching

When $|K_s| + |K_i| > |K_p|$ it is possible to find some angle between the signal and idler K -vectors for which vector momentum conservation and hence phase-matching is achieved. When using beams of finite cross-sectional area this type of phase-matching has the disadvantage that the interaction volume is decreased compared to the case of collinear interactions.

Figure 2.10 shows the relative orientation of the wave vectors with respect to the crystal axis, C . The phase-matching angle θ_p between K_p and C can be varied by rotating the crystal. In non-collinear geometry, there are two distinct propagation geometries of the parametric waves about the direction of the pump. In the first case $\theta_s < \theta_i$, i.e. the signal wave is propagating at a closer angle to the C axes than the idler (figure 2.10a), in the second case $\theta_s > \theta_i$ and the situation is reversed (figure 2.10b). Figure 2.10 shows also the direction of energy propagation (Poynting vector) for each of the three waves.

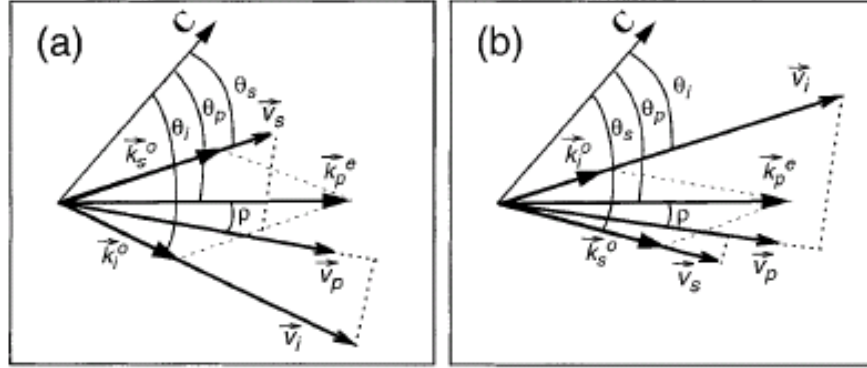


Figure 2.10. Orientation with respect to the crystal axis of wave vectors and energy propagation vectors for pump, signal, and idler [28].

The propagation angle θ_s is related to angle θ_p and indices of refraction for ordinary and extraordinary waves, according to [28]:

$$\theta_s = \theta_p \pm a \cos \frac{n_{op}^2 n_{ep}^2 (1 + \beta)^2 + (n_{os}^2 - \beta^2 n_{oi}^2) [n_{ep}^2 + (n_{op}^2 - n_{ep}^2) (\sin \theta_p)^2]}{2(1 + \beta) n_{os} n_{op} n_{ep} \sqrt{n_{ep}^2 + (n_{op}^2 - n_{ep}^2) (\sin \theta_p)^2}} \quad (2.28)$$

where $\beta = \lambda_s / \lambda_i$ is the ratio between the wavelengths of the signal and the idler waves inside the crystal. Minus (plus) sign in front of $a \cos$ corresponds to the beam geometry addressed in figure 2.10a, b. In a similar manner, the propagation angle of the idler wave θ_i is found to be [28]:

$$\theta_i = \theta_p \pm a \cos \frac{n_{op}^2 n_{ep}^2 (1 + \beta)^2 + (n_{os}^2 - \beta^2 n_{oi}^2) [n_{ep}^2 + (n_{op}^2 - n_{ep}^2) (\sin \theta_p)^2]}{2\beta(1 + \beta) n_{oi} n_{op} n_{ep} \sqrt{n_{ep}^2 + (n_{op}^2 - n_{ep}^2) (\sin \theta_p)^2}} \quad (2.29)$$

It is also clear from figure (2.10) that the three wave vectors must lie in a plane so that:

$$\phi_{Idler} = \phi_{Signal} + \pi \quad (2.30)$$

2.4 OPO Cavity Configurations

Tunability is a fundamental characteristic of all parametric devices. With the pump providing input at the fixed wavelength λ_p , small changes of the refractive index around the phase-matching condition will change the signal and idler wavelengths such that a new phase-matching condition is achieved. Tuning is possible by making use of the angular dependence of the birefringence of anisotropic crystals.

Figure 2.11 illustrates different configurations that make use of the parametric interaction process of three waves. The simplest device is a nonresonant configuration, namely an optical parametric amplifier (OPA) exhibited in figure 2.11(a). In this case, a pump beam and a signal beam are present at the input. If the output of a Q -switched laser is focused into the crystal and if the intensity of the pump is sufficiently high and phase-matching conditions are met, gain is obtained for the signal wave and at the same time an idler wave is generated. Typically, an OPA is used if the signal obtained from an optical parametric oscillator (OPO) is too weak and further amplification is desired.

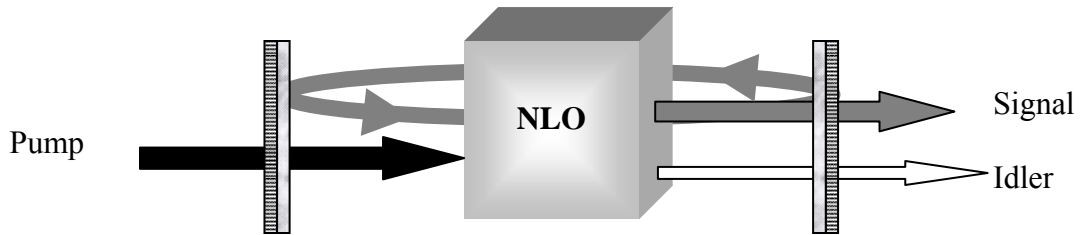
The most common optical parametric device is the singly resonant oscillator depicted in Figs. 2.11(b) and (c). In this device, the crystal is located inside a resonator that provides feedback at either the signal or idler frequency. In the example illustrated, the pump beam enters through a mirror that is highly transmitting at the pump wavelength and highly reflective for the signal wavelength. In figure 2.11(b) the opposite mirror, which is the output coupler, has typically 80–95% reflectivity for the signal wavelength, and

high transmission for the idler and pump beam. Only the signal wavelength is resonant in the cavity, and a small fraction is coupled out through the front mirror. In the configuration in figure 2.11(c) the pump beam is reflected at the output mirror and makes one return pass through the crystal. Since the input mirror through which the pump enters is highly transmissive for this wavelength, no resonance condition is set up for the pump wavelength. However, threshold is lowered, because on the return path the pump beam provides gain for the resonant signal wave.

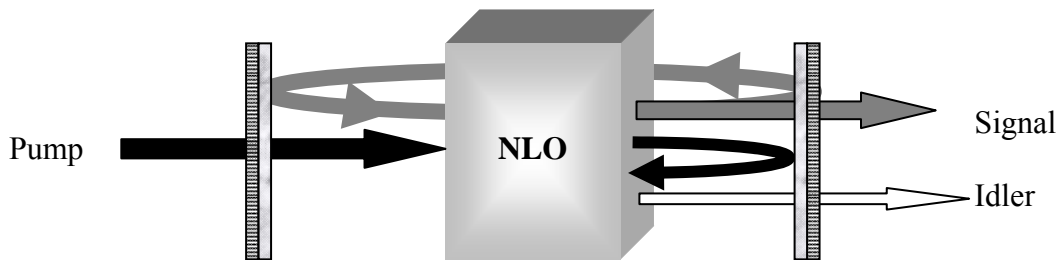
Figure 2.11(d) depicts a doubly resonant oscillator (DRO), which provides feedback at both the signal and idler wavelengths. The double-resonance condition, in which both the signal and the idler waves are simultaneously resonant within the optical cavity, lowers the threshold significantly. However, this advantage of a DRO is off-set by a reduction in stability and tunability. Maintaining the doubly resonant condition in a common resonator requires that the pump be single frequency and stable, and that the OPO cavity length be actively controlled to maintain the resonance condition. The considerably lower threshold of a DRO makes it possible to obtain parametric gain at the low-power densities achievable under CW conditions.



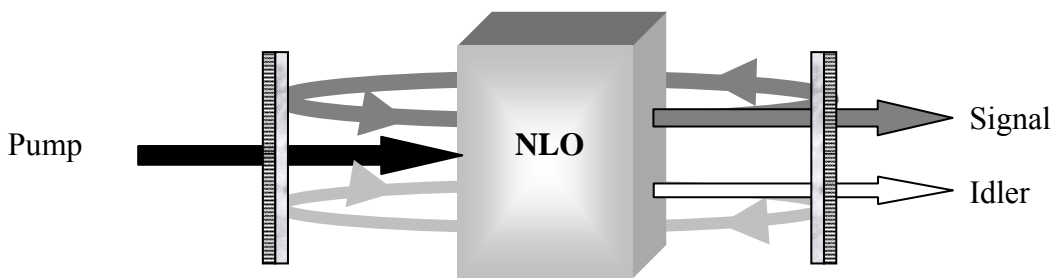
(a) Optical parametric amplifier.



(b) Singly resonant OPO.



(c) Singly resonant with pump beam reflected.



(d) Doubly resonant OPO.

Figure 2.11 Configurations of parametric interactions [55].

2.5 The Effects of Focusing on Parametric Oscillation

The Gaussian beam contracts to a minimum diameter $2w_0$ at the beam waist where the phase front is planar, if one measures z from this waist. The spot size $w(z)$ at the distance z from the beam waist is given by [55]:

$$w(z) = w_0 \left[1 + \left(\frac{\lambda z}{\pi w_0^2} \right)^2 \right]^{0.5} \quad (2.31)$$

where w_0 is the minimum radius at the beam waist. The full divergence angle for the fundamental mode is given by [55];

$$\theta_{div} = \left(\frac{2\lambda}{\pi w_0} \right) = 1.27 \left(\frac{\lambda}{2w_0} \right) \quad (2.32)$$

If $R(z)$ is the radius of curvature of the wavefront that intersects the axis at z then:

$$R(z) = z \left(1 + \left(\frac{\pi w_0^2}{\lambda z} \right)^2 \right) \quad (2.33)$$

Thus, the optimum focusing can be shown to be when the beams are focused to the centre of the crystal such that $\sqrt{2} \times \text{beam dia. crystal centre} = \text{beam dia. crystal edge}$. This is called confocal focusing as shown in figure 2.12.

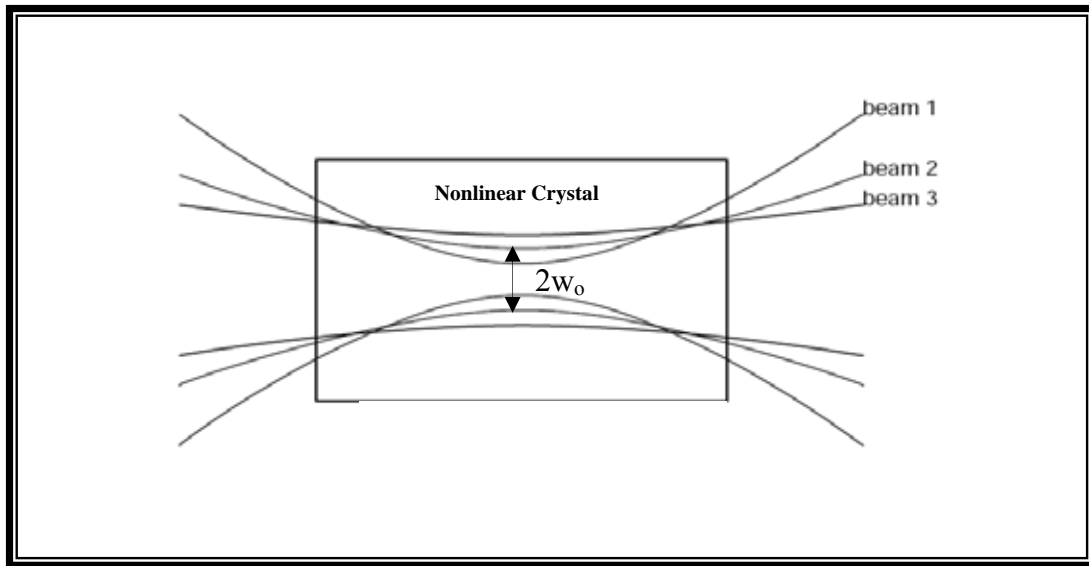


Figure 2.12 Optimum focusing for nonlinear interaction [49].

- Beam 3 is not tightly focused; the resulting power density is reduced leading to low nonlinear conversion.
- Beam 2 is correctly focused giving a reasonable power density over the entire length of the crystal.
- Beam 1 is very tightly focused giving a high power density at the centre of the crystal. However, the divergence of the beam means that the power density at the edges of the crystal is reduced.

As a general rule, tight focusing of the interacting beams results in higher power density and consequently higher nonlinear efficiency. However, two factors may limit the degree of focusing

- High power densities may damage the nonlinear material.
- The divergence of a tightly focused beam limits the length of crystal over which the high power density can be maintained.

3. The Characteristics of Non-collinear Phase-matching in Uniaxial and Biaxial Crystals

3.1 Introduction

A non-collinear phase matching method is presented here for calculating the characteristics of both uniaxial and biaxial crystals.

In this work, silver Gallium Sulfide (AgGaS_2 or AGS) which is an example of a negative uniaxial crystal with high nonlinear optical coefficient and high optical transmission from 0.5-12 μm makes it realistic to generate infrared parametric radiation (3-5 μm) region. Its most characteristic is that it is one of the few crystals which can be pumped by commercially available 1.064 μm Nd:YAG laser to achieve phase-matched down-conversion into the $\lambda > 5\mu\text{m}$ region [56].

A recent attention has been focused on the utilization of nonlinear potassium titanyl phosphate (KTP) which is an example of a positive biaxial crystal for optical parametric oscillator (OPO) technique. The KTP crystal features suitable tuning parameters in infrared and visible wavelength range 0.3-4.5 μm has found extensive applications as an eye-safe radiation source. The expressions for calculation of phase-matching characteristics for type II noncritically phase-matched are carried out.

3.2 Tuning of Nonlinear Crystal

The propagation of the laser beam through the nonlinear crystal and the generation of new wavelengths are affected by the refractive index. Thus the refractive indices for the ordinary and extraordinary rays in uniaxial crystals need to be determined. The fast and slow rays in biaxial crystals also depend on the wavelength and the direction of the propagation.

Calculations of the wave vector of the pump, signal and idler rays depend on the type of phase matching, and hence the phase matching condition need to be fulfilled. The calculation of the three-wave down-conversion interaction requires the use of conservation of energy and conservation of momentum commonly referred to as phase matching. The flow chart of the calculation of the refractive indices and wave vectors of the three waves was shown in (Appendix D).

3.2.1 Calculation of Refractive Index for Uniaxial Crystal

The procedure for calculating the refractive index for uniaxial crystal can be summarized as follows:

- a. The principal indices of refraction of any crystal for ordinary and extraordinary waves n_o and n_e respectively can be chosen from Sellmeier type index dispersion that depends on the wavelength [52].
- b. The polar angle θ_p of the pump beam propagates through the crystal with respect to its optical axis that has been chosen. The propagation direction in uniaxial crystal does not depend on the azimuthal angle ϕ_p as expressed in equation (2.19), which could simplified to the following form:

$$n_e(\theta) = \frac{n_o n_e}{(n_e^2 \cos^2 \theta + n_o^2 \sin^2 \theta)^{1/2}} \quad (3.1)$$

The refractive index of an ordinary wave does not depend on the polar angle, but the refractive index of an extraordinary wave does.

- c. The refractive index of the pump wave and those for the generated signal and idler waves has been calculated, taking into account the type of phase matching.

In uniaxial crystal, the ordinary wave travels slower than the extraordinary (see Appendix C). The phase matching achieved with the refractive indices of the pump, signal and idler waves as follows:

For Type I:

$$\begin{aligned} n_p(\lambda_p, \theta_p) &= n_e(\lambda_p, \theta_p) \\ n_s(\lambda_s, \theta_s) &= n_o(\lambda_s) \\ n_i(\lambda_i, \theta_i) &= n_o(\lambda_i) \end{aligned} \quad (3.2)$$

For Type II:

$$\begin{aligned} n_p(\lambda_p, \theta_p) &= n_e(\lambda_p, \theta_p) \\ n_s(\lambda_s, \theta_s) &= n_o(\lambda_s) \\ n_i(\lambda_i, \theta_i) &= n_e(\lambda_i, \theta_i) \end{aligned} \quad (3.3)$$

For type III:

$$\begin{aligned} n_p(\lambda_p, \theta_p) &= n_e(\lambda_p, \theta_p) \\ n_s(\lambda_s, \theta_s) &= n_e(\lambda_s, \theta_s) \\ n_i(\lambda_i, \theta_i) &= n_o(\lambda_i) \end{aligned} \quad (3.4)$$

3.2.2 Calculation of Refractive Index for Biaxial Crystal

The following steps describe briefly the procedure for calculating the refractive indices for biaxial crystal:

- a. The principal indices of refraction n_x , n_y and n_z of the crystal can be chosen from Sellmeier type index dispersion that depends on the wavelength.
- b. The polar angle θ_p and the azimuthal angle ϕ_p of the pump beam propagating through the crystal have been chosen such that the principal axis of the crystal is taken as the reference.

To find the indices of refraction n_{fast} and n_{slow} in a given direction, equation (2.25) may be used:

$$\begin{aligned} n_{fast}(\lambda, \theta, \phi) &= \left(\frac{2}{B + \sqrt{B^2 - 4C}} \right)^{1/2} \\ n_{slow}(\lambda, \theta, \phi) &= \left(\frac{2}{B - \sqrt{B^2 - 4C}} \right)^{1/2} \end{aligned} \quad (3.5)$$

The refractive indices of the fast and slow rays in bi-directional crystals depend on the polar and azimuthal angles of propagation.

- c. The refractive index of the pump wave and those for the generated signal and idler waves has been calculated, taking into account the type of phase matching.

For biaxial crystal, the phase matching achieved with the refractive indices of the pump, signal and idler waves as follows:

For type I:

$$\begin{aligned}
 n_p(\lambda_p, \theta_p, \phi_p) &= n_{fast}(\lambda_p, \theta_p, \phi_p) \\
 n_s(\lambda_s, \theta_s, \phi_s) &= n_{slow}(\lambda_s, \theta_s, \phi_s) \\
 n_i(\lambda_i, \theta_i, \phi_i) &= n_{slow}(\lambda_i, \theta_i, \phi_i)
 \end{aligned} \tag{3.6}$$

For type II:

$$\begin{aligned}
 n_p(\lambda_p, \theta_p, \phi_p) &= n_{fast}(\lambda_p, \theta_p, \phi_p) \\
 n_s(\lambda_s, \theta_s, \phi_s) &= n_{fast}(\lambda_s, \theta_s, \phi_s) \\
 n_i(\lambda_i, \theta_i, \phi_i) &= n_{slow}(\lambda_i, \theta_i, \phi_i)
 \end{aligned} \tag{3.7}$$

For type III:

$$\begin{aligned}
 n_p(\lambda_p, \theta_p, \phi_p) &= n_{fast}(\lambda_p, \theta_p, \phi_p) \\
 n_s(\lambda_s, \theta_s, \phi_s) &= n_{slow}(\lambda_s, \theta_s, \phi_s) \\
 n_i(\lambda_i, \theta_i, \phi_i) &= n_{fast}(\lambda_i, \theta_i, \phi_i)
 \end{aligned} \tag{3.8}$$

3.3 Tracing Behaviors of the phase-matching angle in non-collinear phase matched optical parametric oscillators

Under certain phase-matching conditions, a pair of signal and idler can be phase matched simultaneously, and hence two output wavelengths can be obtained from an optical parametric oscillator (OPO) if the signal wave oscillates in the cavity. This phenomenon is called tracing behavior of the phase matching angle, which means that the phase-matched signal wavelength is a monotonically increasing or decreasing function of crystal orientation angle.

In the present work, we propose that in non-collinear phase-matching configurations it is possible to realize tracing phenomenon with the pump beam wavelengths falling in the wavelength ranges of available high-power laser systems. In particular, our calculations with the aid of equation (2.21) predicted the tuning curve in type I phase-matched AgGaS₂ OPO with pump wavelength at 1.064μm in non-collinear phase-matching configurations

as shown in figure.3.1. The solid line in figure.3.1 is simulated based on the Sellmeier's equation [57], which gives the best agreement with experimental data. Also, we found that, near certain phase-matching angles, phase matching could be simultaneously achieved over quite broad spectral widths as shown in figure.3.2. Meanwhile, near the turning point of the phase - matching curve, we implemented an OPO with broad signal and idler spectral widths (3-5 μm) in the signal and (1.35-1.64 μm) in the idler. With certain simple tuning mechanisms, such a coherent light source of broad spectral width should find many applications in spectroscopic measurements and others.

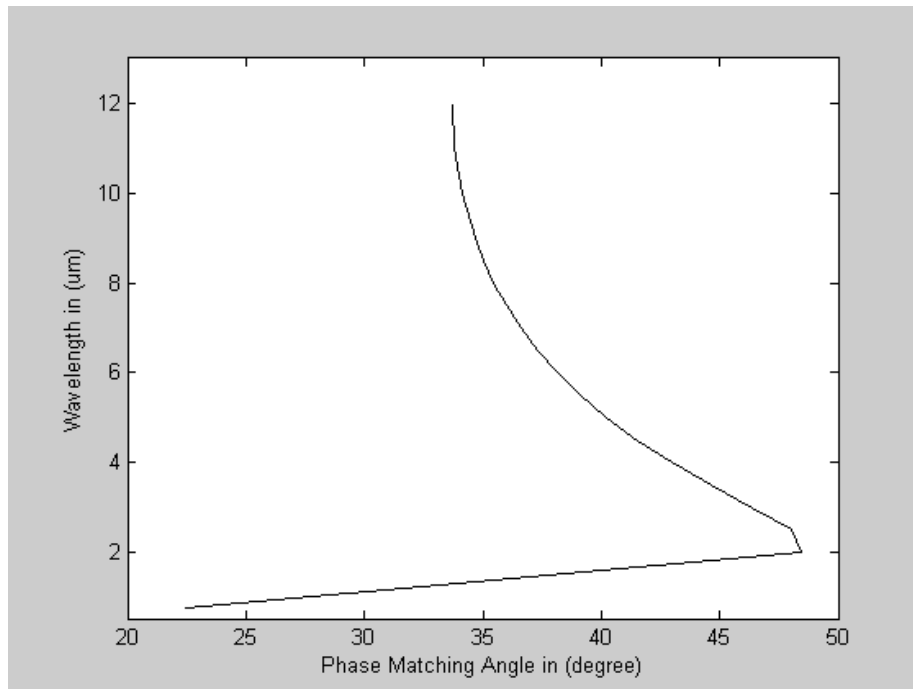


Figure.3.1 Tuning curve of AgGaS₂ at type I phase matching.

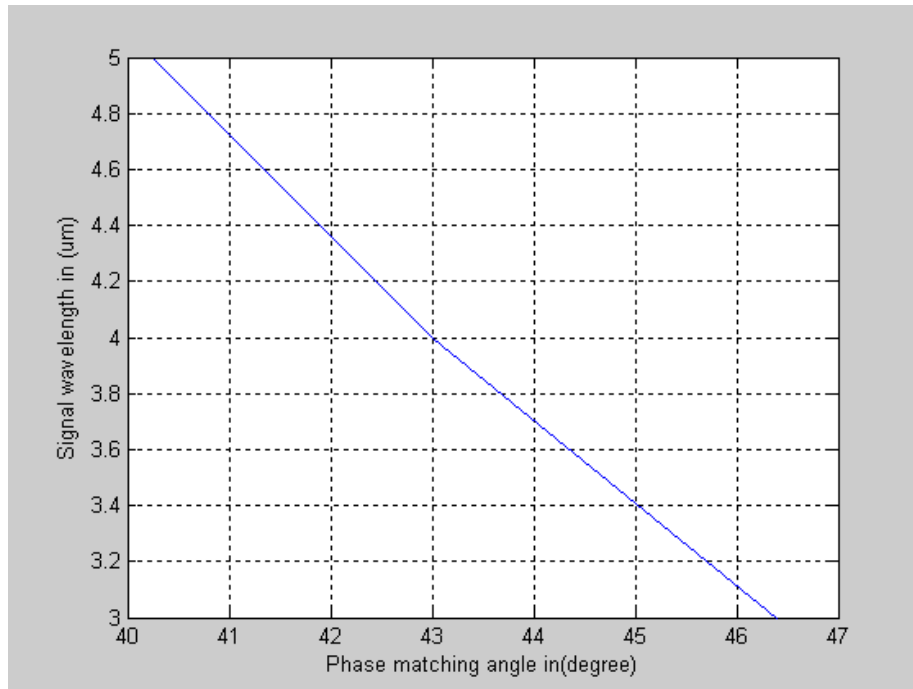


Figure.3.2 Signal wavelengths versus phase matching angle of AgGaS₂ at type I phase matching

3.4 The direction of the generated waves in uniaxial crystal

The AgGaS₂ crystal is an example of a negative uniaxial crystal. The transmission range in such crystal lies between 0.53μm and 12 μm. For different phase matching angles θ_p the maximum conversion efficiency of the crystal and the momentum phase mismatching (ΔK) for type I phase matching have been calculated. The crystal pumped by ns ($\lambda_p=1.064\mu\text{m}$) Nd:YAG laser. The transmission of this crystal make it realistic to generate the signal wavelength in the range of atmospheric transparency (3-5μm), thus the idler wavelength will be in the range of (1.35-1.64μm) as shown in figures 3.3 – 3.6.

Figures 3.3 and 3.4 show the variation of the momentum phase mismatching (ΔK) in the band of the signal wavelength (3-5μm) with the signal polar angle θ_s at different values of phase matching angles θ_p for type I phase

matching. It can be seen that as θ_p increased the value of (ΔK) increased in a manner that will decrease the conversion efficiency of the crystal. At $\theta_p = 46.4^\circ$ there is no phase matching between the pump, signal and idler waves because the condition of phase matching cannot be satisfied.

Figures 3.5 and 3.6 show the variation of the maximum conversion efficiency of the AgGaS₂ crystal at type I phase matching with respect to the momentum phase mismatch (ΔK) at different phase matching angles θ_p .

As can be seen from figure.3.5, when the phase matching angle $\theta_p = 40.25^\circ$ the conversion efficiency of the 3 μm wavelength is higher than that of the 4 μm and 5 μm wavelengths respectively. As θ_p increased (i.e. $\theta_p = 43^\circ$) the conversion efficiency decreased over the whole range (3-5 μm) and the higher conversion efficiency is obtained at $\lambda_s = 5\mu\text{m}$ as shown in figure.3.6.

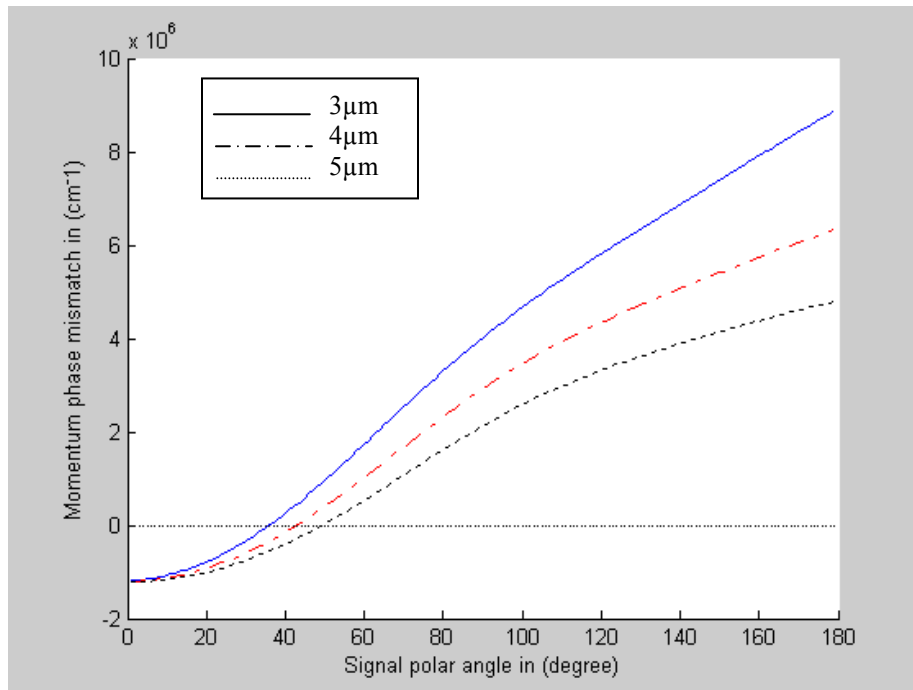


Figure.3.3 Momentum phase mismatch of AgGaS₂ versus signal polar angle for type I phase matching at $\theta_p = 40.25^\circ$

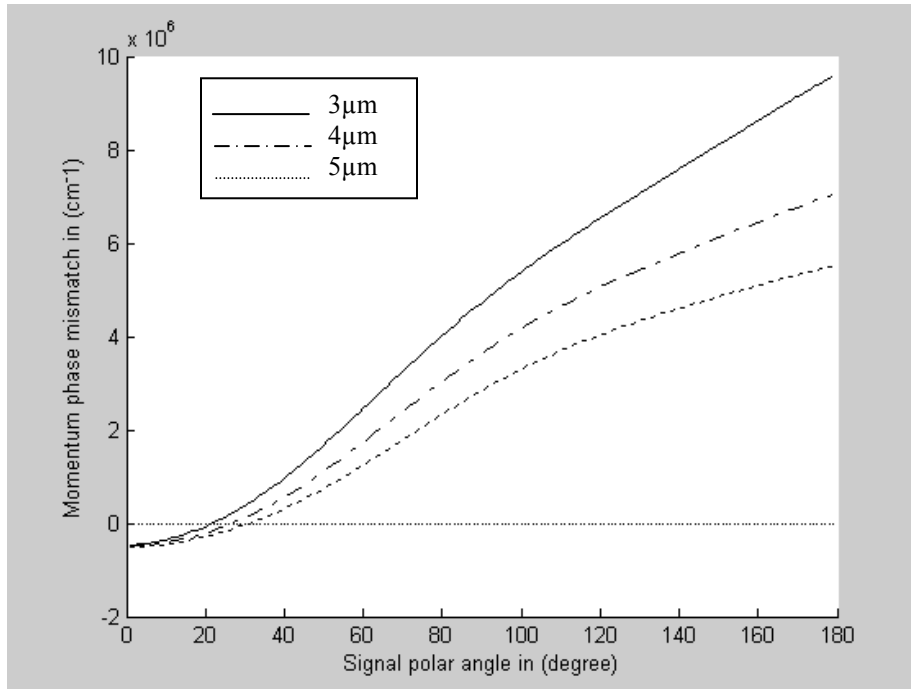


Figure.3.4 Momentum phase mismatch of AgGaS₂ versus signal polar angle for type I phase matching at $\theta_p=43^\circ$

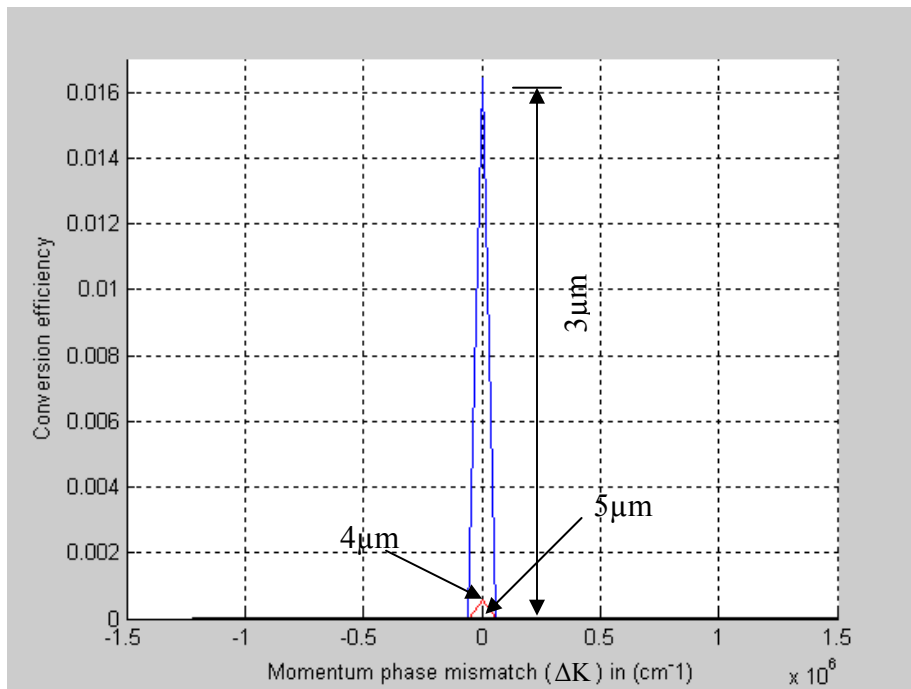


Figure.3.5 Conversion efficiency of AgGaS₂ versus Momentum phase mismatch for type I phase matching at $\theta_p=40.25^\circ$

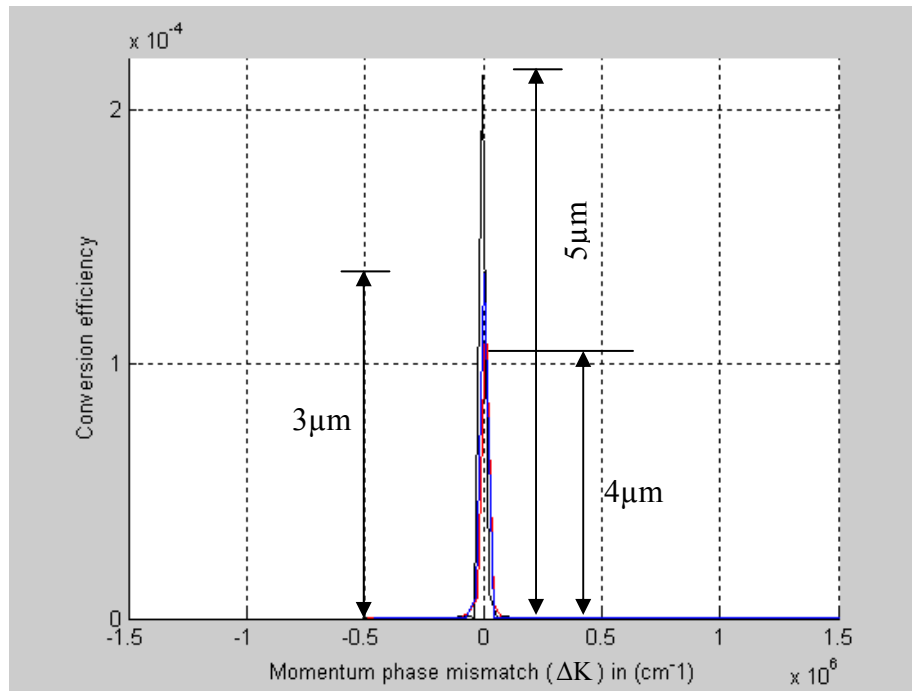


Figure.3.6 Conversion efficiency of AgGaS₂ versus Momentum phase mismatch for type I phase matching at $\theta_p=43^\circ$

For non-collinear phase matching, however, there is no one-to-one correspondence between θ_p and generated wavelengths. For each phase-matching angle θ_p there is a possible signal and idler wavelengths, generated at different angles θ_s and θ_i . For any particular value of θ_p , it is possible to generate the whole parametric spectrum, covering the entire interval between 3 and 5 μm . In this case, different wavelengths are produced at a variety of different angles θ_s and θ_i , centered on the pump beam direction, giving rise to characteristic cone-shaped beams.

Figures 3.7-3.10 show the signal polar angle θ_s , idler polar angle θ_i , signal azimuthal angle ϕ_s and idler azimuthal angle ϕ_i as a function of phase matching angle θ_p for type I phase matching. The signal polar angle θ_s

decreases with increasing the phase matching angle θ_p while the idler polar angle θ_i increased linearly and the value of θ_s is always higher than that of θ_i which means that the propagation of the idler wave is very close to the optic axis of the crystal as shown in figures 3.7 and 3.8 respectively.

The signal azimuthal angle φ_s increased in the $-x,y$ plane as θ_p increased while the idler azimuthal angle φ_i increased in the x,y plane, thus the separation between them is constant and equal to π as shown in figures 3.9 and 3.10.

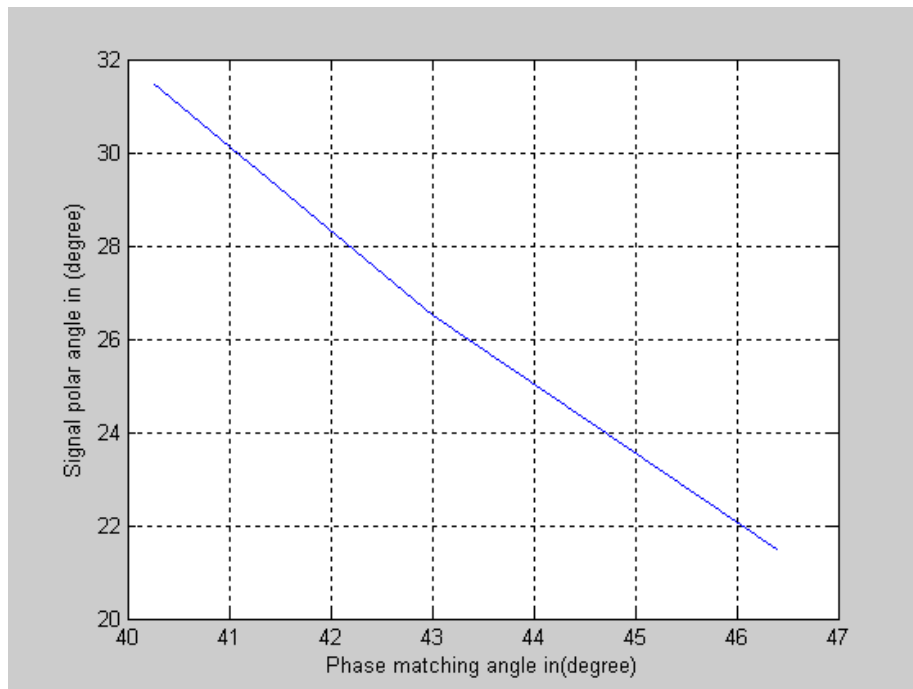


Figure.3.7 Signal polar angle of AgGaS₂ versus phase matching angle for type I phase matching

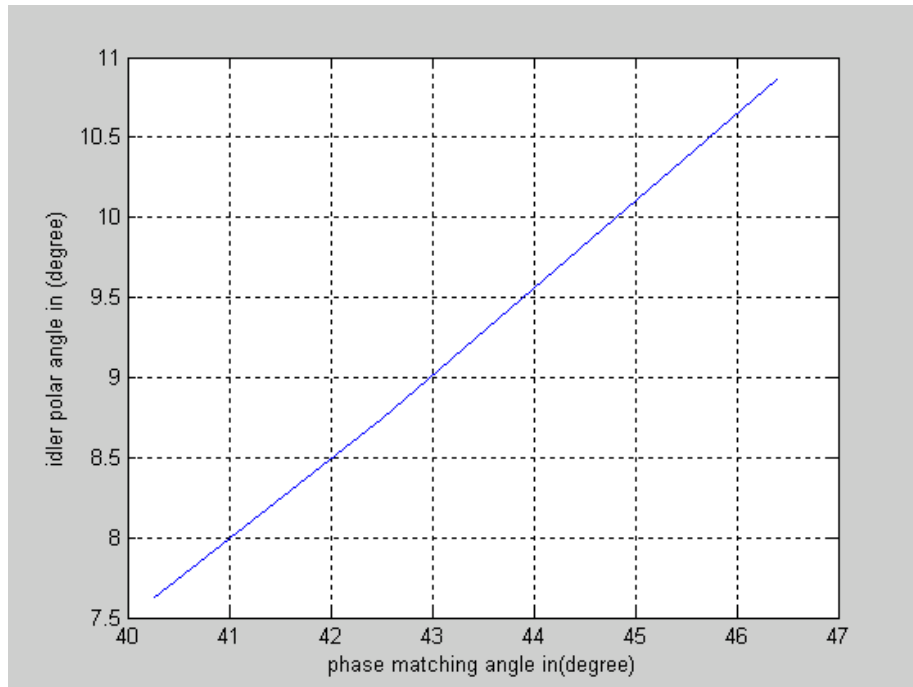


Figure.3.8 Idler polar angle of AgGaS₂ versus phase matching angle for type I phase matching

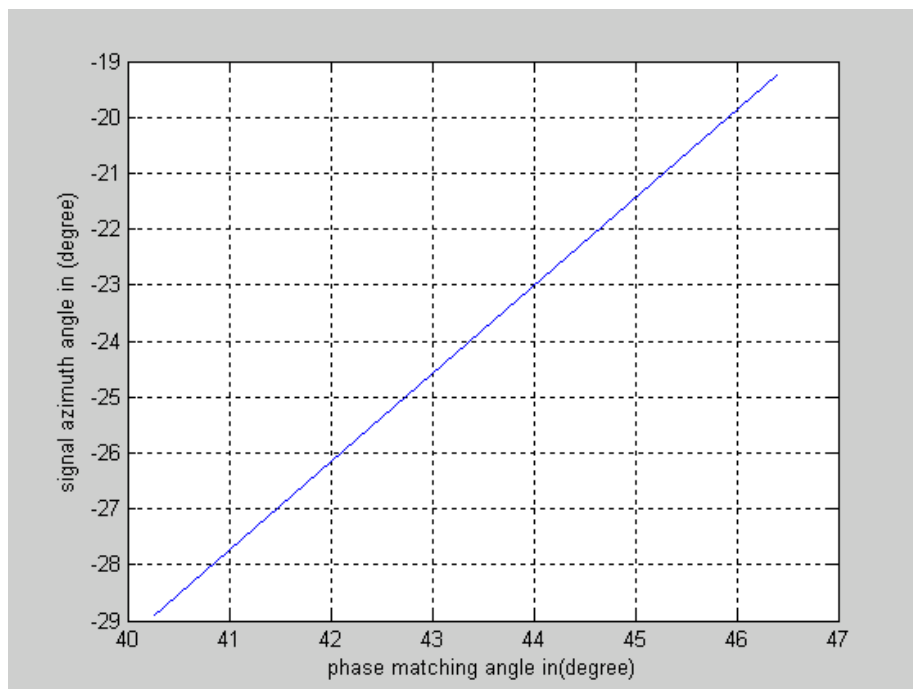


Figure.3.9 Signal azimuth angle of AgGaS₂ versus phase matching angle for type I phase matching

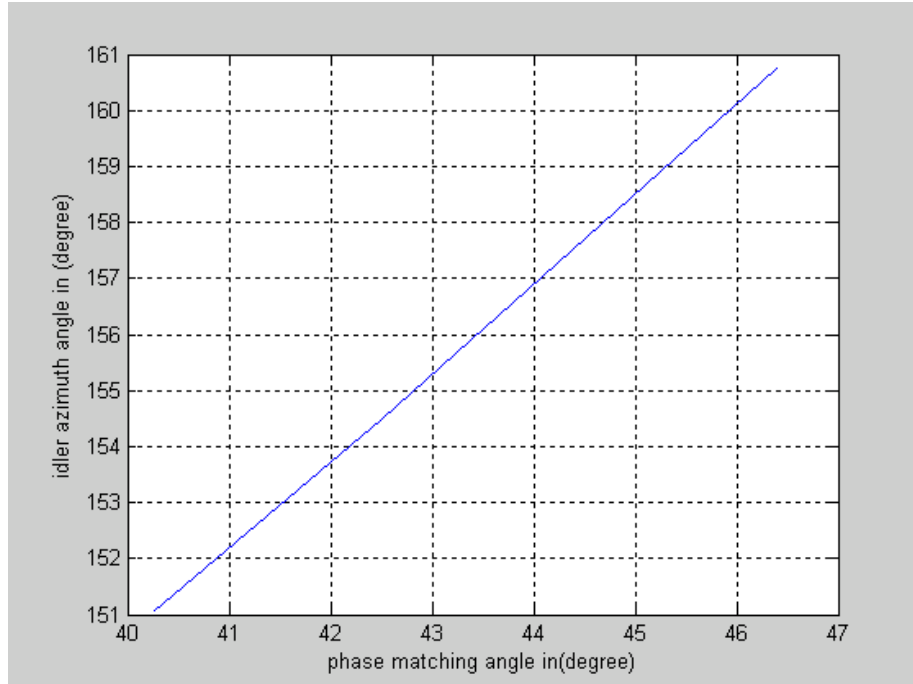


Figure.3.10 Idler azimuth angle of AgGaS₂ versus phase matching angle for type I phase matching

At the phase matching angle $\theta_p=40.25^\circ$ the signal polar angle θ_s increased linearly as λ_s increased while the signal azimuthal angle ϕ_s exhibits negative gradient in $-x,y$ plane. The idler polar angle θ_i and the idler azimuthal angle ϕ_i increased linearly as λ_i increased in the band of (1.35-1.64 μm) and the separation between the signal and idler azimuthal angles is constant and equal to π as shown in figures 3.11-3.14.

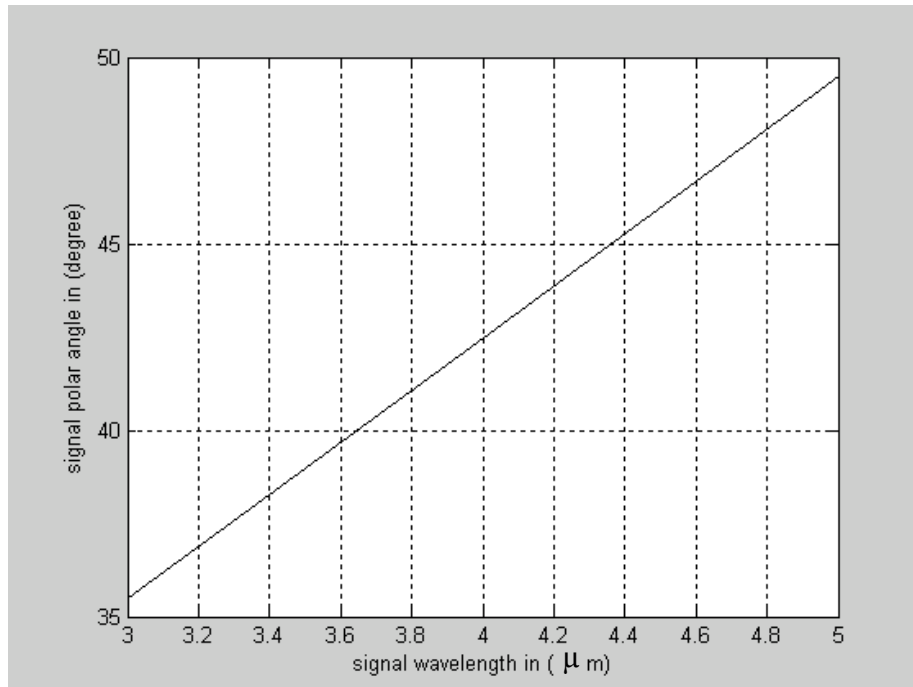


Figure.3.11 Signal polar angle of AgGaS_2 versus Signal wavelength within the range $(3-5)\mu\text{m}$ for type I phase matching at $\theta_p=40.25^\circ$

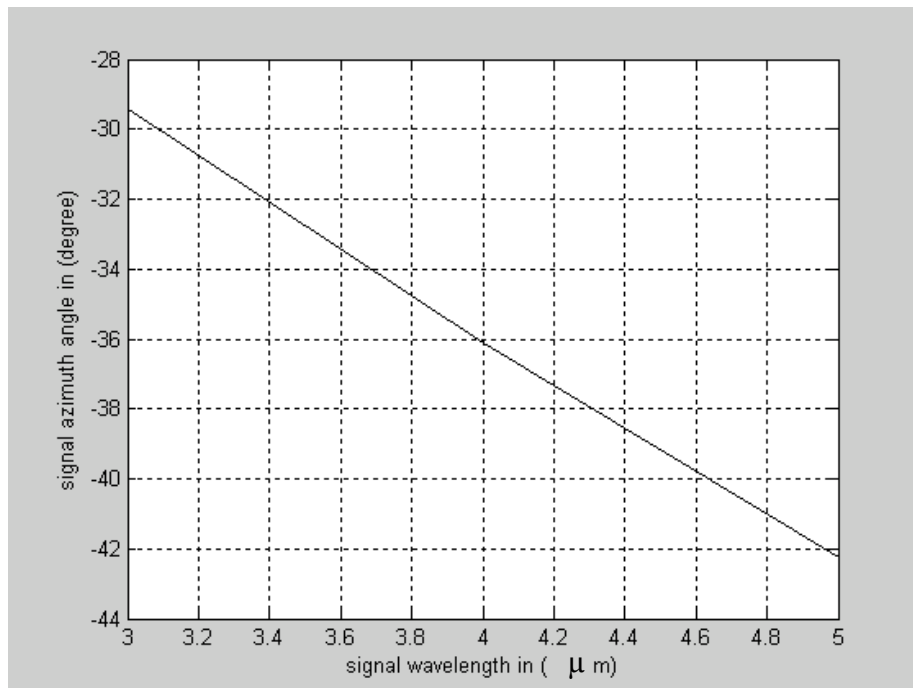


Figure.3.12 Signal azimuth angle of AgGaS_2 versus Signal wavelength within the range $(3-5)\mu\text{m}$ for type I phase matching at $\theta_p=40.25^\circ$

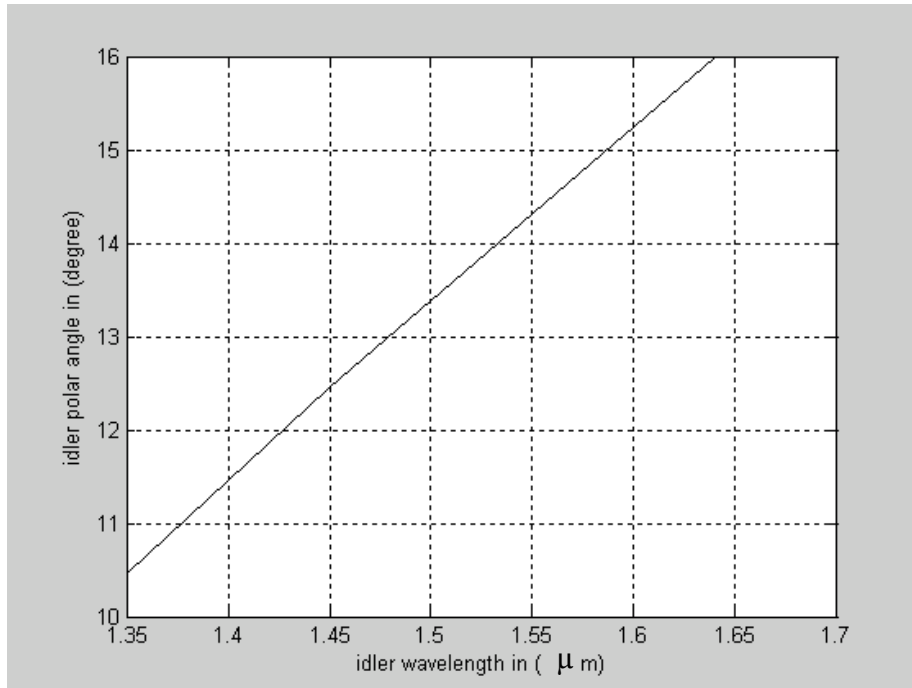


Figure.3.13 Idler polar angle of AgGaS_2 versus idler wavelength within the range $(1.35\text{-}1.64)\mu\text{m}$ for type I phase matching at $\theta_p=40.25^\circ$

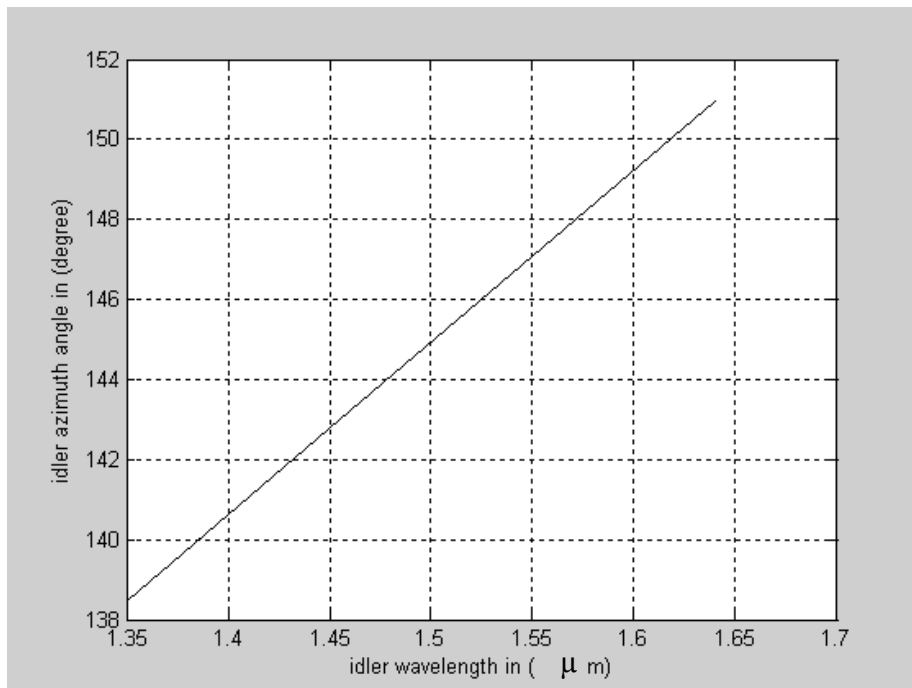


Figure.3.14 Idler azimuth angle of AgGaS_2 versus idler wavelength within the range $(1.35\text{-}1.64)\mu\text{m}$ for type I phase matching at $\theta_p=40.25^\circ$

Over the range of the signal wavelengths under consideration (3-5 μm), phase matching may occur as the phase matching angle θ_p increased. Figures 3.15-3.18, show the influence of the signal polar angle θ_s , signal azimuthal angle φ_s , idler polar angle θ_i and idler azimuthal angle φ_i of AgGaS₂ for type I phase matching at $\theta_p=43^\circ$. As λ_s increased from 3 to 5 μm the signal polar angle θ_s increased and the signal azimuthal angle φ_s decreased linearly in $-x,y$ plane. The idler polar angle θ_i increased linearly in the band of the idler wavelengths (1.35-1.64 μm) but its value is less than θ_s which means that the propagation of idler wave is very close to the optic axis of the crystal. The idler azimuthal angle φ_i increased as λ_i increased and the separation between φ_s and φ_i is constant and equal to π .

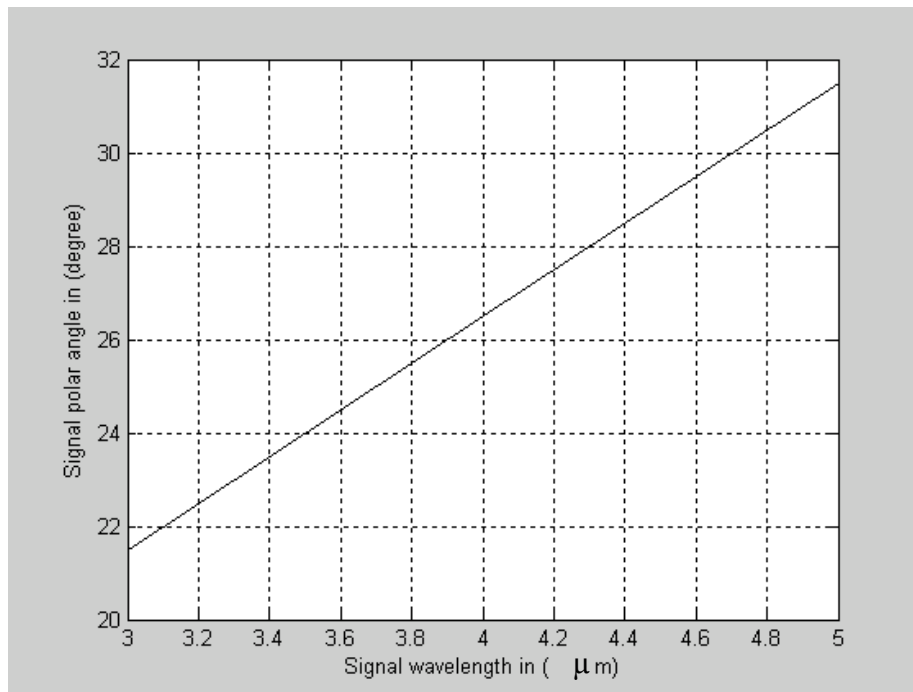


Figure.3.15 Signal polar angle of AgGaS₂ versus signal wavelength within the range (3-5) μm for type I phase matching at $\theta_p=43^\circ$

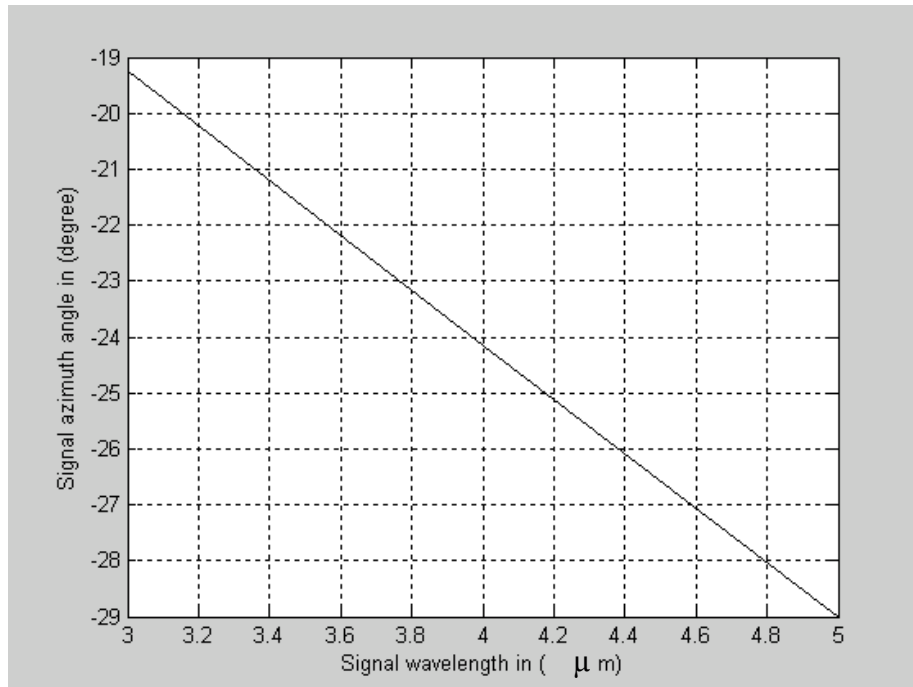


Figure.3.16 Signal azimuth angle of AgGaS_2 versus signal wavelength within the range $(3-5)\mu\text{m}$ for type I phase matching at $\theta_p=43^\circ$

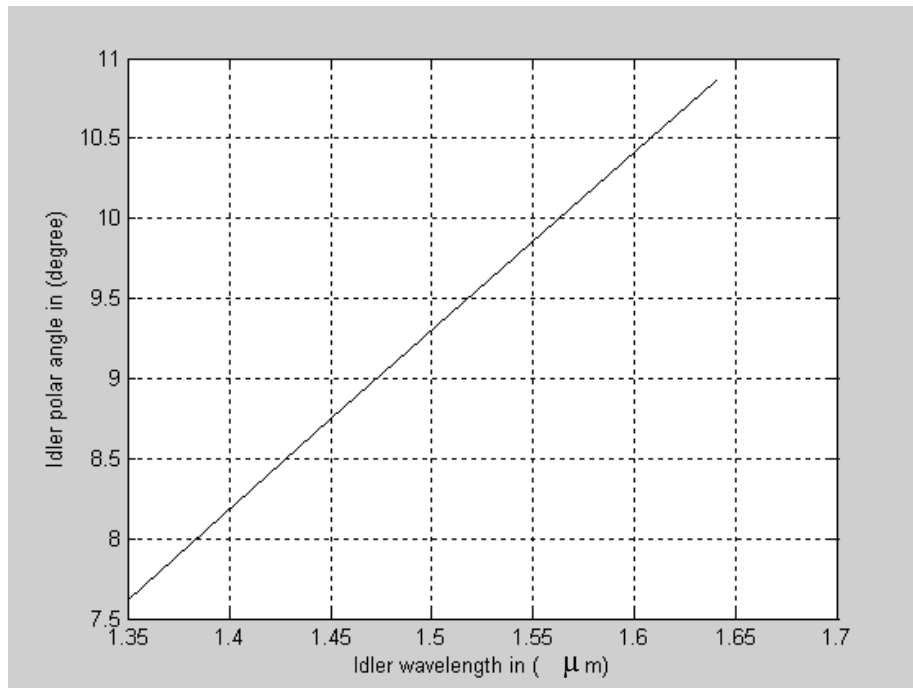


Figure.3.17 Idler polar angle of AgGaS_2 versus idler wavelength within the range $(1.35-1.64)\mu\text{m}$ for type I phase matching at $\theta_p=43^\circ$

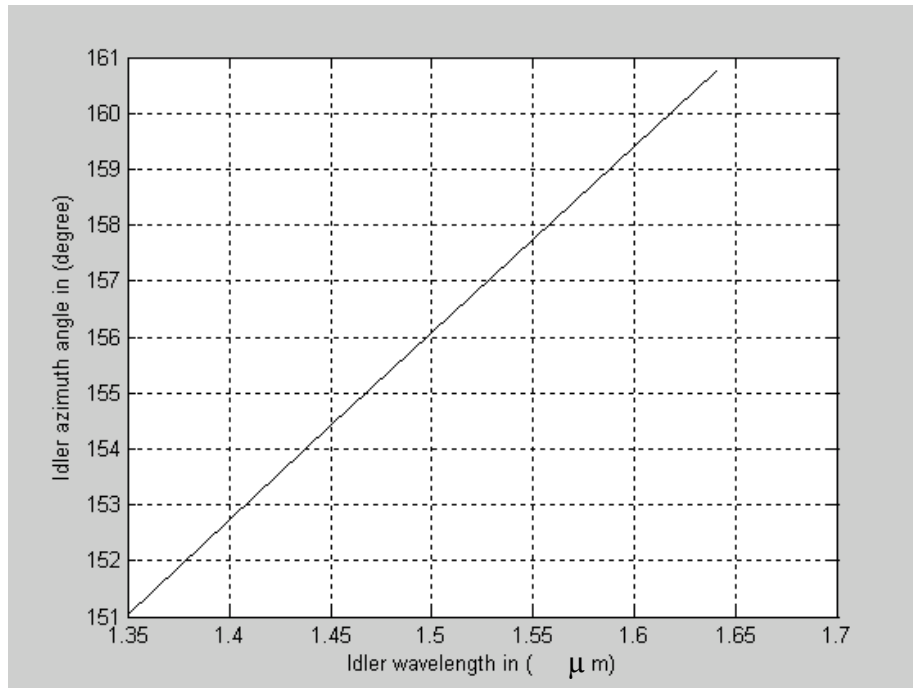


Figure.3.18 Idler azimuth angle of AgGaS_2 versus idler wavelength within the range $(1.35\text{-}1.64)\mu\text{m}$ for type I phase matching at $\theta_p=43^\circ$

3.5 The direction of the generated waves in biaxial crystal

One of the most effective methods for generating eye-safe radiation is based on an optical parametric oscillator using crystals in the KTP family, pumped by radiation from solid-state lasers. KTP crystal which is an example of biaxial crystal has high radiation resistance, high nonlinear optical coefficients, and ensures lasing under noncritically phase matching conditions. Because of the indicated properties, they make it possible to convert the wavelength of emission from Nd^{+3} lasers at $\lambda_p=1.064\mu\text{m}$ to the wavelength $\lambda_s=1.61\mu\text{m}$, thus the idler wavelength is $3.2\mu\text{m}$. Under noncritically phase matching (NCPM) condition, the momentum phase mismatch and the maximum conversion efficiency have been calculated at different values of pumping azimuthal angles ϕ_p . Figures 3.19 and 3.20 show the momentum phase mismatch for type II noncritically phased matched as a

function of signal polar angle at different pump azimuthal angles ϕ_p . It can be seen that under phase matching condition (i.e. $\Delta K=0$) the three component of the wave vectors intersect at the same point which represent phase matching signal polar angle. In biaxial crystal the condition of (NCPM) is not true unless $\phi_p=0, 90^\circ, 180^\circ$, etc. under these conditions the maximum conversion efficiency has been calculated as a function of the momentum phase mismatch as shown in figures 3.21 and 3.22. It can be seen that at type II phase matching the maximum conversion efficiency appears at $\theta_p=90^\circ$ when $\phi_p=90^\circ$ and at $\phi_p=180^\circ$ and the conversion efficiency at $\phi_p=180^\circ$ is lower than that at $\phi_p=90^\circ$, thus it can be concluded that the conversion efficiency increased as the pump azimuthal angle decreased and the conversion efficiency for biaxial crystal is a pump azimuthal angle dependent.

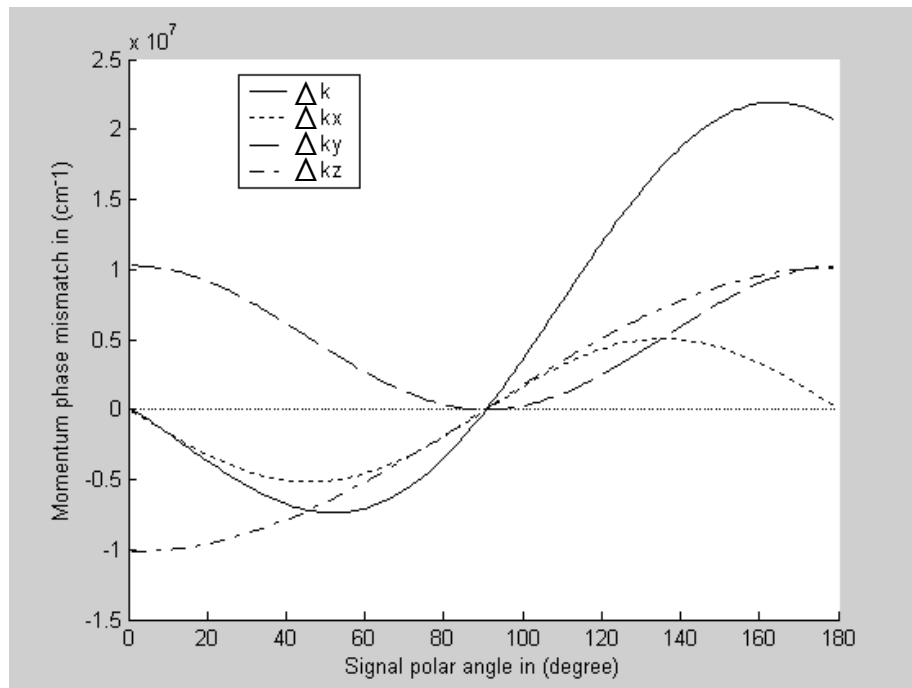


Figure. 3.19 Momentum phase mismatch of KTP versus signal polar angle for type II (NCPM) at $\phi_p=90^\circ$

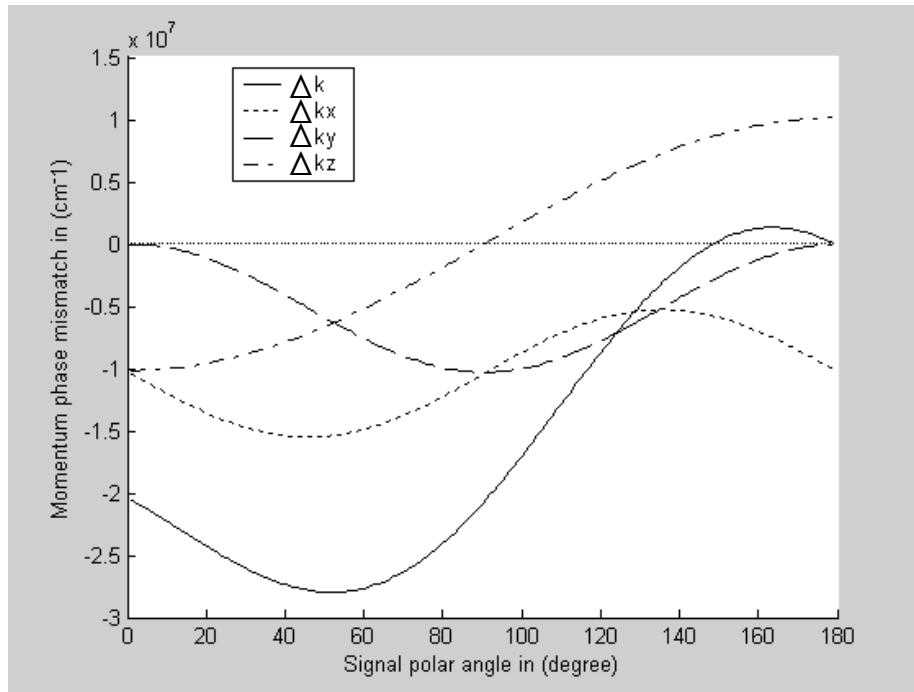


Figure. 3.20 Momentum phase mismatch of KTP versus signal polar angle for type II (NCPM) at $\phi_p=180^\circ$

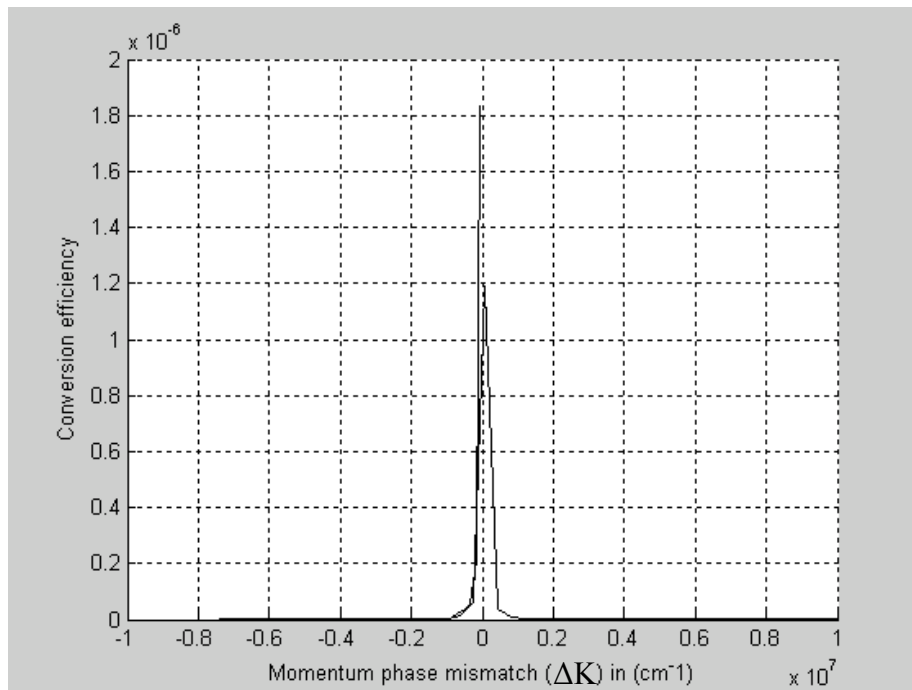


Figure.3.21 Conversion efficiency of KTP versus momentum phase mismatch for (NCPM) at $\phi_p=90^\circ$

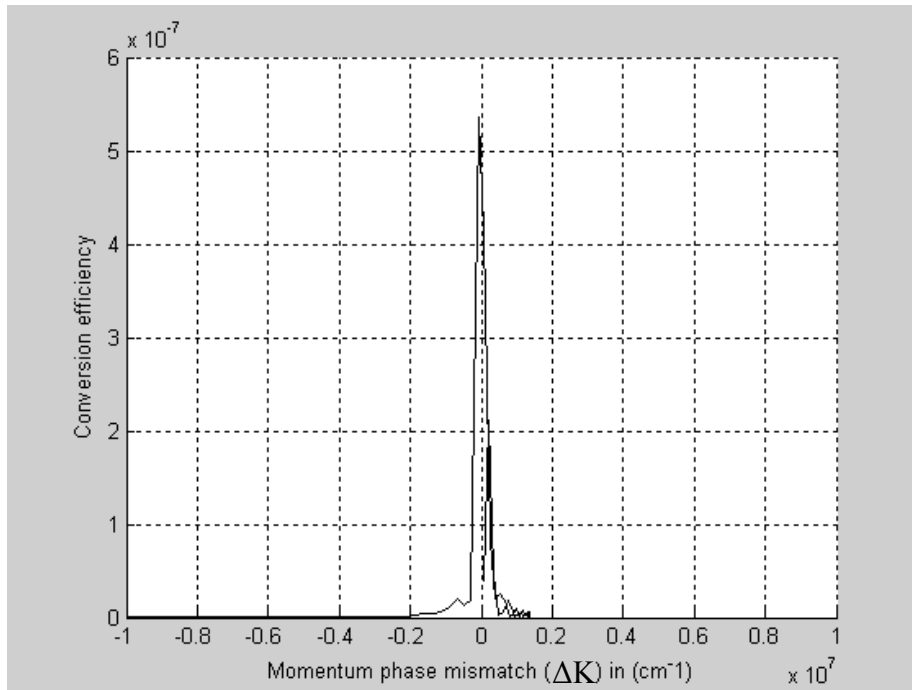


Figure.3.22 Conversion efficiency of KTP versus momentum phase mismatch for (NCPM) at $\varphi_p=180^\circ$

At different pumping azimuthal angles φ_p the signal and idler polar angles have been calculated for (NCPM) and plotted in figures 3.23 and 3.24. These figures indicate that the signal polar angle increased linearly as φ_p increased while the idler polar angle decreased and as φ_p increased the separation between the signal wave and the optic axis of the crystal and between the signal and idler waves are wide which means that the idler wave propagate very close to the optic axis of the crystal so one may deduce that the signal and idler polar angles are a pump azimuthal angle dependent.

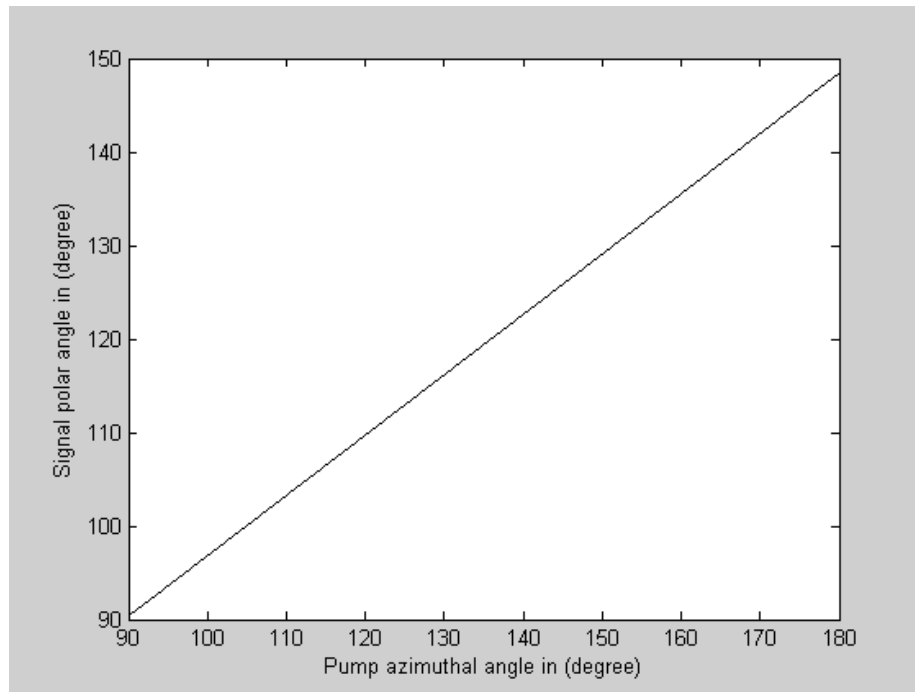


Figure. 3.23 signal polar angle of KTP versus pump azimuthal angle for type II (NCPM)

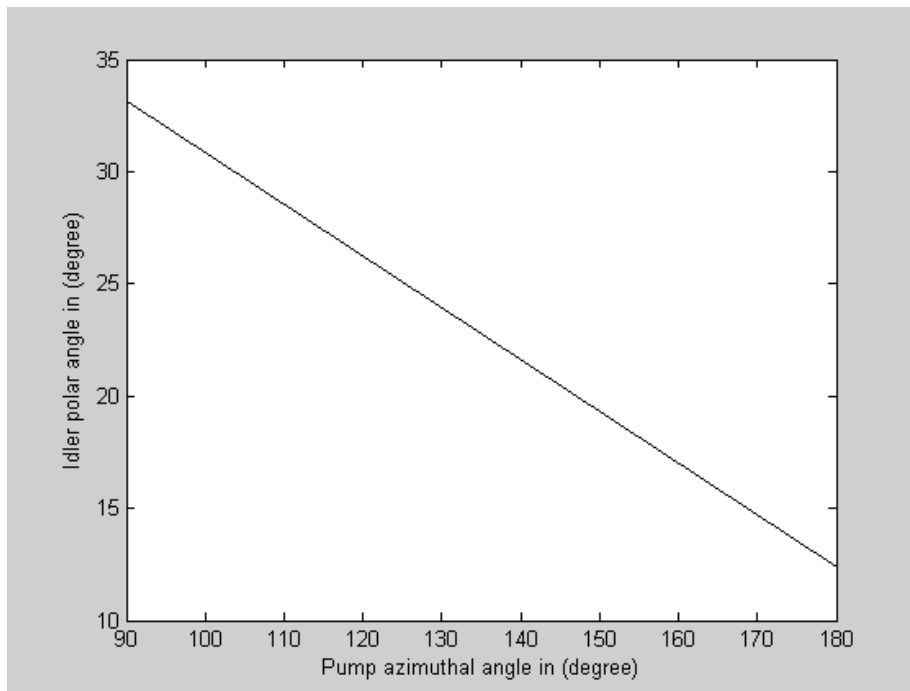


Figure. 3.24 Idler polar angle of KTP versus pump azimuthal angle for type II (NCPM)

The signal azimuthal angles increased in $-x,y$ plane as ϕ_p increased and simultaneously the idler azimuth angles increased in x,y plane and the separation between them is constant and equal to π as shown in figures. 3.25 and 3.26 respectively.

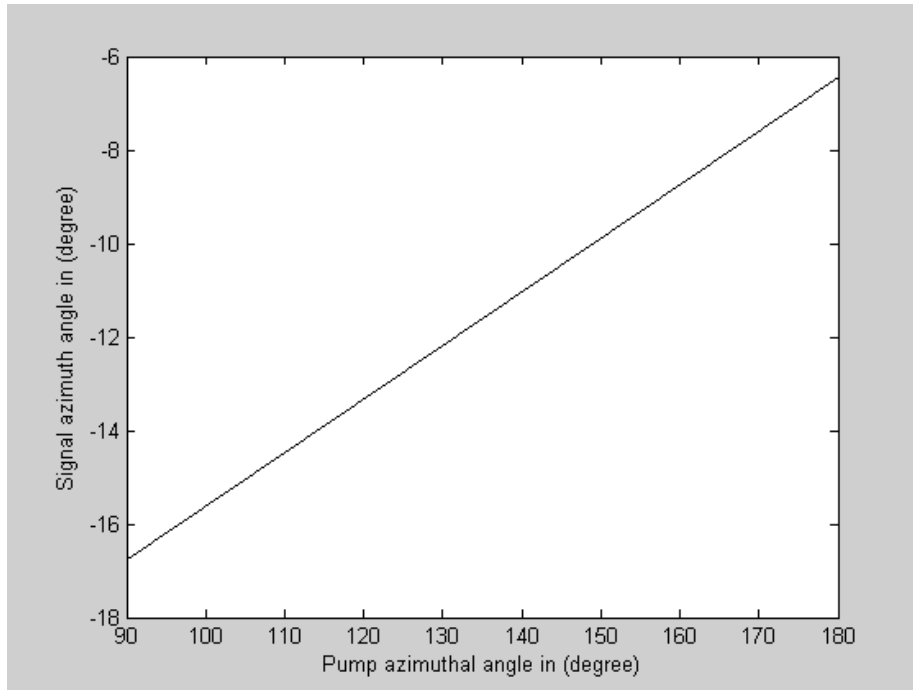


Figure. 3.25 Signal azimuth angle of KTP versus pump azimuthal angle for type II (NCPM)

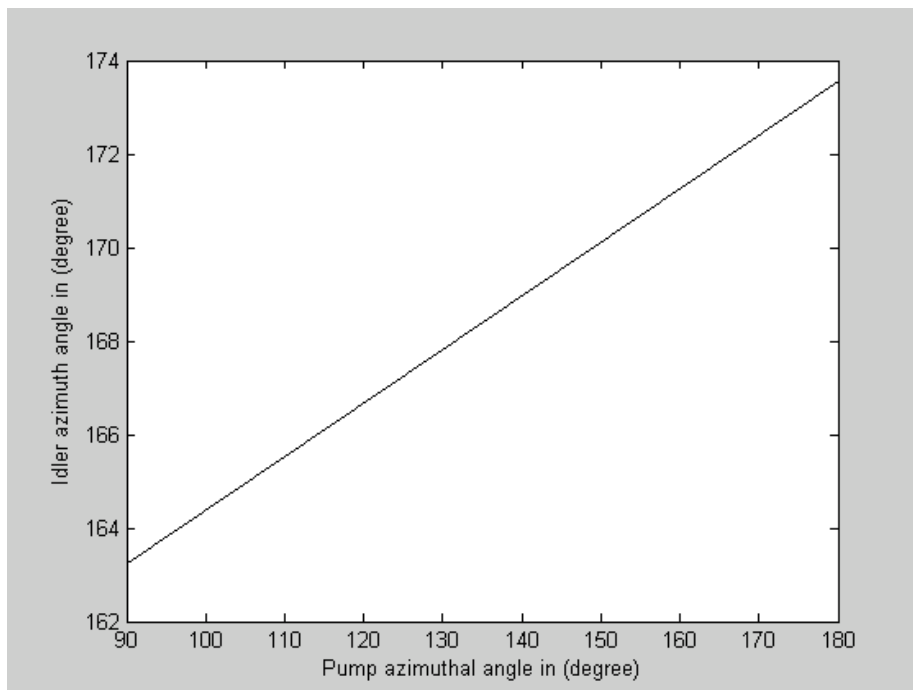


Figure. 3.26 Idler azimuth angle of KTP versus pump azimuthal angle for type II (NCPM)

4. Performance Modeling of an OPO

4.1 Wide-tunable AgGaS₂ Optical Parametric Oscillator

4.1.1 Introduction

Solid state lasers operated in the range of atmospheric transparency (3-5 μm , 8-12 μm) is of great interest for many applications such as eye-safety lidars, target designations, obstacle avoidance, and infrared countermeasures. Optical parametric oscillator (OPO) is an effective tool to cover the range.

In the present work, considering the low damage threshold, the methods to reduce the oscillating threshold are discussed. AgGaS₂ type-I singly resonant optical parametric oscillator (SRO OPO) pumped by a ns 1.064 μm Nd:YAG laser is demonstrated theoretically. We put our emphasis on the interesting parametric wavelength range within 3-5 μm . A comparison on the threshold energy density is made between the single pump pass SRO OPO and the double pump pass OPO.

4.1.2 OPO Cavity Configuration

The most common optical parametric device is the singly resonant oscillator with two identical flat mirrors M_1 and M_2 depicted in figure 4.1. In this device, the AgGaS₂ crystal with $10 \times 7 \text{ mm}^2$ in cross section, 20mm in length, $\theta = 43^\circ$ and $\phi = 45^\circ$ cut for type-I phase matching is located inside a resonator that provides feedback at the signal frequency. In order to reduce the loss so as to the oscillation threshold, both cross sections are well antireflection AR coated: high transparent $\text{HT}_{1.06} > 99\%$ at pump wavelength 1.06 μm , and also at signal and idler wavelengths $\text{HT}_{3.5} \sim 97.5\% - 99\%$,

$HT_{1.35-1.64} \sim 97\%-98.5\%$, respectively. As illustrated in figure 4.1, the pump beam enters through a mirror M_1 that is highly transmitting at the pump wavelength $HT_{1.06} > 95\%$ and highly reflective for the signal wavelength $HR_{3.5} > 99-99.4\%$. The opposite mirror M_2 , which is the output coupler, has a high reflectivity for the signal wavelength, and $HT_{1.35-1.64} > 88-98\%$ transmission for the idler and pump beam. Only the signal wavelength is resonant in the cavity, and a small fraction is coupled out through the front mirror M_2 .

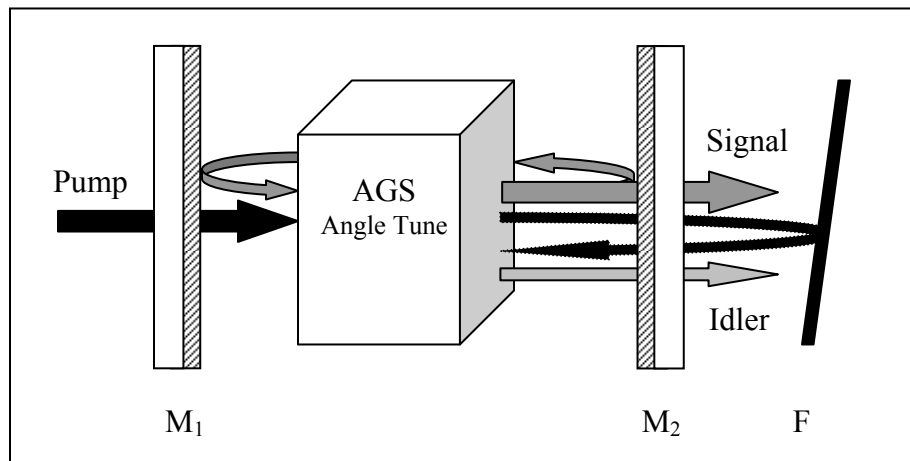


Figure 4.1 Schematic of $AgGaS_2$, SRO OPO Cavity

4.1.3 Analysis of Oscillation Threshold

Due to the low damage threshold in AGS crystal, how to lower the pump threshold is considered firstly. In order to describe the threshold pump energy density (oscillation threshold) of a pulsed single- and double pump pass single resonant oscillator, a simplified theoretical model including the effects of Poynting vector walk-off is used [57]. Simplified expression for the threshold pump energy density (threshold fluency) is given by

$$I_{th} = \frac{2.25}{kg_s l_{eff}} \frac{\tau}{(1+\gamma)^2} \left\{ \frac{L}{2c\tau} \ln\left(\frac{P_n}{P_s}\right) + 2\alpha l + \ln\frac{1}{\sqrt{R}} + \ln 4 \right\}^2 \quad (4.1)$$

Where g_s, l_{eff} and k are the signal spatial mode coupling coefficient and the effective parametric gain length and the interaction coefficient listed below, respectively.

$$g_s = \frac{W_p^2}{W_p^2 + W_s^2}, \quad l_{eff} = l_w \operatorname{erf}\left(\frac{\sqrt{\pi}}{2} \frac{l}{l_w}\right), \quad k = \frac{2w_s w_i d_{eff}^2}{n_s n_i n_p \epsilon_o c^3} \quad (4.2)$$

The walk-off length l_w is given by

$$l_w = \frac{\sqrt{\pi}}{2} \frac{W_p}{\rho} \sqrt{\frac{W_p^2 + W_s^2}{W_p^2 + W_s^2/2}} \quad (4.3)$$

where w_s, w_i are frequencies for the signal and idler light, d_{eff} is effective nonlinear coefficient; n_s, n_i, n_p are refractive indexes for signal, idler and pumping light, respectively; c is the light velocity; τ is the pulse width for pumping light; L, l are the cavity length and the crystal physical length, respectively; γ is the ratio of backward to forward pump field amplitude inside the crystal; α is the coefficient of field absorption in the crystal; $\ln\left(\frac{P_n}{P_s}\right)$ is the ratio of the threshold power to noise power, R is the effective cavity loss (the product of mirror reflectivities).

The relations between the Gaussian mode electric field radii W_p, W_s and the resonant spot radii \bar{W}_s are given in Appendix A.

If the ratio of backward to forward pump field amplitude γ is fixed to zero and SRO is considered, the threshold pump intensity of a pulsed singly resonant oscillator including the effect of Poynting vector walk-off is concluded as follows

$$I_{th} = \frac{2.25}{kg_s l_{eff}} \tau \left\{ \frac{L}{2c\tau} \ln\left(\frac{P_n}{P_s}\right) + 2\alpha l + \ln\frac{1}{\sqrt{R}} + \ln 2 \right\}^2 \quad (4.4)$$

4.1.4 Theoretical Results

Double pump pass means that pump wave passes through the nonlinear crystal twice i.e. the pump laser is not fed back into the OPO cavity when pump laser is not vertical to $1.064 \mu m$ reflective filter, F, but the pump laser can be fed back into the cavity for a double pump pass by adjusting the filter, F, vertical to pump laser as shown in figure 4.1. It is an effective method to lower the pump threshold. Figure 4.2 shows a comparison between single- and double pump pass (DSRO, double-pump singly resonant, SSRO, single-pump singly resonant). It clear that the threshold energy density of SSRO is about 2.8 orders of magnitude higher than that of DSRO for type I phase matching. The threshold energy density increases linearly with the signal wavelength and has a maximum value of $0.38 J/cm^2$ and $1.06 J/cm^2$ at $(5 \mu m)$ for DSRO and SSRO respectively.

The different ratio of backward to forward pump field amplitude inside the crystal follows with the different threshold. With increase of γ , threshold declines obviously as shown in figure 4.3.

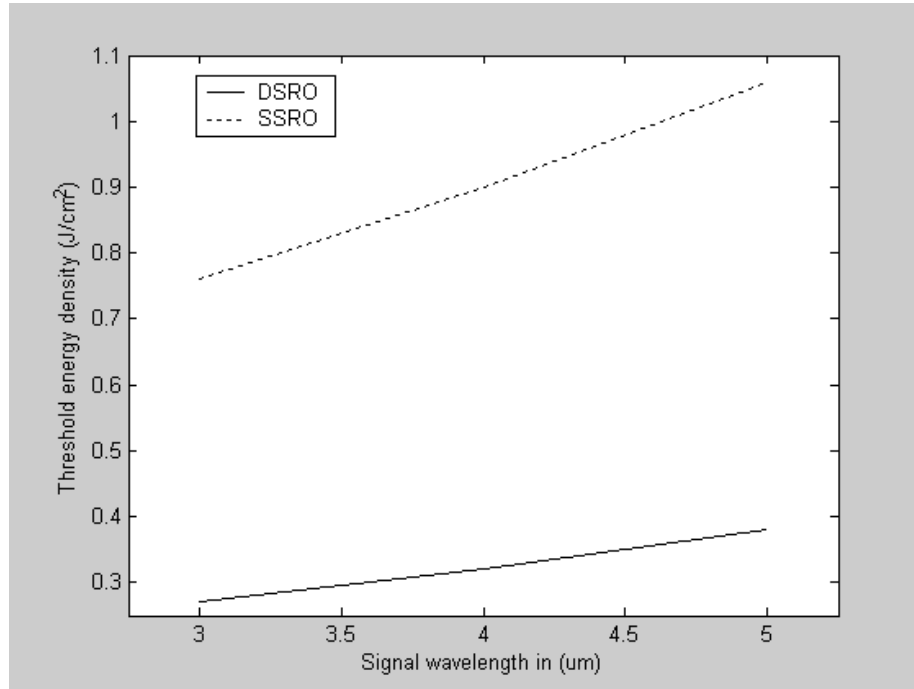


Figure.4.2 Comparison between oscillation threshold of the single and double pump pass for $L=3\text{cm}$, $l_c=2\text{cm}$ and $W_p=2\text{mm}$.

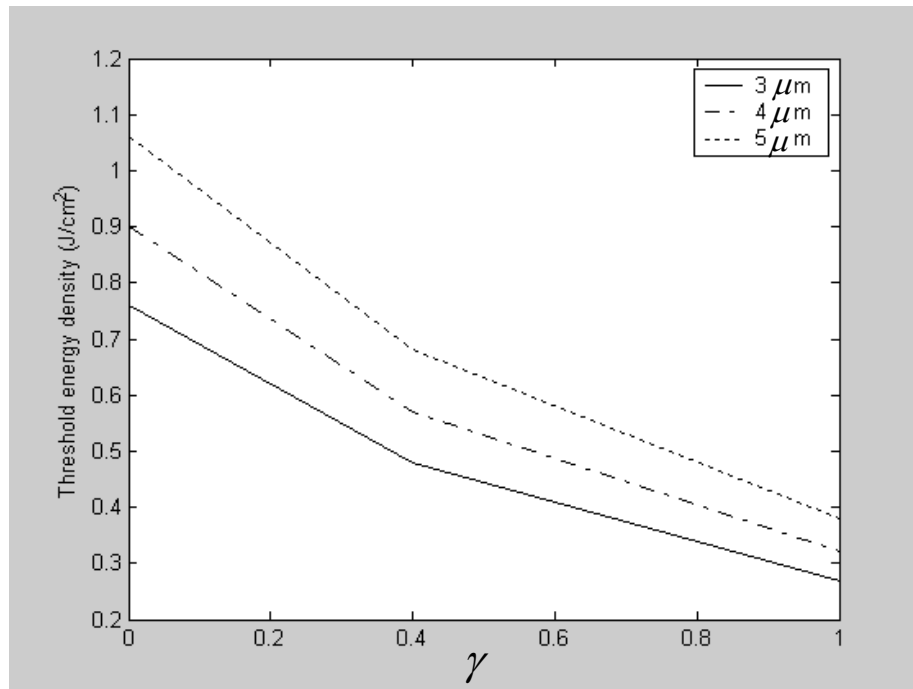


Figure.4.3 Threshold pump energy density as a function of the ratio of backward to forward field amplitude in crystal γ for DSRO, $L=3\text{cm}$, $l_c=2\text{cm}$ and $W_p=2\text{mm}$.

Threshold pump energy density is mainly determined as a function of cavity length, crystal physical length, pump spot size and pump pulse width. The influences of these parameters on the threshold were investigated as shown in figures 4.4-4.7. It is clear that the longer the cavity length is, the higher the threshold as shown in figure 4.4. When the crystal length is less than 2cm, the threshold is abruptly increased and when the length exceeds 3.5 cm, it nearly keeps flat as shown in figure 4.5. The increase in threshold as well as the decrease in gain is due to the small pump spot size as a result of Poynting vector walk-off as in figure 4.6. The benefit of the relatively shorter pulse width, as indicated in figure 4.7, is to produce a lower threshold energy density. It is also evident that the threshold increases with the output wavelength (threshold at $5\mu\text{m}$ > than that at $4\mu\text{m}$ > than that at $3\mu\text{m}$) as can be seen from figures 4.4-4.7.

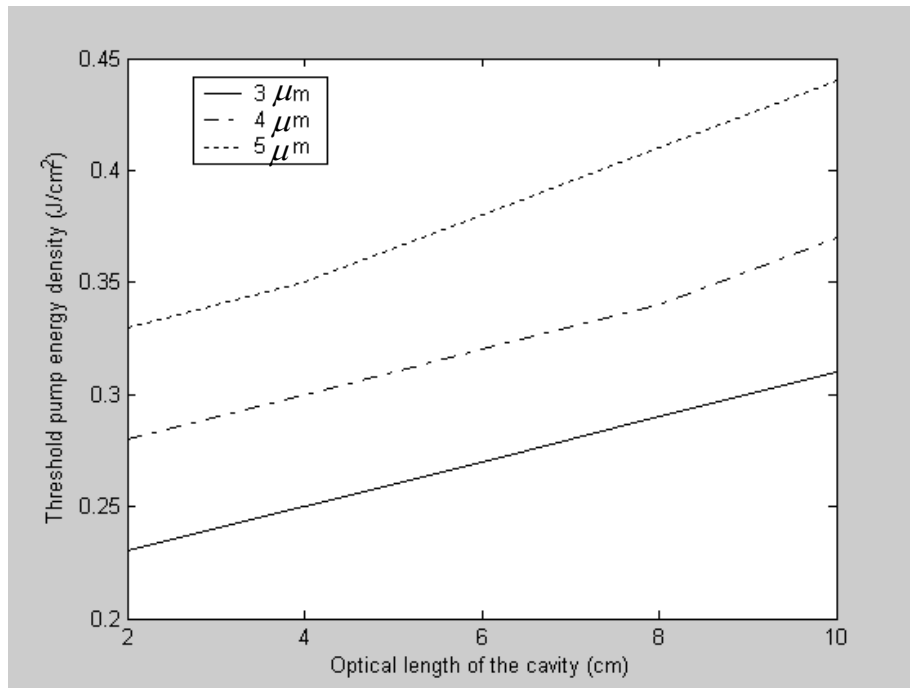


Figure 4.4 Threshold energy density as a function of OPO cavity length. Solid line, dash dot line, dot line corresponding to $3\mu\text{m}$, $4\mu\text{m}$, $5\mu\text{m}$ of signal wavelength, respectively.

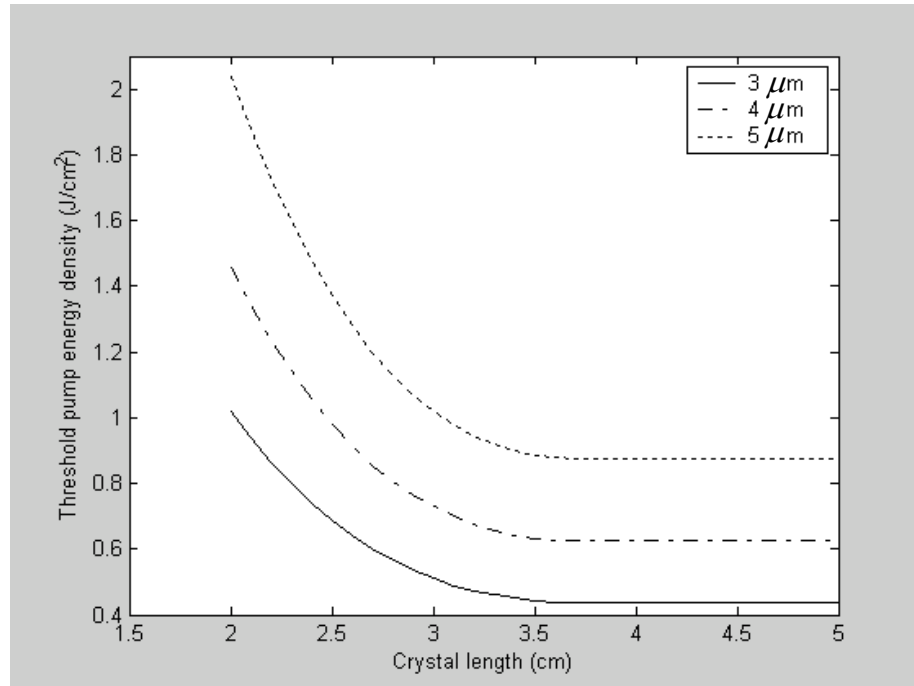


Figure. 4.5 Threshold energy density as a function of the crystal length. Solid line, dash dot line, dot line corresponding to $3\mu\text{m}$, $4\mu\text{m}$, $5\mu\text{m}$ of signal wavelength, respectively.

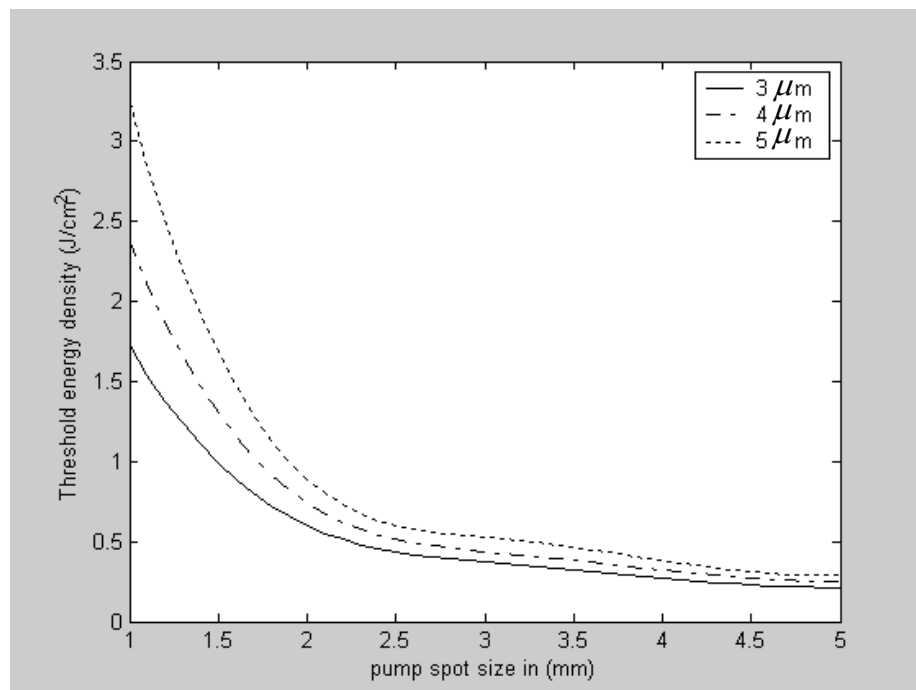


Figure.4.6 Threshold energy density as a function of pump spot size. Solid line, dash dot line, dot line corresponding to $3\mu\text{m}$, $4\mu\text{m}$, $5\mu\text{m}$ of signal wavelength, respectively.

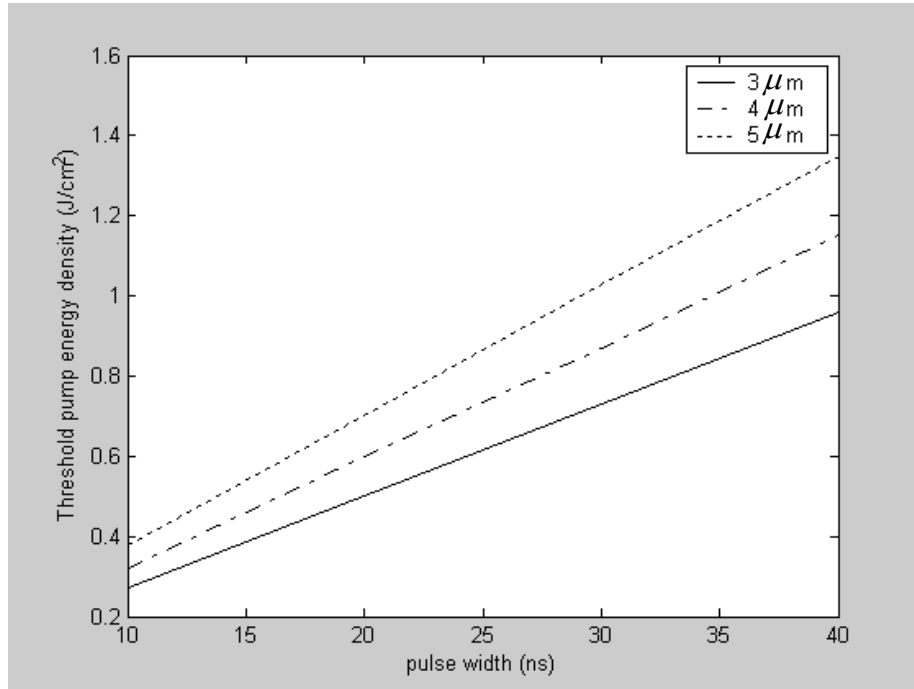


Figure.4.7 Threshold energy density as a function of pump pulse width. Solid line, dash dot line, dot line corresponding to $3\mu\text{m}$, $4\mu\text{m}$, $5\mu\text{m}$ of signal wavelength, respectively.

It can be interpreted as the oscillation threshold is inversely proportional to the product of the idler and signal angular frequency as given in Eq.(4.1), so as to the product of the two wavelength; the effective nonlinear coefficient d_{eff} is decreasing at the range of 3-5 μm as well as the gain in the AGS crystal, the oscillation threshold is inversely proportional to d_{eff} , too. Thus a larger threshold is predicted at longer output wavelength certainly.

4.2 Pulsed Confocal Unstable Optical Parametric Oscillators

4.2.1 Introduction

Optical parametric oscillators (OPOs) are very attractive solid-state sources for the generation of eye-safe wavelengths. Significant

improvements in the performance of the OPOs have taken place in the past years, largely owing to the development of high-quality nonlinear optical crystal and efficient pump laser sources [58]-[60]. One of the greatest challenges for OPOs in the long-range laser applications is to obtain good beam quality along with high energy, i.e. high-brightness OPOs are required.

A confocal positive-branch unstable resonator is a wonderful optical solution to the conflicting demands of high beam quality and high energy in OPO [61]. The unstable resonator effectively filters out laser modes with high-spatial-frequency components by a combination of laser-mode magnification and feedback of only the lowest-order spatial modes. But the high-loss characteristic limits the unstable resonator to high-gain systems. The unstable resonator becomes the ideal cavity for high-energy OPO with large-volume mode and high beam quality. It has been theoretically [62, 63] and experimentally [64]-[68] demonstrated that the confocal positive-branch unstable resonators generate near-to-diffraction-limited signal beams.

The threshold of nanosecond OPO devices is an important parameter for many practical applications. Compared with plane-parallel resonator, although advantage in improving beam quality has indeed been outstanding, threshold of unstable resonator remains rather high [67]. This is mainly due to geometrical loss caused by mode expansion in the unstable resonator. It is demonstrated that there is only one unique pair of conjugate points for a given unstable resonator and wave traveling in any direction inside the resonator is considered as a spherical wave coming from the corresponding conjugate point [61]. Therefore the threshold theoretical model based on plane-wave assumption is no longer valid for the unstable OPO.

The present work details the derivation of the threshold model based on the spherical wave assumption for a confocal positive-branch unstable resonator OPO. This model gives the threshold pump peak intensity and threshold pump energy as a function of important parameters such as the cavity magnification factor M , cavity physical length L , full width half maximum (FWHM) of the input pump pulse intensity T , crystal length l_c , output mirror reflectance to signal R , pump beam radius r_p and separation between crystal to output mirror L_2 .

4.2.2 OPO Cavity Design

The property of confocal positive-branch unstable resonator determines that one of the conjugate points is positioned at infinity and the other one is confocal point F . Therefore forward wave in the resonator is considered as plane wave and backward wave is regarded as spherical wave from the confocal point. A primary advantage of this configuration is that it automatically produces a collimated output beam.

The confocal positive-branch unstable OPO, formed by concave mirror M_1 and convex mirror M_2 , is schematically illustrated in figure 4.8, where signal field E_s is assumed to be resonant. The pump is collimatedly coupled in through M_1 , and the signal is partially coupled out through M_2 . R_1 and R_2 are curvature radii of input mirror and output mirror, respectively (R_2 is with a minus sign for the convex mirror case). The cavity physical length is set by $L = (R_1 + R_2) / 2 + l_c (1 - 1/n_s)$ to satisfy confocal condition, where n_s is the refractive index to signal of the nonlinear crystal. Owing to the geometrical magnification of the unstable resonator, the signal beam is expanded during one round trip by the cavity magnification factor $M = -R_1/R_2$. As shown in figure 4.8, L_1 and L_2 describe separation between input mirror center to front

surface of nonlinear crystal and between back surface of nonlinear crystal to output mirror center, respectively.

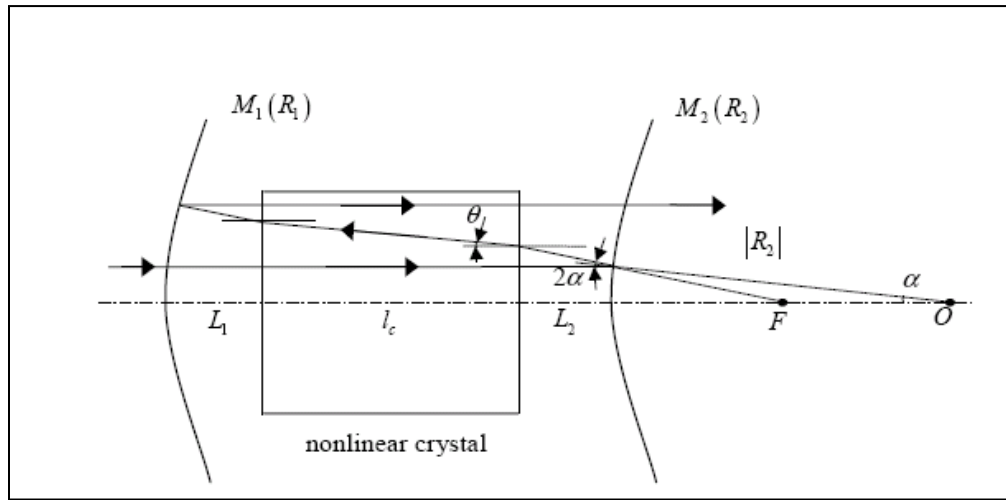


Figure.4.8. Confocal unstable singly resonant OPO. The Input Mirror M_1 is a concave mirror, which is highly reflecting at the signal wavelength and highly transmitting at the pump and idler wavelengths. The output coupler M_2 is a convex mirror, which is highly reflective at the pump wavelength, highly transmitting at the idler wavelength, and has signal reflectance R .

The input mirrors M_1 for all resonators were coated for 98% transmission at the pump wavelength of $1.064\mu\text{m}$, 95% transmission at the idler wavelength of $3.2\mu\text{m}$, and 99.8% reflectance at the signal of $1.61\mu\text{m}$. The output mirrors M_2 for all resonators were highly reflecting at the $1.064\mu\text{m}$ pump wavelength, 82% reflecting at the $1.61\mu\text{m}$ signal wavelength, and 99% transmission at the $3.2\mu\text{m}$ idler wavelength.

4.2.3 Theoretical Threshold Model

This model was proposed to describe the threshold pump intensity and threshold pump energy of a pulsed double – pass pumped confocal unstable singly resonant oscillator (SRO). This model is appropriate for non – critically phase matched for which there is no walk-off.

4.2.3.1 SRO single pass gain solution based on spherical wave

In this model, the wave field profile is assumed to be circular symmetrical around z-axis. The spherical wave field traveling in the unstable resonator with the wave-vector \vec{K} which has two components: longitudinal component K_z and transverse component K_r , is defined by [69]:

$$E_j(r, z, t) = \frac{1}{2} [E_j(r, z) e^{i(K_z z + K_r r - \omega t)} + c.c.] \quad (4.5)$$

Where

$$E_j(r, z) = \frac{A_j(r_o, z)}{M'_j} \quad j=p, s, i \quad (4.6)$$

is a Fourier component of the optical electric field of pump, signal or idler. Here r and z are not independent variables, but related by $r = r_o + \theta_j z$. Where r_o is corresponding to the transverse coordinate at the entrance to the crystal, i.e. at $z = 0$. The angle $\theta_j = 2\alpha / n_j$ depicted in figure 4.8 is the refractive angle in the crystal for the incidence 2α and n_j is the refractive index of the nonlinear crystal at angular frequency ω_j . $M'_j(z)$ describes the magnification factor to beam diameter, and is defined as the ratio of distance between considered point (r, z) and confocal point to distance between the corresponding incident point $(r_o, 0)$ and confocal point, or equivalently

$$M'_j(z) = r / r_o.$$

From Maxwell's equations [70], we can get

$$\nabla^2 E_j(r, z, t) - \mu_o \sigma \frac{\partial E_j(r, z, t)}{\partial t} - \mu_o \epsilon_o \frac{\partial^2 E_j(r, z, t)}{\partial t^2} = \mu_o \frac{\partial^2 P_j(r, z, t)}{\partial t^2} \quad (4.7)$$

Substituting Eq. (4.5) into Eq. (4.7) for each frequency component, in the slowly varying amplitude approximation and no consideration of diffraction and walk-off which can be ignored in the case of the noncritically phase-matched operation, the equations describing the nonlinear optical parametric oscillation are given by [69]:

$$\begin{cases} \frac{\partial E_s(r, z)}{\partial z} + \alpha_s E_s(r, z) = iN_s E_p(r, z) E_i^*(r, z) e^{i\Delta K_r r} e^{i\Delta K_z z} \\ \frac{\partial E_i(r, z)}{\partial z} + \alpha_i E_i(r, z) = iN_i E_p(r, z) E_s^*(r, z) e^{i\Delta K_r r} e^{i\Delta K_z z} \\ \frac{\partial E_p(r, z)}{\partial z} + \alpha_p E_p(r, z) = iN_p E_s(r, z) E_i(r, z) e^{-i\Delta K_r r} e^{i\Delta K_z z} \end{cases} \quad (4.8)$$

Where

$$\alpha_j = \frac{\mu_o \sigma_j w_j}{2K_j \sqrt{1 + \theta_j^2}} + \frac{i\theta_j^2 K_{jz}}{2} \quad (4.9)$$

is the absorption coefficient and the interaction coefficient is

$$N_j = \frac{w_j d_{eff}}{n_j c \sqrt{1 + \theta_j^2}} \quad (4.10)$$

where d_{eff} is the effective nonlinear coefficient of the crystal.

In the assumption of no pump depletion which is reasonable near threshold, $A_p(r_o, z)$ remains constant along z-direction and it can be written as $A_p(r_o)$. Substituting Eq. (4.6) into Eq. (4.8), yields

$$\begin{cases} \frac{\partial A_s(r, z)}{\partial z} + \alpha_s A_s(r, z) = iN_s A_p(r, z) A_i^*(r, z) e^{i\Delta K_r r_o} e^{i\Delta k' z} \\ \frac{\partial A_i(r, z)}{\partial z} + \alpha_i A_i(r, z) = iN_i A_p(r, z) A_s^*(r, z) e^{i\Delta K_r r_o} e^{i\Delta k' z} \end{cases} \quad (4.11)$$

Satisfying the boundary condition of zero idler field at the entrance to the crystal, the solution to Eq. (4.11) is

$$A_p(r_o, z) = e^{-\alpha z} e^{j\Delta K' l / 2} A_s(r_o, 0) \left[\cosh(g(r_o)z) - \frac{j\Delta K'}{2g(r_o)} \sinh(g(r_o)z) \right] \quad (4.12)$$

where

$$g(r_o) = \sqrt{N_s N_i |A_p(r_o)|^2 - (\Delta K' / 2)^2} \quad (4.13)$$

The input pump intensity is temporal-spatial Gaussian defined by $I_p(r, t) = I_{po} e^{-\left(\frac{t}{\tau_p}\right)^2} e^{-\left(\frac{r}{r_p}\right)^2}$, where τ_p is the $1/e$ intensity half width of the pump pulse. For a pulsed OPO operation where pump duration is much longer than one round-trip time of the cavity, the pump intensity can be assumed to be constant during a single cavity transit.

Substituting Eq. (4.6) into Eq. (4.12) and ignore phase mismatch, the signal field at the end of the crystal is

$$E_s(M'_s(l_c)r, l_c) = e^{-\alpha l_c} \frac{E_s(r, 0)}{M'_s(l_c)} \cosh \left(\beta_o l_c e^{-\left(\frac{r}{\sqrt{2}r_p}\right)^2} \right) \quad (4.14)$$

where

$$\beta_o = \sqrt{\frac{2N_s N_i}{n_p c \epsilon_o} I_{po} e^{-\left(\frac{t}{\tau_p}\right)^2}} \quad (4.15)$$

is a time dependant gain coefficient.

4.2.3.2 Double-pass pumped case

The forward waves traveling in a confocal unstable resonator are the plane waves propagating along the z-direction. Let $M_s^f = 1$ and $\theta = 0$ in Eq. (4.14) and assume that perfect phase matching is satisfied, the signal at the end of nonlinear crystal on the forward transit is

$$E_s^f(r, l_c) = E_s^f(r, 0) e^{-\alpha_f l_c} \cdot \cosh \left(\beta_f l_c e^{-\left(\frac{r}{\sqrt{2}r_p}\right)^2} \right) \quad (4.16)$$

where α_f is the forward field absorption coefficient. The forward parametric gain coefficient is

$$\beta_f = \sqrt{\frac{2N_s^f N_i^f}{n_p c \epsilon_o} I_{p0} e^{-\left(\frac{r}{\tau_p}\right)^2}} \quad (4.17)$$

where

$$N_j^f = \frac{w_i d_{eff}}{c n_j}, \quad j = s, i \quad (4.18)$$

is the forward interaction coefficient.

After the reflection of output mirror, the signal field before the output mirror is

$$E_{sr}^b(r) = \sqrt{R} \cdot E_s^f(r, l_c) \quad (4.19)$$

and we let γ_o be the ratio of backward to forward pump field, the pump field before the output mirror at the start of the backward transit is

$$E_{pr}^b(r) = \gamma_o \cdot E_p^f(r) \quad (4.20)$$

According to characteristics of spherical wave, the wave field at the entrance of the crystal on the backward transit is

$$E_j^b(M_1 r, 0) = \frac{E_{jr}^b(r)}{M_1} \quad (4.21)$$

where $M_1 = 1 + 2L_2 / |R_2|$ is defined as the magnification factor to wave traveling from output mirror to the back surface of nonlinear crystal. If we let wave field in the crystal on the backward transit to be $E_j^b(r(z), z) = A_j^b(r_o, z) / M_{2j}(z)$, where

$$M_{2j}(z) = 1 + \frac{2}{n_j(|R_2| + 2L_2)} z \quad (4.22)$$

describes the magnification factor to wave traveling from the back surface of nonlinear crystal to the arbitrary z-plane in the crystal.

From Eq. (4.12), with the assumption of no wave-vector mismatch, or $\Delta K' = 0$, the signal field at the end of the crystal on the backward transit is

$$E_s^b(M_{2j}(l_c)r, l_c) = e^{-\alpha_b l_c} e^{\frac{i\Delta K' l_c}{2}} \frac{E_s^b(r, 0)}{M_{2j}(l_c)} \cosh \left(\beta_b l_c e^{-\left(\frac{r}{\sqrt{2M_1 r_p}}\right)^2} \right) \quad (4.23)$$

where α_b is the backward field absorption coefficient. The backward parametric gain coefficient is

$$\beta_b = \sqrt{\frac{2N_s^b N_i^b}{n_p c \epsilon_o} \cdot \frac{\gamma_o^2 I_{po}}{M_1^2} e^{-\left(\frac{t}{\tau_p}\right)^2}} \quad (4.24)$$

where

$$N_j^b = \frac{w_i d_{eff}}{c n_j \sqrt{1 + \theta_j^2}}, j = s, i \quad (4.25)$$

is the backward interaction coefficient.

The property of spherical wave which determines the signal field propagating to the plane wave before the input mirror is

$$E_{sround}(M_{3s}r) = \frac{E_s^b(r, l_c)}{M_{3s}} \quad (4.26)$$

where $M_{3s} = 1 + 2n_s L_1 / (M_{1n_s} |R_2| + 2l_c)$ is defined as the magnification factor to wave traveling from the front surface of the nonlinear crystal to input mirror on the backward transit.

According to Eqs. (4.16), (4.19), (4.21) and (4.23) the signal field after one round trip in the confocal unstable resonator is therefore, given by

$$E_{sround}(r) = \sqrt{R} e^{-(\alpha_f + \alpha_b) l_c} \frac{E_{start0} e^{-\left(\frac{r/\sqrt{2M_s}}{\sqrt{2M_r}}\right)^2}}{M} \cosh \left(\beta_f l_c e^{-\left(\frac{r}{\sqrt{2M_r}}\right)^2} \right) \cosh \left(\beta_b l_c e^{-\left(\frac{r}{\sqrt{2M_r}}\right)^2} \right) \quad (4.27)$$

where $M = M_{3s} M_{2s}(l_c) M_1$ is the cavity geometrical magnification factor and equal to $-R_1 / R_2$.

After one round trip in the unstable resonator, the signal spot size r_s is narrowed by the Gaussian-profile parametric gain and broadened by the

geometrical magnification of unstable resonator and diffraction. For m th transit, the initial signal power is

$$P_{m-1} = \int_0^{\infty} \left(\frac{1}{2} n_s c \varepsilon_o \right) |E_{start}(r)|^2 \cdot 2\pi r dr = \left(\frac{1}{2} n_s c \varepsilon_o \right) |E_{start}(r)|^2 \cdot \pi r_s^2 \quad (4.28)$$

and the signal power after one round trip using Eq. (4.27) is

$$\begin{aligned} P_m &= \int_0^{\infty} \left(\frac{1}{2} n_s c \varepsilon_o \right) |E_{round}(r)|^2 \cdot 2\pi r dr \\ &= \frac{R}{M^2} e^{-2(\alpha_f + \alpha_b)l_c} \left(\frac{2\pi}{2} n_s c \varepsilon_o \right) |E_{start}|^2 \int_0^{\infty} e^{-\left(\frac{r}{M r_s}\right)^2} \cosh^2 \left(\beta_f l_c e^{-\left(\frac{r}{\sqrt{2} M r_p}\right)^2} \right) \cosh^2 \left(\beta_b l_c e^{-\left(\frac{r}{\sqrt{2} M r_p}\right)^2} \right) r dr \end{aligned} \quad (4.29)$$

The signal power using the relation $\cosh^2 \phi = \frac{e^{2\phi}}{4 + \frac{1}{2}}$ is

$$P_m = P_{m-1} \left\{ \text{Re}^{-2(\alpha_f + \alpha_b)l_c} \left[\frac{1}{16} \left(\frac{r_{s1}}{r_s} \right)^2 e^{2\beta_f l_c (1+\gamma)} + \frac{1}{8} \left(\frac{r_{s2}}{r_s} \right)^2 e^{2\beta_f l_c \gamma} + \frac{1}{8} \left(\frac{r_{s3}}{r_s} \right)^2 e^{2\beta_f l_c} + \frac{1}{4} \right] \right\} \quad (4.30)$$

where

$$\left\{ \begin{aligned} \frac{1}{r_{s1}^2} &= \frac{1}{r_s^2} + \frac{\beta_f l_c (1+\gamma)}{r_p^2} + \frac{4\beta_f l_c \gamma}{(R_2 n_s)^2} \\ \frac{1}{r_{s2}^2} &= \frac{1}{r_s^2} + \frac{\beta_f l_c \gamma}{r_p^2} + \frac{4\beta_f l_c \gamma}{(R_2 n_s)^2} \\ \frac{1}{r_{s3}^2} &= \frac{1}{r_s^2} + \frac{\beta_f l_c}{r_p^2} \end{aligned} \right\} \quad (4.31)$$

Equation (4.30) can be easily iterated numerically to compute threshold, incrementing pump peak intensity until a defined threshold is reached.

The threshold energy was calculated by integration over the temporal and spatial pump intensity profile and given by

$$Q = \int_0^{\infty} \int_0^{\infty} I_p(r, t) dt 2\pi r dr = I_{po} \pi^{1.5} r_p^2 \tau_p \quad (4.32)$$

In this model, there are no mirrors acting on the idler field. If there were some weak idler feedback, the backward gain would be affected by this but it would be too small to consider after that.

4.2.4 Theoretical Results

KTP crystal is an example of biaxial crystal and its dimensions under consideration was $5 \times 5 \times 20 \text{ mm}$, where the type-II non-critical phase matching is satisfied at $1.61 \mu\text{m}$ signal and $3.2 \mu\text{m}$ idler wavelengths when a $1.064 \mu\text{m}$ pump wavelength was used. We take the effective nonlinear coefficient to be 3.3 pmV^{-1} and the refractive indices to signal, idler and pump wave are 1.7284, 1.7026 and 1.744, respectively [71].

Figure 4.9 shows the threshold energy against cavity physical length with $R = 0.82$, $l_c = 20 \text{ mm}$, a 4mm-diameter, 20ns-duration (FWHM) pump beam and different cavity magnification factors. The overall trend of the threshold energy is increasing with cavity physical length and cavity magnification factor. In a confocal unstable resonator, the divergence of the signal beam is reduced by $1/M$ in each round trip. Therefore larger cavity

magnification is preferable concerning high beam quality. However that means larger geometrical loss and consequently higher threshold.

In the practical application, a proper cavity magnification factor should be chosen to balance the conflicting requirement between high beam quality and low threshold.

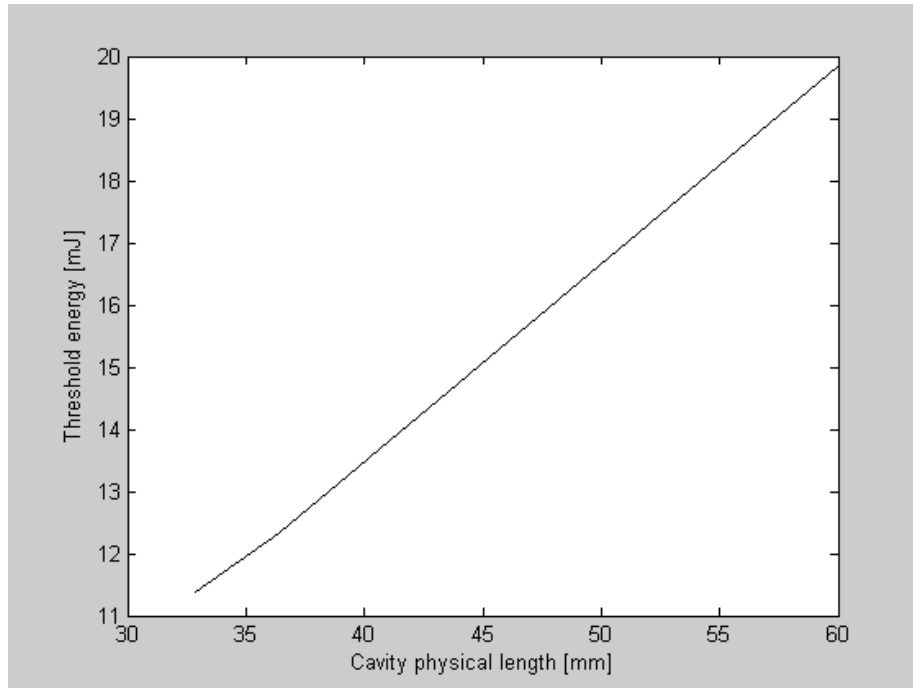


Figure 4.9. Threshold energy versus cavity physical length for various cavity magnification factors. $l_c=20$ mm, $2W_p=4$ mm, $R=0.82$, $\tau=20$ ns.

The threshold energy versus KTP crystal length is shown in figure 4.10. The threshold decreases with crystal length. The unstable resonator with large cavity magnification factor possesses higher threshold, but the threshold differences among the unstable resonators with various cavity magnification factors are decreased with crystal length. When a KTP crystal with length longer than 40mm is used, the threshold difference

between $M=1.33$ and $M=1.19$ was within 8%. Therefore there is no need for longer crystal concerning the reduction of threshold.

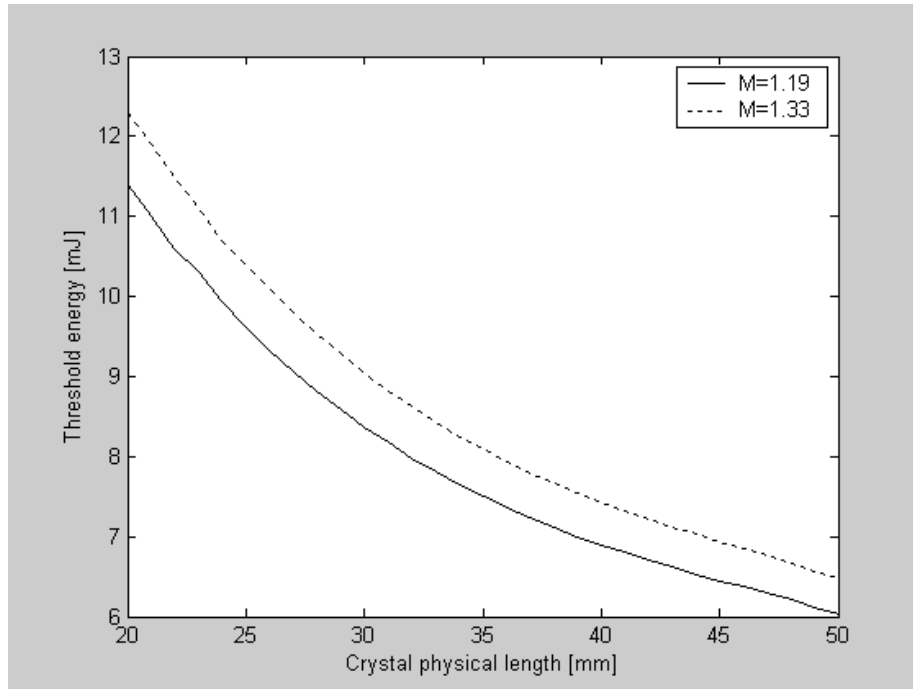


Figure 4.10. Threshold energy versus crystal length. $2W_p=4$ mm, $R=0.82$, $\tau=20$ ns.

Figure 4.11 shows the unstable threshold energy against output mirror reflectance to signal with different magnification factors M , $l_c=20$ mm, $2W_p=4$ mm, $\tau=20$ ns. We also plot threshold energy versus the pump FWHM pulse width for $l_c=20$ mm, $2W_p=4$ mm and $R=0.82$ in figure 4.12. The threshold energy decreases with signal reflectance and increases with pump pulse width. The signal reflectance of the output mirror must therefore be relatively large to maintain a reasonable threshold.

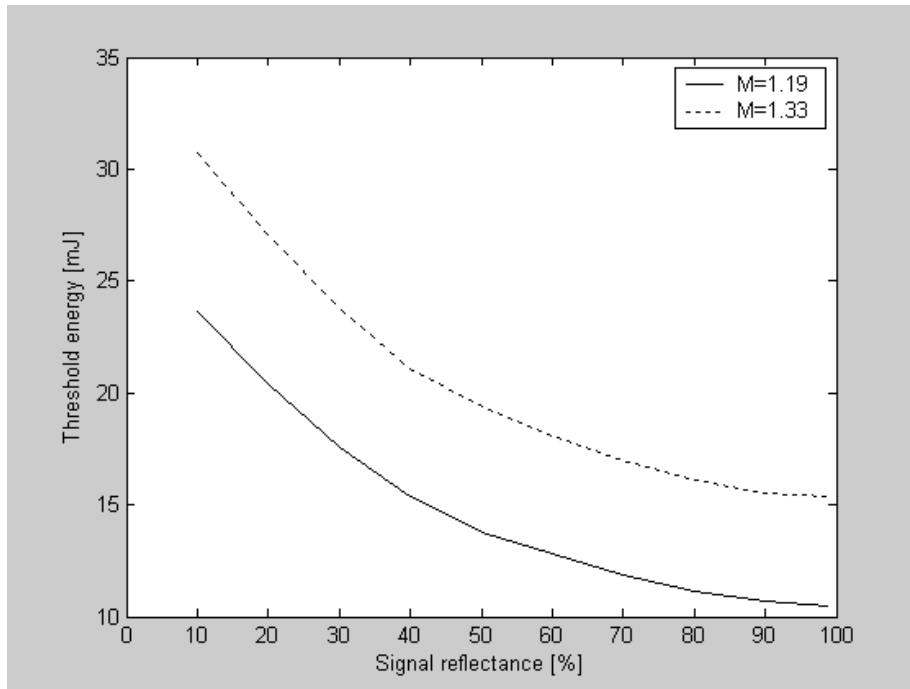


Figure 4.11. Threshold energy versus reflectance to signal of output mirror. $l_c=20$ mm, $2W_p=4$ mm, $\tau=20$ ns.

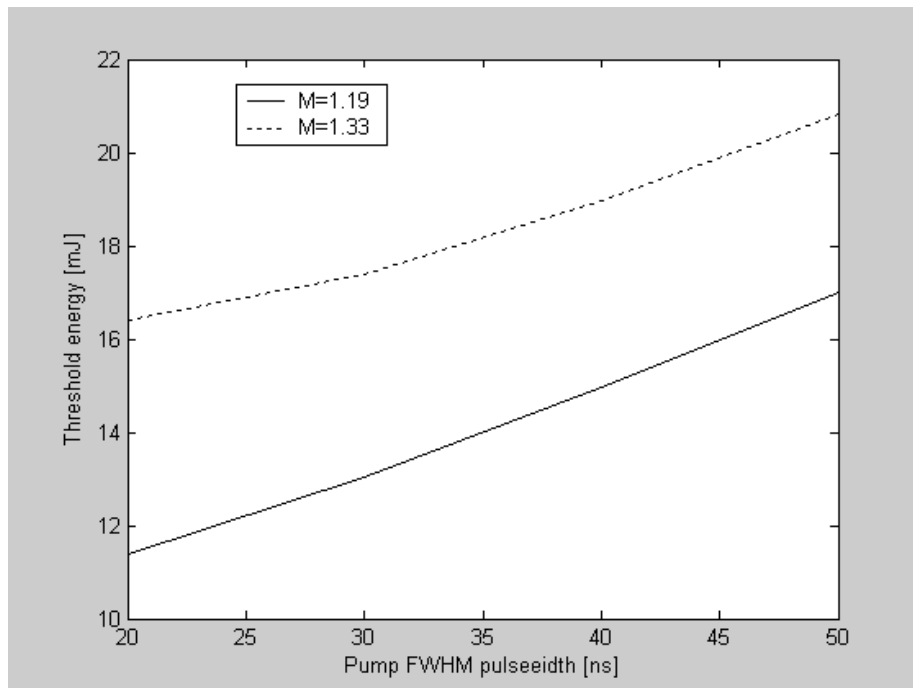


Figure. 4.12. Threshold energy versus pump pulse width. $l_c=20$ mm, $2W_p=4$ mm, $R=0.82$.

In figures 4.9-4.12 respectively, the nonlinear crystal is placed in the middle of the resonator, i.e., $L_1=L_2=(L-l_c)/2$. We present the threshold energy dependent of crystal position in the resonator in figure 4.13. For an unstable resonator with the given cavity physical length, crystal length and cavity magnification, the threshold increases with separation L_2 between crystal and output mirror. As shown in figure 4.13, a threshold increment occurs when the ratio of L_2 to $(L-l_c)$ changes from 0 to 1 for a confocal unstable resonator with $M=1.33$, $L=36$ mm and $l_c=20$ mm. This is because that smaller magnification factor M_1 due to smaller distance L_2 leads to larger backward parametric gain, then lower threshold. This threshold change is also obvious for a short-cavity OPO. This conclusion shows that the nonlinear crystal is better to be placed close to output mirror in the unstable resonator application in order to reduce threshold.

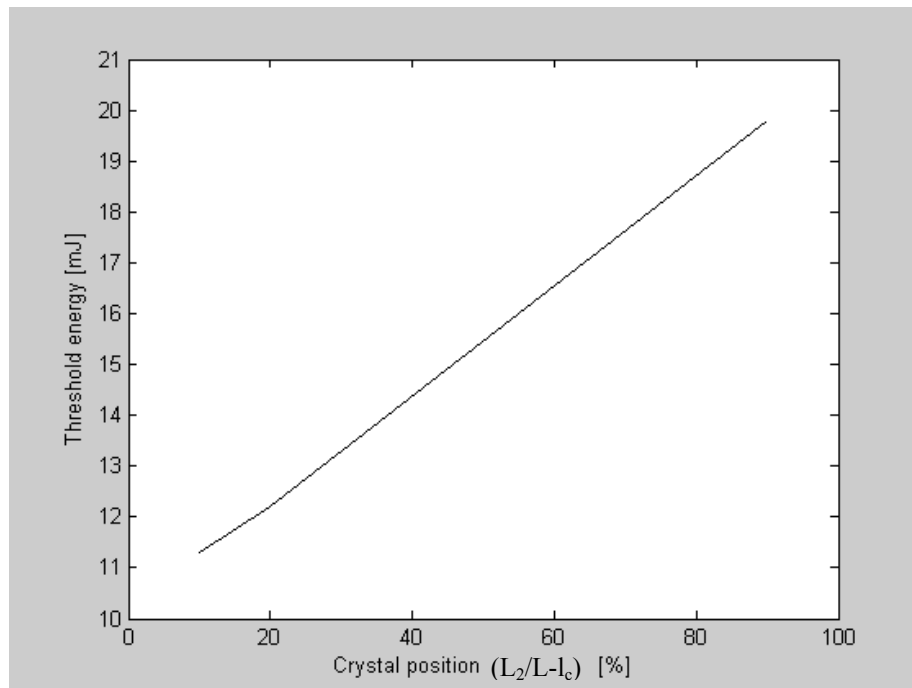


Figure.4.13. Threshold energy versus crystal position. Solid line shows results of our model for $M=1.33$, $L=36$ mm, $l_c=20$ mm, $2W_p=4$ mm, $R=0.82$, $\tau=20$ ns.

5. Conclusions and Suggestions for Future Work

5.1 Conclusions

The process of spontaneous parametric down-conversion, in which a “pump” photon is effectively split into a pair of lower energy “signal” and “idler” photons in a nonlinear optical medium, has proved abundantly useful in the last decade. The twin photons, which are entangled in energy, momentum, and emission time, have been used in a variety of striking demonstrations of the most non classical aspects of quantum theory. In addition, the down-converted photons had applications in the field of metrology, where they can be used to determine the quantum efficiency of photon-counting detectors, and also to determine the spectral radiance of an infrared source. The photon correlations of down-converted light enable these measurement applications to be performed in a fundamentally absolute manner as opposed to conventional methods, which rely on previously calibrated standards.

Calculation of the three-wave down-conversion interaction requires the use of conservation of energy and conservation of momentum, commonly referred to as phase matching. Because the process is nonresonant, a down-converted photon may be emitted over a wide range of wavelengths, so long as the energy and momentum conservation conditions for the pair of photons are met. The individual photons of a pair may also propagate along different directions; this is referred to as non-collinear phase matching. Collinear phase matching, where the incident photon and the output pair of photons propagate in the same direction inside the crystal, while the non-collinear geometry is more difficult to calculate and thus is poorly documented. One of the advantages of non-collinear phase matching

over the collinear case is that it enables easy discrimination between each of the two down-converted photons and the pump beam.

We have proposed a theoretical model for a double-pass pumped singly resonant confocal unstable OPO which relies on the spherical wave theory. The model includes the influence of the cavity magnification factor, cavity physical length, pump pulse width, output coupling and crystal position in the resonator on the threshold of unstable resonator. In the special case this model can be applied to calculate the threshold of the plane-parallel resonator when $M = 1$ and $R_2 = \infty$. The threshold of a confocal unstable resonator increases with the cavity magnification factor, cavity physical length and pump pulse width, and decreases with signal reflectance of output mirror and crystal length..

Two different magnifications factors are investigated in our calculations: $M=1.33$ with $R_1=219\text{mm}$ and $R_2=-163\text{mm}$, $M=1.5$ with $R_1=309\text{mm}$ and $R_2=-206\text{mm}$. In the two cases above, the cavity physical length was set to satisfy the confocal condition, and the nonlinear crystal is placed in the middle of the resonator. We also select the case with $M=1.33$ and $L=36\text{mm}$ to observe the threshold energy varying with the crystal position inside the unstable resonator. We also conclude that the nonlinear crystal is placed close to the output mirror benefits to reduce the threshold.

The method presented here for calculating non-collinear phase-matching allows experimental configurations including either uniaxial or biaxial crystals to be modeled in detail. These computational techniques can provide preliminary answers to a variety of questions that must be asked about a particular down-conversion source before it is constructed in the laboratory, such as “Over what range of wavelengths is down-conversion possible? What should the ‘cut’ of the crystal’s optical axis be? At what

angles can we expect to find certain wavelengths emitted from the crystal?” and so on. The program made available here is the comprehensive scheme that can provide answers to such questions for both collinear and non-collinear phase-matching, and in both uniaxial and biaxial crystals. We hope that the broad pool of calculable crystal data included with this work (both uniaxial and biaxial crystal are included) and wide spectral ranges that can now be computationally investigated will aid other researchers in designing their parametric down-conversion experiments.

5.2 Suggestions for Future Work

- a. Using the phenomenon of retracing behavior of the phase matching angle (RBPM) in non-collinear phase-matched optical parametric oscillators. These phenomena were more prominent with a shorter pump wavelength. Near some specific phase-matching angles there existed broad-signal wavelength ranges over which the phase-matching condition could be simultaneously reached.
- b. Design of a symmetric double quantum well (ADQW) structure for realizing an optical parametric oscillators without phase-matching. The huge nonlinear susceptibility $\chi^{(2)}$ of (ADQW) structure pumped by *Q*-switched CO₂ laser will provide enough gain to realize such an OPO.
- c. Design of a pulsed singly resonant Gaussian Reflectivity Mirror (GRM) confocal unstable OPOs for the single-pass pumped version and also for the double-pass pumped version including the effects of transverse effective gain aperture. The (GRM) is an effective solution to reduce the threshold of unstable OPO.

-
- d. Reducing the oscillation threshold and obtain the stable operation of the cavity by the use of new nonlinear crystals such as Zinc germanium phosphide, ZnGeP_2 (ZGP) which is one of the nonlinear crystals that are most suitable for optical parametric oscillators (OPOs) in the Mid-IR range.

List of Symbols and Abbreviations

c	Light Speed ($3 \times 10^8 \text{ m.s}^{-1}$)
d_{eff}	Effective Nonlinear Optical Coefficient (pm.V^{-1})
E	Electric Field Component of Electromagnetic Wave (V.m^{-1})
g_s	Signal Spatial Mode Coupling Coefficient
J_0	Threshold Pump Intensity (W.cm^{-2})
ΔK	Momentum Phase Mismatch (cm^{-1})
L	Cavity Length (cm)
L_c	Coherence Length (cm)
l_c	Crystal Physical Length (cm)
l_{eff}	Effective Parametric gain Length (cm)
l_w	Walk-off Length (cm)
M	Cavity geometrical Magnification Factor
N	Effective Mode Index
n	Refractive Index
P	Polarization
Q	Threshold Energy (J)
R	Effective Cavity Loss (The Product of Mirror Reflectivities)
S	Propagation Direction of the Cosine vector
W	Gaussian Beam Radius (m)
ADQW	Asymmetric Double Quantum Well
AR	Antireflection
CW	Continuous Wave
DFG	Difference frequency Generation
DRO	Doubly Resonant Oscillator
DSRO	Double-Pump Singly Resonant

e-ray	Extraordinary Ray
FWHM	Full Width Half Maximum
fs	Femtosecond
GRM	Gaussian Reflectivity Mirror
HT	High Transparent
IR	Infrared
NCPM	Noncollinear Phase Matching
ns	Nanosecond
o-ray	Ordinary Ray
OPA	Optical Parametric Amplification
OPG	Optical Parametric Generation
OPO	Optical Parametric Oscillator
PP	Periodically Poled
QPM	Quasi Phase matching
RBPM	Retracing Behavior of the Phase matching
SFG	Sum Frequency Generation
SHG	Second Harmonic Generation
SRO	Singly Resonant Oscillator
SSRO	Single-Pump Singly Resonant
ZGP	Zinc germanium Phosphide

List of Greek Letters

α	Coefficient of Field Absorption in the Crystal (cm^{-1})
β	Parametric Gain Coefficient
ϵ_0	Permittivity of Free Space ($8.85 \times 10^{-12} \text{ F.m}^{-1}$)
θ	Polar Angle (degree)
θ_{PM}	Phase Matching Angle (degree)
λ	Wavelength (μm)
ρ	Walk-off Angle (degree)
φ	Azimuthal Angle (degree)
ω	Angular Frequency (rad.s^{-1})
χ	Susceptibility
τ	Pulse duration (ns)
γ	Ratio of Backward to Forward pump Field Amplitude Inside The Crystal

List of Subscripts

b	Backward Transit
c	Cladding
e	Extraordinary
f	Forward Transit
g	Guiding
i	Idler
o	Ordinary
p	Pump
PM	Phase Matching
s	Signal

-
- [1] Handbook of Optics. Bass, M, et.al., Fiber Optics and Nonlinear Optics: Vol IV. Optical Parametric Oscillators (2nd ed., PP. 22-1 – 22-65). New York: McGraw-Hill (2001).
- [2] P.A. Franken, A.E. Hill, C.W. Peters, and G. Weinrich, “Generation of optical harmonics, Phys.Rev.Lett” **7**, 118-119 (1961).
- [3] J. A. Armstrong, N. Bloembergen, J. Ducuing, and P. S. Pershan, “Interactions between light waves in a nonlinear dielectric,” Phys. Rev., **127**, 1918–1939 (1962).
- [4] R. H. Kingston, “Parametric amplification and oscillation of optical frequencies,” Proc. IRE, **50**, 472 (1962).
- [5] N. M. Kroll, “Parametric amplification in spatially extended media and application to the design of tunable oscillators at optical frequencies,” Phys. Rev. **127**, 1207–1211 (1962).
- [6] C. C. Wang and G. W. Racette, “Measurement of parametric gain accompanying optical difference frequency generation,” Appl. Phys. Lett., **6**, 169–171 (1965).
- [7] J. A. Giordmaine and R. C. Miller, “Tunable coherent parametric oscillation in LiNbO at optical frequencies,” Phys. Rev. Lett., **14**, 973–976 (1965).
- [8] S. A. Akhmanov, A. I. Kovrigin, V. A. Kosolov, A. S. Piskarskas, V. V. Fadeev, and R. V. Khokhlov, “Tunable parametric light generator with KDP crystal,” JETP Lett., **3**, 241–245 (1966).
- [9] G. D. Boyd and A. Ashkin, “Theory of parametric oscillator threshold with single-mode optical masers and observation of amplification in LiNbO₃,” Phys. Rev., **146**, 187–198 (1966).

- [10] R. G. Smith, J. E. Geusic, H. J. Levinstein, S. Singh, and L. G. van Uitert, "Continuous optical parametric oscillator in $\text{Ba}_2\text{NaNb}_5\text{O}_{15}$," *Appl. Phys. Lett.*, **13**, 308 (1968).
- [11] R. L. Byer, M. K. Oshman, J. F. Young, and S. E. Harris, "Visible CW parametric oscillator," *Appl. Phys. Lett.*, **13**, 109–111 (1968).
- [12] S. E. Harris, "Tunable Optical Parametric Oscillator," *Proc. IEEE*, **57**, 2096–2113 (1969).
- [13] R. L. Herbst and R. L. Byer, "Singly resonant CdSe infrared parametric oscillator," *Appl. Phys. Lett.*, **21**, 189–191 (1972).
- [14] R. L. Byer, R. L. Herbst, R. S. Feigelson, and W. L. Kway, "Growth and application of [01.4] LiNbO₃," *Opt. Commun.*, **12**, 427–429 (1974).
- [15] R. L. Byer and R. L. Herbst, "Tunable electromagnetic oscillator using [01.4] grown LiNbO₃ and method," U.S. Patent 3 922 561, 25 (1975).
- [16] R. L. Byer, R. L. Herbst, and R. N. Fleming, "A broadly tunable IR source," in *Laser Spectroscopy*, S. Haroche, J. C. Pabay-Payroula, T. W. Hansch, and S. E. Harris, Eds. Berlin, Germany: Springer-Verlag, 1975.
- [17] C. Chen, B. Wu, A. Jiang, and G. You, "A new type ultraviolet SHG crystal $\beta\text{-BaB}_2\text{O}_4$," *Sci. Sin. Ser. B*, **28**, 235 (1985).
- [18] C. T. Chen, R. C. Eckardt, Y. X. Fan, and R. L. Byer, "Recent developments in beta barium borate," in *Proc. SPIE* **681**, 12–19 (1986).
- [19] Y. X. Fan, R. C. Eckardt, R. L. Byer, J. Nolting, and R. Wallenstein, "Visible BaB_2O_4 optical parametric oscillator pumped at 355 nm by a single axial-mode pulsed source," *Appl. Phys. Lett.*, **53**, 2014–2016, (1988).

-
- [20] Y. X. Fan, R. C. Eckardt, R. L. Byer, C. Chen, and A. D. Jiang, "Barium borate optical parametric oscillator," *IEEE J. Quantum Electron.*, **25**, 1196–1199 (1989).
- [21] C. L. Tang, W. R. Bosenberg, T. Ukachi, R. J. Lane, and L. K. Cheng, "Optical parametric oscillators," *Proc. IEEE*, **80**, 365–374 (1992).
- [22] J. G. Haub, M. J. Johnson, and B. J. Orr, "Continuously tunable injection-seeded beta barium borate optical parametric oscillator: Spectroscopic applications," *Appl. Phys. Lett.*, **58**, 1718–1720(1991).
- [23] J. G. Haub, R. M. Hentschel, M. J. Johnson, and B. J. Orr, "Controlling the performance of a pulsed optical parametric oscillator: A survey of techniques and spectroscopic applications," *J. Opt. Soc. Amer. B*, **12**, 2128–2141(1995).
- [24] Lawrence A. W. Gloster, Zhi Xing Jiang, and Terence A. King," Characterization of an Nd:YAG-Pumped β -BaB₂O₄ Optical Parametric Oscillator in Collinear and Non-collinear Phase-Matched Configurations" *IEEE J. Quantum Electronics*, **30**, 12(1994).
- [25]. T. Wilhelm, J. Piel, E. Riedle," Sub-20-fs pulses tunable across the visible from a blue-pumped single-pass noncollinear parametric converter" *Opt. Lett.* **22**, 1494 (1997).
- [26] G. Gerullo, M. Nisoli, S. Stagira, S. De Silvestri," Sub-8-fs pulses from an ultrabroadband optical parametric amplifier in the visible" *Opt. Lett.* **23**, 1283 (1998).
- [27] A. Shirakawa, I. Sakane, T. Kobayashi," Pulse-front-matched optical parametric amplification for sub-10-fs pulse generation tunable in the visible and near infrared" *Opt. Lett.* **23**, 1292 (1998).

- [28] V. Krylov, J. Gallus, U.P. Wild, A. Kalintsev, A.Rebane, “Femtosecond non-collinear and collinear parametric generation and amplification in BBO crystal”, *Appl. Phys. B* 70, 163–168 (2000).
- [29] k. Finsterbusch R.Urschel and H. Zacharias,” Tunable, high-power, narrow-band picosecond IR radiation by optical parametric amplification in KTP” *Appl. Phys. B* 74, 319–322 (2002).
- [30] H. Vanherzeele,” Picosecond laser system continuously tunable in the 0.6-4-micrometer range” *Appl. Opt.* **29**, 2246 (1990).
- [31] L. Carrion, J.P. Girardeau-Montaut: *Opt. Comm.* **152**, 347 (1998).
- [32] T. Nishikawa, N. Uesugi,” Effects of walk-off and group velocity difference on the optical parametric generation in KTiOPO₄ crystals” *J. Appl. Phys.* **77**, 4941 (1995).
- [33] Y.F. Chen, S.W. Chen, Y.C. Chen, Y.P. Lan, S.W. Tsai “Compact efficient intracavity optical parametric oscillator with a passively Q-switched Nd :YVO₄/Cr⁴⁺ :YAG laser in a hemispherical cavity”, *Appl. Phys. B* 77, 493–495 (2003).
- [34] G.Anstett, G.Goritz, D.Kabs, R.Urschel, R.Wallenstein, A.Borsutzky “Reduction of the spectral width and beam divergence of a BBO OPO by using collinear type II phase matching and back reflection of the pump beam. *Appl.Phys. B*72, 583 (2001).
- [35] N.Kondr atyuk, O.Manko, A.Shagov ,” Features of the angle tuned Phase matched OPO with pump beam reflected”, In *Laser Optics 2003: Solid State Lasers and nonlinear Frequency Conversion*, edited by V.Ustugov, Proceedings of SPIE 5478 ,189 (SPIE, Bellingham,WA,2004).
- [36] Y.F. Chen, S.W. Chen, L.Y. Tsai, Y.C. Chen, C.H. Chien “Efficient sub-nanosecond intracavity optical parametric oscillator pumped with

- a passively Q-switched Nd:GdVO₄ laser”, *Appl. Phys. B* 79, 823–825 (2004).
- [37] G.K.H. Kitaeva, V.V. Tishkova, I.I. Naumova, A.N. Penin, C.H. Kang, S.H. Tang “Mapping of periodically poled crystals via spontaneous parametric down-conversion “, *Appl. Phys. B* 81, 645–650 (2005).
- [38] A. I. Vodchits, V. I. Dashkevich, N. S. Kazak, V. K. Pavlenko, V. I. Pokryshkin, I. P. Petrovich, V. V. Rukhovets, A. S. Kraskovskii, and V. A. Orlovich1” Eye-Safe Radiation Source Based on an Optical Parametric Oscillator”, *Journal of Applied Spectroscopy*, **73**, 2(2006).
- [39] X. Liang, J. Bartschke, M. Peltz, J.A. L’huillier,” Non-collinear nanosecond optical parametric oscillator based on periodically poled LN with tilted domain walls”, *Appl. Phys. B* 87, 649–653 (2007).
- [40] P. N. Butcher and D. Cotter, “The Elements of Nonlinear Optics”, Eds:P. L. Knight and W. J. Firth, *Cambridge Studies in Modern Optics* 9, Cambridge University Press, UK (1990).
- [41] R. W. Minck, R. W. Terhune and C. C. wang, “Nonlinear Optics,” *Procc. IEEE*, **54**, 10(1966).
- [42] W. H. Louisell, *Coupled-Mode and Parametric Electronics*. New York: Wiley, 1960.
- [43] D. A. Kleinman,” Nonlinear Dielectric Polarization in Optical Media” *Phys. Rev.*, 126 1977 (1962).
- [44] F. T. Arecchi, E. O. Schulz-Doubois, “*Laser Hanndbook*,” Vol. 1, 1972.
- [45] T. Sminia, “Frequency conversion by nonlinear optics: narrow bandwidth sources and applications,” Ph.D Thesis, ACADEMISCH PROEFSCHRIFT, Dec. 2003.

- [46] M. Born and E. Wolf, Principles of Optics, 7th ed. (Cambridge University Press, Cambridge, United Kingdom, 1999).
- [47] E. E. Wahlstrom, Optical Crystallography, 4th ed. (John Wiley and Sons, Inc., New York, 1951).
- [48] R. W. Boyd. Nonlinear Optics. Academic, 1992.
- [49] M. Pagett, “Notes for modern and nonlinear optics”, m.padgett@physics.gla.ac.uk, internet source.
- [50] A. Yariv and P. Yev, Optical Waves in Crystals (John Wiley & Sons, New York, 1984).
- [51] V.G. Dimitriev, G.G. Gurzadyan and D.N. Nikogosyan, Handbook of Nonlinear Optical Crystals, 2nd ed., New York, Springer, 1991.
- [52] P. G. Nutting, “Dispersion Formulas Applicable to Glass,” J. Opt. Soc.Am., **2–3**, 61–65(1919).
- [53] M . Herzberger , “Colour Correction in Optical Systems and a New Dispersion Formula , ” Opt .Acta **6** : 197 – 215 (1959) .
- [54] M . Herzberger and C . D . Salzberg , “Refractive Indices of Infrared Optical Materials and Color Correction of Infrared Lenses , ” J . Opt . Soc .Am . **52** : 420 – 427 (1962) .
- [55] W. Koechner, ”Solid-State Laser Engineering”, 5th ed., Springer, 1999.
- [56] K. L. Vodopyanov, J. P. Maffetone, I. Zwieback, and W. Ruderman, “AgGaS₂ optical parametric oscillator continuously tunable from 3.9 to 11.3 μm ,” Appl. Phys. Lett. **75**, 1204-1206 (1999).
- [57] S. J. Brosnan, and R. L. Byer, “Optical parametric oscillator threshold and linewidth studies,” IEEE J.Quantum. Electron, **QE-15**, 415-431 (1979).
- [58] “Feature issue on optical parametric oscillation and amplification,” J. Opt. Soc. Am. B **10**, 1656-1791(1993).

-
- [59] “Feature issue on optical parametric oscillators and amplifiers,” *J. Opt. Soc. Am. B* **10**, 2148-2243 (1993).
- [60] “Feature issue on optical parametric devices,” *J. Opt. Soc. Am. B* **12**, 2084-2320 (1995).
- [61] A. E. Siegman, *Lasers* (University Science Books, Mill Valley, Calif., 1986), pp.858-913.
- [62] W. A. Neuman and S. P. Velsko, “Effect of cavity design on optical parametric oscillator performance,” in *Advanced Solid-State Lasers*, A. Payne and C. R. Pollock, eds., Vol.1 of OSA Trends in Optics and Photonics Series (Optical Society of America, Washington, D. C., 1996), pp.177-178.
- [63] M. K. Brown and M. S. Bowers, “High energy, near diffraction limited output from optical parametric oscillators using unstable resonators,” in *Solid State Lasers VI*, R. Scheps, ed., *Proc. SPIE* **2986**, 113-122 (1997).
- [64] J. N. Farmer, M. S. Bowers, and W. S. Schaprf, Jr., “High brightness eye safe optical parametric oscillator using confocal unstable resonators,” in *Advanced Solid-State Lasers*, M. M. Fejer, H. Injeyan, and U. Keller, eds., Vol. 26 of OSA Trends in Optics and Photonics Series (Optical Society of America, Washington, D. C., 1999), pp.567-571.
- [65] B. C. Johnson, V. J. Newell, J. B. Clark, E. S. McPhee, “Narrow-bandwidth low-divergence optical parametric oscillator for nonlinear frequency-conversion applications,” *J. Opt. Soc. Am. B* **12**, 2122-2127 (1995).
- [66] G. Hansson, H. Karlsson, F. Laurell, “Unstable resonator optical parametric oscillator based on quasi-phase-matched RbTiOAsO₄,” *Applied Optics* **40**, 5446-5451 (2001).

- [67] S. Pearl, Y. Ehrlich, S. Fastig, S. Rosenwaks, "Nearly diffraction-limited signal generated by a lower beam-quality pump in an optical parametric oscillator," *Applied Optics* **42**, 1048-1051 (2003).
- [68] S. Chandr, T. H. Allik, J. A. Hutchinson, M. S. Bowers, "Improved OPO brightness with a GRM non-confocal unstable resonator," in *Advanced Solid-State Lasers*, S. A. Payne and C. R. Pollock, eds., Vol.1 of OSA Trends in Optics and Photonics Series (Optical Society of America, Washington, D. C., 1996), pp.177-178.
- [69] Mali Gong, Shanshan Zou, Gang Chen, Ping Yan, Qiang Liu, and Lei Huang, "Threshold Studies of Pulsed Confocal Unstable Optical Parametric Oscillators," *Optics Express*, Vol. 12, No. 13, 28 June 2004.
- [70] R. L. Byer, "Optical parametric oscillator," in *Treatise in Quantum Electronics*, H. Rabin and C. L. Tang, eds. (Academic, New York, 1975), pp. 587-702.
- [71] W. J. Alford, A. V. Smith, "Wavelength variation of the second-order nonlinear coefficients of KNbO_3 , KTiOPO_4 , KTiOAsO_4 , LiNbO_3 , LiIO_3 , $\beta\text{-BaB}_2\text{O}_4$, KH_2PO_4 , and LiB_3O_5 crystals: a test of Miller wavelength scaling," *J. Opt. Soc. Am. B* **18**, 524-533 (2001).
- [72] P. Canarelli, Z. Benko, A. H. Hielscher, R. F. Curl, and F. K. Tittel, "Measurement of Nonlinear Coefficient and Phase Matching Characteristics of AgGaS_2 ," *IEEE Journal of Quantum Electronics*, **28**, 1 (1992).
- [73] Robert C. Eckardt, Member IEEE, Hisashi Masuda, Yuan Xuan Fan, AND Robert L. Byer, Fellow IEEE, "Absolute and Relative Nonlinear Optical Coefficients of KDP, KD^*P , BaB_2O_4 , LiIO_3 , MgO:LiNbO_3 , and KTP Measured by Phase-Matched Second-Harmonic Generation", *IEEE Journal of Quantum Electronics*, **26**, 5 (1990).

الخلاصة

في هذا البحث تم إجراء دراسته حاسوبية باستخدام برنامج (MATLAB) الاصدار (6.5) لحساب خصائص البلورات اللاخطية الاحادية والثنائية اذ اخذ بنظر الاعتبار التطابق الطوري غير الموحد خطياً لمذبذب معلمي بصري لبلوره متفرده بعرض نبضة ضخ (10-40) نانوثانية.

لقد تم اجراء دراسته نظريه لمرنان احادي لبلورة ($AgGaS_2$) للتطابق الطوري - النوع الأول لمنظومة مذبذب معلمي بصريه مضخه بواسطة ليزر النديميوم - ياك ذو الطول الموجي (1.064) مايكروميتر والعامل بنمط إحكام عامل النوعيه حيث تم الحصول على موجة اشاره ذات طول موجي (3-5) مايكرومتر في عملية تحويل ذات مرحله واحده. لقد تم اجراء مقارنه نظريه بين حد العتبه لكثافة طاقة الضخ لمنظومة مذبذب معلمي بصريه احادية الضخ ومنظومه ثنائية الضخ.

لقد تم عرض نموذج نظري لحساب حد عتبه كثافة طاقه الضخ قائم على فرضية الموجات الكرويه لمرنان احادي نبضي لمذبذب معلمي بصري مزدوج الضخ متحد البؤره موجب التفرع غير مستقر. نتائج هذا النموذج كانت لبلورة (KTP) من النوع الثاني للتطابق الطوري غير الحرج لمنظومة مذبذب معلمي بصريه لموجة اشاره ذات طول موجي (1.61) مايكرومتر وموجه عاطله ذات طول موجي (3.2) مايكرومتر.

كما تم عرض حد العتبه لطاقة الضخ لمنظومة مذبذب معلمي بصريه كداله لعدة معاملات مهمه مثل عامل تكبير التجويف, طول التجويف, طول البلوره, عرض نبضة الضخ, إنعكاسية الخرج بالنسبه لموجة الاشاره وكذلك موقع البلوره داخل المرنان.

Abstract

This work presents a computational calculation method of calculating the characteristics of non-collinear phase matching for a single-crystal down-conversion OPO with pump pulse durations on the order of (10-40) nanoseconds using MATLAB (version 6.5).

A nanosecond AgGaS₂ type-I singly resonant optical parametric oscillator pumped by a *Q*-switched 1.064 μ m Nd:YAG laser was demonstrated theoretically. Continuously tunable (3-5 μ m) radiation for a signal wave has been achieved in a single stage conversion process. A theoretical comparison on the threshold pump energy density is made between the single pump pass SRO OPO and the double pump pass one. Also a theoretical threshold model based on the spherical wave assumption for a pulsed double-pass pumped singly resonant confocal positive-branch unstable optical parametric oscillator (OPO) has been proposed. The threshold model results for a 1.064 μ m pumped KTP OPO, where type-II non-critical phase matching was satisfied at 1.61 μ m signal and 3.2 μ m idler wavelengths. The OPO threshold as a function of important parameters such as the cavity magnification factor, cavity physical length, crystal length, pump pulsewidth, output coupler reflectance to signal and crystal position inside the resonator has been presented.



جمهورية العراق
وزارة التعليم العالي والبحث العلمي
الجامعة التكنولوجية
قسم هندسة الليزر والبصريات الالكترونية

دراسة اداء منظومة تذبذب علميه بصريه للبورات اللاخطييه (KTP و $AgGaS_2$)

رساله مقدمه الى
الجامعة التكنولوجيه قسم هندسة الليزر والبصريات الالكترونيه كجزء من متطلبات نيل شهادة
الدكتوراه فلسفه في اختصاص
هندسة الليزر

من قبل
محمد جلال عبد الرزاق
ماجستير (2002)

باشراف

الاستاذ الدكتور
محمد صالح مهدي

الاستاذ الدكتور
فريد فارس رشيد

1429 هجري

2008 ميلادي

Contents

Chapter One: Introduction

1.1 Definition of Nonlinear Optics	1
1.2 Optical Parametric Amplification and Oscillation	2
1.3 OPO Technique: Past and Present	4
1.4 Aim of the Project	11

Chapter Two: Second Order Nonlinear Optical Conversions

2.1 Basic Principles of Second Order Nonlinear Optical Conversions	13
2.1.1 Three Wave Interactions in 2 nd Order NLO Process	16
2.1.2 Effective Second-Order Nonlinear Coefficient	19
2.2 Nonlinear Optical Materials	20
2.2.1 Basic Properties	20
2.2.2 Optical Properties of Materials	20
2.3 Phase Matching and Conversion Efficiency	23
2.3.1 Methods for Phase-Matching	24
2.3.1.1 Dielectric Waveguide Phase-Matching	26
2.3.1.2 Birefringent Phase Matching	27
2.3.1.2.1 Walk off	32
2.3.1.3 Quasi Phase-Matching	34
2.3.1.4 Non-collinear Phase-Matching	35
2.4 OPO Cavity Configurations	37
2.5 The Effects of Focusing on Parametric Oscillation	40

Chapter Three: The Characteristics of Non-collinear Phase-matching in Uniaxial and Biaxial Crystals

3.1 Introduction	42
3.2 Tuning of Nonlinear Crystal	43
3.2.1 Calculation of Refractive Index for Uniaxial Crystal	43
3.2.2 Calculation of Refractive Index for Biaxial Crystal	45
3.3 Tracing Behaviors of the phase-matching angle in non-collinear phase matched optical parametric oscillators	46
3.4 The direction of the generated waves in uniaxial crystal	48
3.5 The direction of the generated waves in biaxial crystal	59

Chapter Four: Performance Modeling Of an OPO

4.1 Wide-tunable, AgGaS₂ optical parametric oscillator

4.1.1 Introduction	65
4.1.2 OPO Cavity Configuration	65
4.1.3 Analysis of Oscillation Threshold	66
4.1.4 Theoretical Results	68

4.2 Pulsed Confocal Unstable Optical Parametric Oscillators

4.2.1 Introduction	72
4.2.2 OPO Cavity Design	74
4.2.3 Theoretical Threshold Model	75
4.2.3.1 SRO single pass gain solution based on spherical wave	76
4.2.3.2 Double-pass pumped case	79
4.2.4 Theoretical Results	83

Chapter Five: Conclusion and Suggestion for Future Work

5.1 Conclusion	88
5.2 Suggestion for Future Work	90
References	92
Appendices	

Republic of Iraq
Ministry of Higher Education and
Scientific Research
University of Technology
Laser and Optoelectronics Engineering
Department



Performance Study of an Optical Parametric Oscillation System for Nonlinear Crystals KTP and AgGaS₂

A Thesis
Submitted to University of Technology Laser and Optoelectronics Engineering
Department
in Partial Fulfillment of the Requirements for the Degree of
Doctor of Philosophy
In
Laser Engineering

by

Mohammed Jalal Abdul-Razzak
M.Sc.2002

Supervised BY

Dr. Fareed F. Rasheed
Professor
A.H.1429

Dr. Mohammed S. Mehde
Professor
A.C.2008